Spin-orbit coupling and chirality in carbon nanotubes
Master Thesis

Frederik Treue
Supervisor: Karten Flensberg

April 30, 2010

Contents

1 Introduction **1**
- 1.1 Carbon nanotubes and quantum computers . . . 1
- 1.2 Organization of the thesis . . . 3

2 Graphene **5**
- 2.1 Basic definitions . . . 5
- 2.2 Symmetry of graphene . . . 6
- 2.3 Bloch's theorem for graphene . . . 7

3 Folding up the nanotube **13**
- 3.1 Chirality and unitcell of the CNT . . . 13
  - 3.1.1 The helical unitcell . . . 14
  - 3.1.2 The translational unitcell . . . 16
  - 3.1.3 Comparing the unitcells . . . 16
- 3.2 Cyclic boundary conditions. Metallic and semiconducting nanotubes . . . 17
- 3.3 σ/π band mixing . . . 20
  - 3.3.1 $\pi - \pi$ orbital coupling . . . 23
  - 3.3.2 $\sigma - \pi$ orbital coupling . . . 24
  - 3.3.3 $\sigma - \sigma$ orbital coupling . . . 26
  - 3.3.4 Selfenergy of the σ orbitals . . . 26
  - 3.3.5 Solving the full CNT hamiltonian . . . 27

4 Spin orbit interaction in CNTs **29**
- 4.1 Basics of the spin-orbit coupling . . . 29
- 4.2 The atomic hamiltonian . . . 30

5 The pertubative hamiltonian **37**
- 5.1 The basic problem . . . 37
- 5.2 The effective spin-orbit/curvature perturbation . . . 38
  - 5.2.1 calculation of $\hat{H}_0$ . . . 41
- 5.3 The pertubative hamiltonian . . . 43

6 Izumidas derivation **45**
6.1 Their coordinatesystem . . . 45
6.2 The effective hamiltonian . . . 46
6.2.1 The $\hat{H}_{CV}$ hamiltonian . . . 47
6.2.2 $\hat{H}_{SO}$ . . . 53
6.2.3 The graphene hamiltonian $\hat{H}_0$ . . . 55
6.2.4 $\hat{H}^{(2)}_{SOCV}$ and $\hat{H}^{(2)}_{CVCV}$ . . . 60

7 Magnetic field **69**
7.1 Zeeman effect . . . 69
7.2 The Aharonov-Bohm effect . . . 70
7.2.1 Numerical results . . . 77

8 Nummerical Hückel calculations **83**
8.1 The extended Hückel method . . . 83
8.1.1 Semi-heuristic argument for EHT . . . 85
8.2 EHT for magnetic field and spin-orbit coupling . . . 86
8.3 A more efficient method . . . 87

9 Conclusion **91**

A $\sigma - \sigma$ coupling elements **93**

B Explicit H_{so} matrix **95**
B.1 Explicit H_{so} matrix . . . 96

C Oddness of derivative operator **97**

D Electromagnetic field in quantummechanics. Canonical and Kinematic impulse **99**

Chapter 1

Introduction

In this first section, I aim to present my personal entry point to the study of carbon nanotubes (CNTs), ie. the reason why I think this particular systems are of any interests. I then outline the thesis organization, ie. present an overview of the chapters.

1.1 Carbon nanotubes and quantum computers

In a standard "classical" computer, every piece of data is represented by a vector of bits which can each take the value of 0 or 1. In the first part of the last century it was shown by Alan Turing and others, that any algorithm could be implemented by repeated application of the NAND gate to this vector.

However, in 1982, Richard Feynman sparked a new field inside physics, mathematics and computer science, when he pointed out that while classical computers can indeed carry out any algorithm, only a subset of the computational operations made available by the Schrodinger equation [2] are described by the classical gates such as the NAND gate. In quantum physics we know that states need not be in either one state or another, but can be in a superposition of eg. state 0 and state 1, and, more importantly, we know that different states may be entangled with each other, eg. the state $|\Psi\rangle = \frac{1}{\sqrt{2}}(|01\rangle + |10\rangle)$ where each state depends on the other state, so that if a measurement is made on the first state, and it is found to be in the "0" position, the other one immediately shifts from being in a superposition of "0" and "1" to being in position "1" with unit certainty. Now, we may imagine having a vector of N such states, or "qubits[1]", and preparing them in a superposition of all 2^N possible (classical) states, ie. if we use $|n\rangle$ to denote the state where the qubits in some given ordering is the binary representation of the number n, we may prepare the state $\frac{1}{\sqrt{2^N}} \sum_n |n\rangle$. Now, if we have an algorithm that we wish to evaluate, one way of formally characterizing the quantum computation (due to Kitaev[3]), is to note we must have some physical system that implement a time development operator U, such that for a given input vector $|i\rangle$, we have that $|o\rangle = U|i\rangle$ is the desired output, for any input vector $|i\rangle$ - such an operation have been shown to be implementable with an array consisting of a number of "quantum gates",

[1] QUantum BITS

each of which is one of 3 basic 1 or 2 qubit operations, reminiscent of the NAND gate mentioned above, shown in e.g. [4] .

Combining these two things, U and $|\Psi\rangle$, we find that we can generate a superposition of all possible *output* states of the system, since $U|\Psi\rangle = U\frac{1}{\sqrt{2^N}}\sum_n |n\rangle = \frac{1}{\sqrt{2^N}}\sum_n |o_n\rangle$ where $|o_n\rangle$ is defined as the algorithms output when given input $|n\rangle$. Since the U operation was used only once, the time needed for this calculation is the same as the time needed to calculate the result for only one input state, and so this principle have been named "quantum parallelism" - however if we try to measure the result of the calculation, the wavefunction will collapse and we will receive only one of the answers, so it was not clear if this scheme provides any advantages over the classical computer, but through the work of e.g. Deutch[5] ,Grover[6] and especially Shor[7], quantum algorithms with significant speedup over classical computation was discovered, some of which also had significance for the society at large.

The theory of quantum computation have developed much in its approx. 30 year long existence, however the implementation of these ideas in actual physical systems have proven to be a formidable challenge in its own respect. There are some fundamental reasons for this, but it all comes down to 5 demands made of a quantum computer, some of which seems mutually exclusive. To qualify as a physical system for quantum computation, a system must have

1. Strong *controllable* interaction, providing a "handle", so we can set the qubit and interact with it.

2. Weak interaction with surroundings, so that when we leave the system, the data contained in the qubit is preserved.

3. Readout: We need a way to measure the state of a qubit once calculation is done.

4. Scalability: One qubit is not (very) interesting - we need easy way to expand the number of qubits for larger calculations

5. A way to make two qubits interact in a controlled way.

So far, probably the most successful implementation of this has been the iontrap quantum computer, first proposed by [1] . However, it is at its core an atomic physics implementation, meaning that all operations is carried out on individual ions in a single trap, making scalability the major problem of this implementation[2]. As an alternative route to the quantum computer, solid state implementations have been considered, since it may be thought that the scalability will be easier here, as has been seen for classical computers. However, here one runs into the problem that most physical variables is strongly coupled to the surroundings in for instance crystals: The charge of a given area is eg. coupled by the strong Coulomb potentials of nearby charges - thus, what we need is a variable that is weakly coupled with the environment. The spin of an (unpaired) electron of a spin-0 atom (to avoid hyperfine interaction) is a potentially good candidate, since the spin is typically relatively weakly interacting with the environment compared to e.g. the charge,

[2]although there are also problems with speed: By design, the quantum computer will never get far above 10^4 quantum gates pr. second

thus fulfilling condition 2 above, but we then need a strong interaction to control the qubit: The magnetic field is an obvious candidate, but changing magnetic field is relatively slow compared to changing electric fields, and thus one could search for a system where one has electric control of the spin. One possible candidate for such a system is carbon nanotubes: They can, on one hand, be made using only C-12 atoms, which have nuclear spin 0, and since the spin-orbit coupling here gives a physical interaction between the motion around the circumference of the nanotube and the spin of the electrons[14], it could thus be hoped, that by electrically controlling the orbital motion of the electrons, one could, in a controlled way, alter their spin, thus fulfilling condition 1 above.

Around the beginning of the work on this thesis, an article showing new, relevant experimental data was published [8] where several unexpected features due to spin-orbit coupling in carbon nanotubes were observed. This prompted us to attempt a more thorough examination of the effects of spin-orbit coupling in carbon nanotubes, which was found independently by us, has a highly nontrivial correlation with the so-called chirality of the nanotube, which is a measure of the specific geometry of a given carbon nanotube.

1.2 Organization of the thesis

This thesis is roughly organized as a gradually more advanced description of the physical effects in a carbon nanotube, each chapter adding a new part to the hamiltonian of the system:

- The first chapter concerns graphene, which forms the basis of the description of the carbon nanotubes, since these may be thought of as rolled up sheets of graphene.
- Then follows a chapter describing the effects of the cylindrical like topology of the carbon nanotube.
- Then we describe the effect of spin-orbit coupling in a nanotube.
- In chapter 5 we describe the first of the results from a numerical simulation of the system, and explain it, using a pertubative approach.
- As an interlude, chapter 6 describes another derivation, reaching the same principal result as us, but with a slightly different, and perhaps more elegant, way of deriving it.
- Then follows a chapter on the effect of applying a magnetic field along the tube axis direction, where we explain some further numerical results.
- Finally, a chapter describes the numerical algorithm used to generate the numerical data in this thesis.

Chapter 2

Graphene

In order to solve the graphene system, we shall employ Bloch's theorem, so we assume that we may deal with an infinite sheet of graphene. We use a tight-binding approximation, ie. we shall assume that the electron wavefunctions can be described as linear combinations of atomic orbitals, also known as the LCAO approximation, so we shall ignore e.g. ionized basis functions - this follows the literature standard for solving graphene, which was first developed for graphite by [30]. First of all, however, we must define the unitcell to be used in these calculations, along with a few other important basics.

2.1 Basic definitions

In figure 2.1 we see the honeycomb lattice of graphene. The first thing one notices (or remembers from basic solid state physics) is that the honeycomb lattice is not a bravais lattice, but rather, composed by two sub(bravais)lattices or in other words, the primitive unitcell will contain two atoms, and thus the two vectors, $\mathbf{a_1}$ and $\mathbf{a_2}$ in figure 2.1 are chosen to be our lattice vectors, and, defining the latticeconstant (the length of the lattice vectors), as a_0, we find through simple geometry that

$$\mathbf{a_1} = a_0 \begin{pmatrix} \frac{\sqrt{3}}{2} \\ \frac{1}{2} \end{pmatrix} \qquad \mathbf{a_2} = a_0 \begin{pmatrix} \frac{\sqrt{3}}{2} \\ -\frac{1}{2} \end{pmatrix} \tag{2.1}$$

From these, it is easy to see that the reciprocal lattice will be spanned by the two vectors:

$$\mathbf{b_1} = \frac{2\pi}{a_0} \begin{pmatrix} \frac{1}{\sqrt{3}} \\ 1 \end{pmatrix} \qquad \mathbf{b_2} = \frac{2\pi}{a_0} \begin{pmatrix} \frac{1}{\sqrt{3}} \\ -1 \end{pmatrix} \tag{2.2}$$

Notice also that from the real lattice, we may gather that the distance between neighboring atoms is $a_{cc} \equiv \frac{a_0}{\sqrt{3}}$, and since the lattice constant is approximately $a_0 = 2.46$ Å[30] we find that $a_{cc} = 1.42$Å.

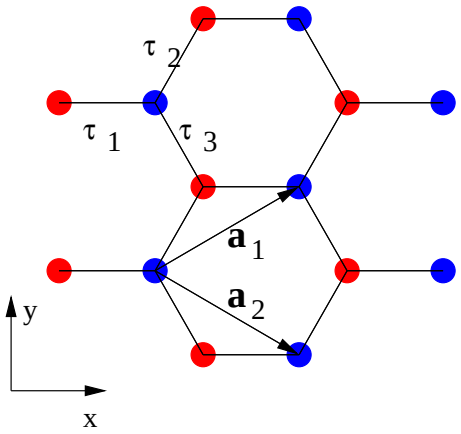

Figure 2.1: The crystal structure of graphene. The red(blue) dots denotes carbon atoms on sublattice A(B) and the lines denote the σ-orbital bonds between the atoms. Note, that with the coordinatesystem shown, the σ orbitals presented in the text denotes the orbitals on the A sublattice sites.

2.2 Symmetry of graphene

In principle, one could now start out with the full hamiltonian for the graphene system, including all 6 electrons (pr. atom). However, a few assumptions vastly decreases the work required. First, we shall assume that the 1s electrons are so tightly bound to the carbon nuclei that they are too far down in the Fermi sea to play any role, reducing our problem to 4 electrons pr. atom. Now, in graphene, the symmetry helps reduce this even further[1]: From figure 2.1 it is obvious that there is a threefold rotation symmetry around each atom, and therefore the crystal field part of the full hamiltonian will also have this symmetry, and consequently it will be easier to solve the system if we can construct atomic orbitals that have this symmetry inbuilt and use them, instead of the usual continuously rotationally symmetric $|nlm\rangle$ (hydrogenic) functions. This is indeed possible: we define the z direction to be perpendicular to the graphene plane, and start out from the wellknown three, realvalued orbitals lying along the 3 axis's, build from the standard $|nlm\rangle$ as follows:

$$\begin{aligned} |p_x\rangle &= \frac{1}{\sqrt{2}}(-|211\rangle + |21-1\rangle) \\ |p_y\rangle &= \frac{i}{\sqrt{2}}(|211\rangle + |21-1\rangle) \\ |p_z\rangle &= |210\rangle \end{aligned} \tag{2.3}$$

and the remaining 2s shell. First we see that the $|p_z\rangle$ shell, since it is invariant under any rotation around the z axis, immediately fulfills the crystal symmetry, and second we make the linear

[1] note, however, that this relies on the planar geometry of the graphene sheet - things become somewhat more involved once we consider the cylindrical CNTs

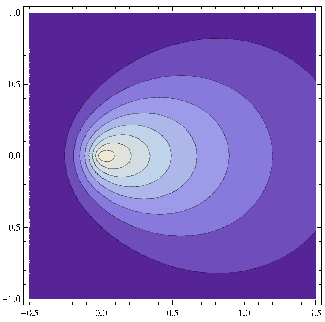

Figure 2.2: The isoprobability curves of the first sigma orbitals. The nucleus is at (0,0) and the units are Ångstrøm, and the neighboring atom would thus be at (1.42,0)

combinations, known as the σ orbitals

$$\begin{aligned}
|\sigma_1\rangle &= \frac{1}{\sqrt{3}}|2s\rangle + \sqrt{\frac{2}{3}}|p_x\rangle \\
|\sigma_2\rangle &= \frac{1}{\sqrt{3}}|2s\rangle - \sqrt{\frac{1}{6}}|p_x\rangle + \frac{1}{\sqrt{2}}|p_y\rangle \\
|\sigma_3\rangle &= \frac{1}{\sqrt{3}}|2s\rangle - \sqrt{\frac{1}{6}}|p_x\rangle - \frac{1}{\sqrt{2}}|p_y\rangle
\end{aligned} \tag{2.4}$$

The isoprobability contours of the $|\sigma_1\rangle$ orbital has been shown in figure 2.2 - We note that the orbitals evidently rotate onto one another under the 3 fold rotation we are considering.

In graphene, the crystal field clearly causes the sp^2 orbitals to have a lower energy than the $|p_z\rangle$ bands, since the sp^2 orbitals get closer to the surrounding, positive nuclei. Therefore 3 out of the 4 electrons in the outer shell of carbon will fall into these orbitals, and form bonds with the 3 surrounding atoms, holding the crystal structure together. The fourth electron could in principle fall into these orbitals as well, but that would cost a large amount of coulomb energy, since they are all halffilled, and so we may assume that it goes into the energetically less favorable, but free, $|p_z\rangle$ orbital, also known as the π orbital. Since these do not form any bonds (graphene is pr. definition a monolayer crystal), it is appropriate to use Bloch's theorem for these electrons, identifying the crystal lattice as the periodic potential.

2.3 Bloch's theorem for graphene

From basic solid state physics, we know that the eigenfunctions of the electrons ($\Psi_{\mathbf{k}n}(\mathbf{r})$) in a periodic potential, $U(\mathbf{r})$, can be chosen to be blochwaves, that is

$$\Psi_{n\mathbf{k}}(\mathbf{r}) = e^{i\mathbf{k}\cdot\mathbf{r}} u_{n\mathbf{k}}(\mathbf{r}) \tag{2.5}$$

where n refers to the band number and $u_{n\mathbf{k}}(\mathbf{r})$ has the same periodicity as the crystal potential, $U(\mathbf{r})$, so they fulfill the Bloch condition

$$\Psi_{n\mathbf{k}}(\mathbf{r}+\mathbf{R}) = e^{i\mathbf{k}\cdot\mathbf{r}+\mathbf{R}}u_{n\mathbf{k}}(\mathbf{r}+\mathbf{R}) = e^{i\mathbf{k}\cdot\mathbf{R}}e^{i\mathbf{k}\cdot\mathbf{r}}u_{n\mathbf{k}}(\mathbf{r}) = e^{i\mathbf{k}\cdot\mathbf{R}}\Psi_{n\mathbf{k}}(\mathbf{r}) \tag{2.6}$$

where $\mathbf{R}$ is a lattice vector.

We now wish to couple this to the atomic orbitals described above, in particular to the π orbitals at each atomic site, since this will put us in a position to use the standard LCAO (Linear Combination of Atomic Orbitals) machinery. This is done by first noting that we may make an inverse Fourier transform of any Bloch wavefunction, that is, any function fulfilling (2.6), since it is periodic in the reciprocal lattice. So

$$\Psi_{n\mathbf{k}}(\mathbf{r}) = \sum_{\mathbf{R}} e^{i\mathbf{k}\cdot\mathbf{R}}\phi_n(\mathbf{r},\mathbf{R}) \tag{2.7}$$

Now, if we can establish that the ϕ_n functions may be represented by atomic orbitals, we will be ready to solve the graphene problem. This will eventually rely on an approximation, but we may make some rigorous progress using the standard Wannier decomposition method, as in chapter 10 of [9], by noting that by virtue of the mechanics of the Fourier transform, we know that

$$\phi_n(\mathbf{r},\mathbf{R}) = \frac{1}{A}\sum_{\mathbf{k}} e^{-i\mathbf{R}\cdot\mathbf{k}}\Psi_{n\mathbf{k}}(\mathbf{r}) \tag{2.8}$$

where A is as usual, the area of the graphene unitcell. From this we may see that the $\phi_n(\mathbf{r},\mathbf{R})$ may be viewed as molecular orbitals on each unitcell, since they may be expressed as a function solely of the difference between $\mathbf{r}$ and $\mathbf{R}$, which is seen by recalling that $\Psi_{n\mathbf{k}}$ fulfills (2.6) and thus, $\phi_n(\mathbf{r},\mathbf{R}) = \phi_n(\mathbf{r}+\mathbf{R_l},\mathbf{R}+\mathbf{R_l})$ where $\mathbf{R_l}$ is a lattice vector, and thus the solution to the problem can be viewed as the $\phi_n(\mathbf{r},\mathbf{R})$ functions placed at each unitcell of the crystal, with the appropriate Bloch phase. Now we make the LCAO assumption that these ϕ_n functions may be expressed as linear combinations of the atomic orbitals present in the unitcell, thus solving two problems with one stroke, namely the problem of connecting the Bloch waves to the atomic orbitals and the complication of the diatomic unitcell, since the molecular orbitals ϕ_n is now assumed to be linear combinations of atomic orbitals, so that, inserting into (2.7), we may express the Bloch wavefunctions as[2]

$$\begin{aligned}\Psi_{n\mathbf{k}}(\mathbf{r}) &= \frac{1}{\sqrt{N}}\sum_{\mathbf{R}} e^{i\mathbf{k}\cdot\mathbf{R}}(a\pi_A(\mathbf{r}-\mathbf{R}) + be^{i\mathbf{k}\cdot\mathbf{l_1}}\pi_B(\mathbf{r}-\mathbf{R}-\mathbf{l_1}))\\ &\equiv a|\psi_{n,\mathbf{k}}\rangle_A + be^{i\mathbf{k}\cdot\mathbf{l_1}}|\psi_{n,\mathbf{k}}\rangle_B\end{aligned} \tag{2.9}$$

where $\mathbf{l_1} = a_0\begin{pmatrix}\frac{-1}{\sqrt{3}}\\ 0\end{pmatrix}$ is the vector between the two atoms in a unitcell, ie. between different sublatices, N is the number of unitcells, the A/B subscripts on the wavefunctions denotes the

[2]One could ask why we don't just use the Wannier functions instead of making this assumption. The main reason for this is, as stated above, that we may find the elements of the Hamiltonian and the overlap matrix,$\mathbf{S}$, for the atomic orbitals, but it is important to remember that the choice of basisfunctions are not fixed by the theory and other sets of functions may serve us better in other circumstances, as we shall indeed see in section 8

sublattice, and a and b are the coefficients to be determined from solving the Schrödinger equation:

$$\hat{H}\Psi_{n\mathbf{k}} = E_n\Psi_{n\mathbf{k}} \tag{2.10}$$

Notice that in (2.9), we explicitly write out the relative blochphase between the atoms in a given unitcell. This may seem slightly at odds with the "molecular orbitals" approach, since we might have made it a part of the coefficient, ie. used $\tilde{b} = be^{i\mathbf{l_1}\cdot\mathbf{k}}$ instead of b - however, this explicit representation will be convenient later, and so it is left in. Now, we have to be slightly careful when we use π orbitals instead of the Wannier functions as in (2.9): Whereas the Wannier functions were orthogonal by construction, the atomic orbitals at different sites are not. This requires a slight modification of the Schrödinger equation: let us define a non-orthonormal, but complete, set of $|\xi_m\rangle$. The fact that the set is complete means that the eigenstates of H may be expressed as $\Psi_{n\mathbf{k}} = \sum_a c_{an\mathbf{k}}|\xi_a\rangle$ - then, if we define the overlap matrix $S_{ab} = \langle\xi_a|\xi_b\rangle$, the usual schrödinger equation (2.10) is

$$\begin{aligned}
\sum_a \hat{H}c_{an\mathbf{k}}|\xi_a\rangle = E_n\sum_a c_{an\mathbf{k}}|\xi_a\rangle \implies \\
\sum_a H_{ba}c_{an\mathbf{k}} = E_n\sum_a c_{an\mathbf{k}}S_{ba} \implies \\
\hat{H}\Psi_{n\mathbf{k}} = E_n\mathbf{S}\Psi_{n\mathbf{k}}
\end{aligned} \tag{2.11}$$

where the first implication follows from multiplying from the left with $\langle\xi_b|$, and the second one follows from the fact that the second line in (2.11) is in fact one row of the equation $\hat{H}\mathbf{c}_{n\mathbf{k}} = E_n\mathbf{S}\mathbf{c}_{n\mathbf{k}}$, where $\mathbf{c}_{n\mathbf{k}}$ is now a column of the coefficients for the nth eigenvector. This equation is equivalent to the last line of (2.11).

Now we apply the schrödinger equation to the LCAO Bloch waves (2.9) in order to find E_n,a and b:

$$\begin{aligned}
\hat{H}\Psi_{n\mathbf{k}}(\mathbf{r}) = \frac{1}{\sqrt{N}}\sum_{\mathbf{R}} e^{i\mathbf{k}\cdot\mathbf{R}}(a\hat{H}\pi_A(\mathbf{r}-\mathbf{R}) + be^{i\mathbf{l_1}\cdot\mathbf{k}}\hat{H}\pi_B(\mathbf{r}-\mathbf{R}-\mathbf{l_1})) = \\
E_{n\mathbf{k}}\mathbf{S}\Psi_{n\mathbf{k}}(\mathbf{r}) = \frac{1}{\sqrt{N}}\sum_{\mathbf{R}} e^{i\mathbf{k}\cdot\mathbf{R}}(a\mathbf{S}\pi_A(\mathbf{r}-\mathbf{R}) + be^{i\mathbf{l_1}\cdot\mathbf{k}}\mathbf{S}\pi_B(\mathbf{r}-\mathbf{R}-\mathbf{l_1}))
\end{aligned} \tag{2.12}$$

Thus, we see that we need the matrix elements of $\hat{H}$ and $\mathbf{S}$ in order to proceed, and in order to make progress with this, we employ our next assumption, namely that only nearest neighbour atoms interact through the hamiltonian, and have a significant overlap. Notice from figure 2.1 that nearest neighbours are always from different sublattices. Clearly, since we have a diatomic unitcell, and since we consider only one atomic orbital pr. atom, the hamiltonian and overlap matrix may be written as 2x2 matrices in the A-B space in which the eigenfunctions (2.9) is described by the vector of the coefficients on the sublattices ie. $\begin{pmatrix} a \\ b \end{pmatrix}$, and consequently, we need $A_{ij} \equiv \langle\psi_{n\mathbf{k}}|_i\mathbf{A}|\psi_{n\mathbf{k}}\rangle_j$ for $\mathbf{A} = \left\{\hat{H}, \mathbf{S}\right\}$, and i,j denoting sublatices. We consider the elements of these matrices one by one:

The H_{AB} and S_{AB} element: As observed above, the graphene crystal have a threefold rotational symmetry, which immediately yields that the transfer integrals between nearest neighbour are equal (since they are rotated onto one another by the symmetry operation), and we denote this transfer integral γ_0. From figure 2.1 one sees that an A sublattice orbital couples to 3 orbitals in the B sublattice, at positions $\mathbf{l_1}, \mathbf{l_2} \equiv a_0 \begin{pmatrix} \frac{1}{2\sqrt{3}} \\ \frac{1}{2} \end{pmatrix}, \mathbf{l_3} \equiv a_0 \begin{pmatrix} \frac{1}{2\sqrt{3}} \\ \frac{-1}{2} \end{pmatrix}$ relative to the A orbital, which leads to the sum over $\mathbf{l}$ in the following derivation:

$$\langle \psi_{n\mathbf{k}'}|_A \hat{H} |\psi_{n\mathbf{k}}\rangle_B = \frac{1}{N} \sum_{\mathbf{R}',\mathbf{R}} e^{i((\mathbf{R}+\mathbf{l_1})\cdot\mathbf{k}-\mathbf{R}'\cdot\mathbf{k}')} \pi_A(\mathbf{r}-\mathbf{R}') \mathbf{H} \pi_B(\mathbf{r}-\mathbf{R}-\mathbf{l_1}) =$$

$$\frac{1}{N} \sum_{\mathbf{R}} e^{i\mathbf{R}\cdot(\mathbf{k}-\mathbf{k}')} \sum_j e^{i\mathbf{l}\cdot\mathbf{k}} \gamma_0 = \delta_{\mathbf{k},\mathbf{k}'} \sum_j e^{i\mathbf{k}\cdot\mathbf{l_j}} \gamma_0 \equiv \Gamma(\mathbf{k})\gamma_0 \tag{2.13}$$

A completely analogous argument yields the S_{AB} element, except that the transport integral γ_0 between neighbours is of cause exchanged with s_0, the overlap integral between neighbours: Thus $S_{AB} = \Gamma(\mathbf{k})s_0$. These calculations also immediately gives us the H_{BA} element since the hamiltonian is hermitian, so $H_{BA} = H_{AB}^*$, in agreement with (2.13), since the only change in the derivation comes from the fact, that while the A sublattice orbitals couple to the B sublattice orbitals at the unitcells at positions $\mathbf{l_1}, \mathbf{l_2}, \mathbf{l_3}$ relative to the original unitcell, the B sublattice couple to A orbitals at relative positions $-\mathbf{l_1}, -\mathbf{l_2}, -\mathbf{l_3}$, which we see is the same as interchanging $\Gamma(\mathbf{k})$ with $\Gamma(\mathbf{k})^*$ in (2.13). Thus, choosing γ_0 real, we have that $H_{BA} = \Gamma(\mathbf{k})^*\gamma_0 = (\Gamma(\mathbf{k})\gamma_0)^* = H_{AB}^*$. This also applies to $S_{BA} = S_{AB}^*$.

Now we turn to the diagonal elements S_{AA} and H_{AA}. Since we know from eg. [10] that the overlap between nearest neighbours is small ($s_0 = 0.129$) and the overlap decreases exponentially with distance (since the $|\pi\rangle$ orbitals have an exponential decaying dependency on distance), we are vindicated in the nearest neighbour assumption, and since the $|\pi\rangle$ orbitals are normalised, the derivation of S_{AA} becomes easy by using the fact that none of the nearest neighbour to the atoms on the A sublattice are themselves part of the A sublatice:

$$\begin{aligned} \langle \psi_{n\mathbf{k}'}|_A \mathbf{S} |\psi_{n\mathbf{k}}\rangle_A &= \frac{1}{N} \sum_{bR',\mathbf{R}} e^{i(\mathbf{R}\cdot\mathbf{k}-\mathbf{R}'\cdot\mathbf{k}')} \pi_A(\mathbf{R}) \mathbf{S} \pi_A(\mathbf{R}') \\ &= \frac{1}{N} \sum_{\mathbf{R},\mathbf{R}'} \delta_{\mathbf{R},\mathbf{R}'} e^{i\mathbf{R}\cdot(\mathbf{k}-\mathbf{k}')} = \delta_{\mathbf{k},\mathbf{k}'} \end{aligned} \tag{2.14}$$

Since this derivation only involves orbitals from the same unitcell, indeed the same atom, it is precisely the same for S_{BB}, so $S_{BB} = S_{AA}$. Furthermore, an analogous derivation gives us H_{AA} (and H_{BB}) except we need to exchange the overlap (1) with the energy of the $|\pi\rangle$ orbital, ie. $\epsilon_0 \equiv \langle\pi|\hat{H}|\pi\rangle$, thus giving $H_{BB} = H_{AA} = \delta_{\mathbf{k},\mathbf{k}'}\epsilon_0$.

Notice that all the elements have a delta Dirac function between $\mathbf{k}$ and $\mathbf{k}'$, proving that eigenfunctions at different points in the Brillouin zone does not couple to one other - this is a (standard) consequence of the assumption of an infinite sheet.

The parameters γ_0 and s_0 are usually found by formally solving the problem, and then fitting the resulting dispersion relation either to DFT calculations or to experiments. In this thesis I use

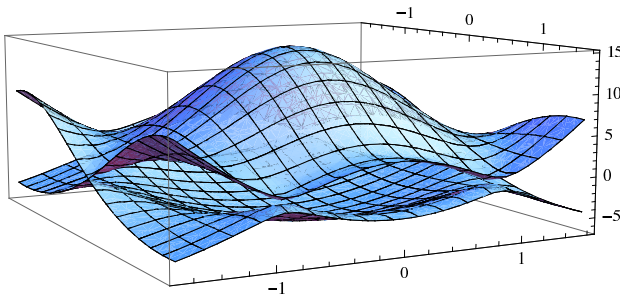

Figure 2.3: The Brillouin zone of graphene. Note the 6 points where the valence and conduction band touch - two of them are in-equivalent, and is conventionally denoted K and K'. The dispersion relation close to these points is linear in k, thus giving rise to the name "Dirac points" for these points. The units are Å^{-1} for the two horizontal axises, and eV for the vertical axis.

the numerical estimates from [10] for the parameters, since they have all the parameters for the σ orbitals as well, which I will use later in the thesis. It should be noted however, that it is not clear how and to what the fit is made since the article cites "private communication" - however, from the plots in the article, it is clear that the parameters produce the wellknown dispersion relation for graphene (compare figure 6a in [10] with eg. figure 2 in [11]).

We then have to solve the following generalized eigenvalue problem:

$$\begin{pmatrix} \epsilon_0 & \gamma_0\Gamma(\mathbf{k}) \\ \gamma_0\Gamma(\mathbf{k})^* & \epsilon_0 \end{pmatrix} \begin{pmatrix} a \\ b \end{pmatrix} = E_n \begin{pmatrix} 1 & s_0\Gamma(\mathbf{k}) \\ s_0\Gamma(\mathbf{k})^* & 1 \end{pmatrix} \begin{pmatrix} a \\ b \end{pmatrix} \tag{2.15}$$

This problem is easily solvable, by noting that $\hat{H}\Psi_n = E_n\mathbf{S}\Psi_n \implies (\hat{H} - E_n\mathbf{S})\Psi_n = 0$, and since this linear equation has nonzero solutions for Ψ_n precisely when the determinant of $\hat{H} - E_n\mathbf{S}$ is zero, we get the following expressions for the two energy bands:

$$\epsilon^+(\mathbf{k}) = \frac{\epsilon_0 - \gamma_0|\Gamma(\mathbf{k})|}{1 + s_0|\Gamma(\mathbf{k})|} \qquad \epsilon^-(\mathbf{k}) = \frac{\epsilon_0 + \gamma_0|\Gamma(\mathbf{k})|}{1 - s_0|\Gamma(\mathbf{k})|} \tag{2.16}$$

The two energy bands have been depicted in figure 2.3.

Note that since $\gamma_0 = -3.033eV$ we have that $\epsilon^+(\mathbf{k}) \geq \epsilon^-(\mathbf{k})$ for all $\mathbf{k}$. By the standard method we find that the eigenfunctions of the graphene hamiltonian may be described as $\begin{pmatrix} a \\ b \end{pmatrix}^{\pm} = \frac{1}{\sqrt{2}} \begin{pmatrix} \frac{\mp\Gamma(\mathbf{k})}{|\Gamma(\mathbf{k})|} \\ 1 \end{pmatrix}$.

We work in the socalled halffilling regime throughout the thesis, meaning simply that there is 1 π band electron pr. carbon atom (ie. the graphene sheet is electrically neutral), so since there are 2 π orbitals pr. atom (due to spin) the lower half of the states in the Brillouin zone is filled, corresponding to the states with energies described by $\epsilon^-(\mathbf{k})$. Thus we see that the points

where $\epsilon^+(\mathbf{k}) = \epsilon^-(\mathbf{k})$ are of special interest, since these are the points where the dispersion relation touches the fermisurface. From (2.16) we see that this happens exactly when $\Gamma(\mathbf{k}) = 0$ - we now also see that if we define $\epsilon_0 = 0$ we have set the Fermi energy $\epsilon_F = 0$. There are two inequivalent points in the Brillouin zone where $\Gamma(\mathbf{k}) = 0$, namely the two socalled diracpoints K and K':

$$K(') = \frac{2\pi}{a}(\frac{1}{\sqrt{3}}, \pm\frac{1}{3}) \tag{2.17}$$

where the $\pm$ distinguishes between K and K'[3]. We are mainly interested in the bandstructure near the fermisurface, since these are the states that will be of interest in a quantum dot setup. Therefore, we expand the energy in a small deviation k around the K and K' point in the Brillouin zone. We have seen that the crucial part is the $\Gamma(\mathbf{K}+\mathbf{k})$, and thus we expand this function around eg. K:

$$\begin{aligned}
&\Gamma(\mathbf{K}+\mathbf{k}) = e^{i\mathbf{l_1}\cdot\mathbf{K}}e^{i\mathbf{l_1}\cdot\mathbf{k}} + e^{i\mathbf{l_2}\cdot\mathbf{K}}e^{i\mathbf{l_2}\cdot\mathbf{k}} + e^{i\mathbf{l_3}\cdot\mathbf{K}}e^{i\mathbf{l_3}\cdot\mathbf{k}} \approx (-\frac{1}{2} - i\frac{\sqrt{3}}{2})(1 + i\mathbf{l_1}\cdot\mathbf{k}) + \\
&(-\frac{1}{2} + i\frac{\sqrt{3}}{2})(1 + i\mathbf{l_2}\cdot\mathbf{k}) + (1 + i\mathbf{l_3}\cdot\mathbf{k}) = (-\frac{1}{2} - i\frac{\sqrt{3}}{2})(1 - i\frac{a_0k_x}{\sqrt{3}}) + \\
&(-\frac{1}{2} + i\frac{\sqrt{3}}{2})(1 + i(\frac{a_0k_x}{2\sqrt{3}} + \frac{a_0k_y}{2})) + (1 + i(\frac{a_0k_x}{2\sqrt{3}} - \frac{a_0k_y}{2})) = \\
&\frac{-a_0\sqrt{3}}{4}(\sqrt{3}k_x + k_y + i(\sqrt{3}k_y - k_x)) \approx \frac{-a_0\sqrt{3}}{2}(k_C^0 + ik_T^0)
\end{aligned} \tag{2.18}$$

where we have defined a new coordinatesystem,

$$\{k_C^0, k_T^0\} = \{\frac{\sqrt{3}}{2}k_x + \frac{1}{2}k_y, -\frac{1}{2}k_x + \frac{\sqrt{3}}{2}k_y\} \tag{2.19}$$

the naming convention of which will become more meaningful in the next chapter. An equivalent calculation for the K' point gives yields $\Gamma(\mathbf{K'} + \mathbf{k}) \approx \frac{-a_0\sqrt{3}}{2}(-k_C^0 + ik_T^0)$. From this we see that the dispersion relation is linear around the K and K' point, giving rise to the term "Dirac points", since the gapless, linear dispersion is also found in relativistic quantum mechanics for massless particles. It is also of worth to note that this leads to the concept of an "effective hamiltonian", ie. a hamiltonian that gives the physics of the interesting states near the Fermi surfaces, which is obtained by inserting the approximated expression of $\Gamma(\mathbf{k})$ from (2.18) into the hamiltonian part (or indeed into $\hat{H} - E_k\mathbf{S}$) from (2.15) to obtain

$$\begin{pmatrix} \epsilon_0 - E_n & (\gamma_0 - E_n s_0)\frac{-a\sqrt{3}}{2}(\tau k_C^0 + ik_T^0) \\ (\gamma_0 - E_n s_0)\frac{-a\sqrt{3}}{2}(\tau k_C^0 - ik_T^0) & \epsilon_0 - E_n \end{pmatrix} \begin{pmatrix} a \\ b \end{pmatrix} = \begin{pmatrix} 0 \\ 0 \end{pmatrix} \tag{2.20}$$

where τ is 1(-1) for K(K').

This concludes the introduction to the physics of graphene.

[3]note, that we can only choose ϵ_0 to 0 as long as we only wish to study states close to these Dirac points. If the size of $\Gamma(\mathbf{k})$ becomes appreciable, we see from (2.16) that it is no longer just an energy shift, and we will have to choose our energy scale to set ϵ_F to 0 explicitly, if we wish to do so

Chapter 3

Folding up the nanotube

We now turn to the task of "rolling up the graphene sheet" into a cylinder called a carbon nanotube or CNT. This gives rise to two effects, namely the imposition of cyclic boundary conditions and the breaking of the graphene plane mirror symmetry, most importantly leading to mixing of the π and σ bands, which were separate in graphene. We shall treat these two effects in turn, but first we need to make some basic definitions, especially concerning the crucial concept of chirality.

3.1 Chirality and unitcell of the CNT

In folding up the CNT we have a choice of how exactly to do so - Essentially we may specify everything about the folding of the nanotube by specifying two equivalent atoms in the graphene lattice that will be folded onto one another - this is done by specifying the chiral vector, $\mathbf{C}$ going from these two sites, and thus going around the circumference, and is illustrated in figure 3.1. We shall use two equivalent methods for specifying the chiral vector:

- by specifying the two numbers n and m, so that $\mathbf{C} = n\mathbf{a_1} + m\mathbf{a_2}$. Because of the sixfold rotational symmetry and the mirror symmetry around a line parallel with a given nearest neighbour bond (see figure 3.1), we see that we may impose the condition $n \geq m \geq 0$. It is customary to denote a CNT by its chiral vector as (n, m) eg. a $(4, 3)$ CNT, and also to denote $(n, 0)$ CNTs as "zigzag" nanotubes, and (n, n) as armchair nanotubes. All other CNTs are denoted "chiral" nanotubes.

- by specifying the radius r of the nanotube (giving the length of $\mathbf{C}$, since obviously $|\mathbf{C}| = 2\pi r$) and the *chiral angle*, θ, which we define as the angle between $\mathbf{C}$ and $\mathbf{a_1}$. From the above restriction on n and m, it is clear that $0 \leq \theta \leq \frac{\pi}{6}$. We see that zigzag nanotubes have $\theta = 0$ and armchair nanotubes have $\theta = \frac{\pi}{6}$. Note that this implies that θ becomes *larger* if we turn $\mathbf{C}$ in a clockwise direction.

We also need to consider the possible unitcells of the CNT. First, we shall prove that we may still use the diatomic unitcell from graphene (although of cause curved) following the derivations of [12], and then we shall consider the larger socalled translational unitcell,which is easier to handle numerically than the primitive unitcell.

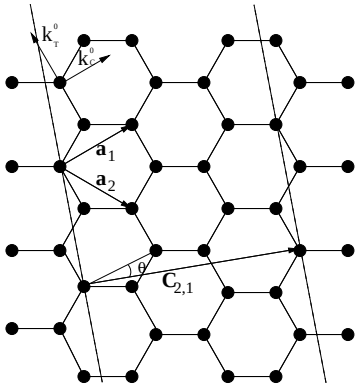

Figure 3.1: The (2,1) chiral vector in a graphene sheet. The two broken lines (perpendicular to $\mathbf{C}$) are folded onto one another, so the chiral vector goes around the circumference. The coordinatesystem $\{\mathbf{k^0_C}, \mathbf{k^0_T}\}$ is also shown.

3.1.1 The helical unitcell

Following [12], we first observe, that the two atoms that make up a unitcell of graphene may be mapped onto the CNT surface by arbitrarily placing the first atom onto the surface, and then, since the vector between two atoms in the same unitcell is $\mathbf{d} = \frac{\mathbf{a_1}+\mathbf{a_2}}{3}$, and since, as we noted above, $\mathbf{C}$ is mapped onto the circumference of the CNT. We may therefore divide $\mathbf{d}$ into an rotation around the tube axis by $\frac{2\pi \mathbf{d}\cdot\mathbf{C}}{|\mathbf{C}|}$ radians, and a translation along the tube axis direction, which is simply $|\mathbf{d}\times\mathbf{C}|$, since Usually (for all but the armchair case) the direction of the $\mathbf{d}$ vector will not coincide with the direction of the $\mathbf{C}$ vector.

Thus the unitcell may be uniquely mapped onto the surface of the nanotube - we now turn to the task of proving that this mapped unitcell is indeed a unitcell of the CNT: First observe, that there may be unitcells at the same coordinate along the tubule axis as the first unitcell placed, but at different angles around the circumference: This happens, if $\mathbf{C}$ can be expressed as a shorter chiral vector, $\tilde{\mathbf{C}} = \tilde{m}\mathbf{a_1} + \tilde{n}\mathbf{a_2}$, times some factor M, since this means that we may reach another unitcell from the first one, by translating $\tilde{\mathbf{C}}$ in the graphene plane, or correspondingly rotating $\frac{|\tilde{\mathbf{C}}|2\pi}{|\mathbf{C}|}$ radians around the tubule axis. Since $\tilde{m}$ and $\tilde{n}$ must both be integers, we see that the shortest $\tilde{\mathbf{C}}$ possible in the direction of $\mathbf{C}$, corresponding to the largest M possible, is the $\tilde{\mathbf{C}}$ for which M is the greatest common divisor of n and m, ie. $M = gcd(n, m)$. This leads us to the first of our lattice vectors for the CNT primitive cell, namely the vector $\mathbf{C}/M$ corresponding to a rotation of $\frac{2\pi}{M}$ around the tubule axis. With this lattice vector alone we can place M unitcells in a helical motif around the circumference of the CNT.

We now desire a second operation, $S(h, \alpha)$ that, when applied successively to this motif, generates the nanotube, ie. we desire a unique pair of integers k and l, such that, given an origo on the CNT, the lattice point of any unitcell may be found by applying the rotational operation, ie. rotating $\frac{2\pi}{M}$ radians around the tube axis, k times, and then applying the helical operation $S(h, \alpha)$ l

times. First we notice that we may couple the $S(h,\alpha)$ operation to a corresponding lattice vector[1] in the graphene plane

$$\mathbf{H} = p\mathbf{a_1} + q\mathbf{a_2} \tag{3.1}$$

by noting that $h = \frac{|\mathbf{H}\times\mathbf{C}|}{|\mathbf{C}|}$ and $\alpha = \frac{\mathbf{C}\cdot\mathbf{H}2\pi}{|\mathbf{C}|^2}$. We may insure that $\mathbf{H}$ and $\frac{\mathbf{C}}{M}$ are indeed lattice vectors, by demanding that $h = \frac{|\mathbf{H}\times\mathbf{C}|}{|\mathbf{C}|}$ be as small as possible: since per definition all unitcells in graphene are alike, all unitcells with the distance $r*h$ perpendicular to $\mathbf{C}$ from a given origo unitcell, can be found by adding $r\mathbf{H}$ (corresponding to r applications of $S(h,\alpha)$ on the CNT) to a unique number of $\tilde{\mathbf{C}}$ (corresponding to a given number of $\frac{|\mathbf{C}|2\pi}{M}$ rotations around the CNT axis) - here r must be an integer, since, if the number h is the minimal distance perpendicular to $\mathbf{C}$ from one unitcell to some other, it is the minimal distance perpendicular to $\mathbf{C}$ from *any* unitcell to some other. Conversely only one linear combination of $\mathbf{H}$ and $\tilde{\mathbf{C}}$ will yield the vector R connecting two given unitcells, since they clearly span the graphene plane.

Thus, all we now need to do is to find the numbers h and α, or equivalently p and q. One way to do this, is to note (as in [12]) that the area covered by the helical motif is

$$A_{motif} = M|\mathbf{a_1}\times\mathbf{a_2}| \tag{3.2}$$

since the area of a unitcell is $|\mathbf{a_1}\times\mathbf{a_2}|$, but at the same time the nanotube can be thought of as a repetition of the helical motif, rotated by α and stacked at distance h along the tubule axis, so there is a new motif for each "step" of distance h along the axis, and thus, the area covered by one motif must be the area of a cylinder of height h and circumference $|\mathbf{C}|$ or, in terms of $\mathbf{H}$,

$$A_{motif} = |\mathbf{H}\times\mathbf{C}| = |(p\mathbf{a_1} + q\mathbf{a_2})\times(n\mathbf{a_1} + m\mathbf{a_2})| = |(pm - qn)||\mathbf{a_1}\times\mathbf{a_2}| \tag{3.3}$$

so that, by comparing the two expressions for the area covered by a helical motif, we have the identity

$$pm - qn = \pm M \tag{3.4}$$

Clearly there are some ambiguities here, owing to the fact that $S(h,\alpha) = S(h,\alpha + j2\pi)$ for any integer j, which leads to $\mathbf{H}$ being indistinguishable from $\mathbf{H} + j\mathbf{C}$, and thus to the pair (p,q) being indistinguishable from $(p+jn, q+jm)$. Also, since the inverse operation of $S(h,\alpha)$, namely $S(-h,-\alpha)$ would work just as well, corresponding to $-\mathbf{H}$ being as good as $\mathbf{H}$, we also have that (p,q) is indistinguishable from $(-p,-q)$ as seen from the $\pm$ in (3.4). Clearly we can reach unambiguity by selecting $n > p \geq 0$, and thus, we may find p and q, and thus α and h from n and m, using (3.4) together with the standard identity

$$|\mathbf{H}|^2 = (\frac{|\mathbf{C}\cdot\mathbf{H}|}{|\mathbf{C}|})^2 + (\frac{|\mathbf{C}\times\mathbf{H}|}{|\mathbf{C}|})^2 \tag{3.5}$$

Since the main purpose of this section is to prove the existence of the diatomic unitcell, we choose not to carry out this calculation: It is sufficient for our purposes to prove its existence.

[1] ie. the vector connecting the two unitcells in graphene which, when mapped onto the CNT surface, will be separated by the length h along the axis, and a rotation of α radians around the axis, so that $S(h,\alpha)$ will translate one onto the other.

3.1.2 The translational unitcell

We now turn to the other possible unitcell, namely the socalled translational unitcell, consisting of a cylinder segment of height $|\mathbf{T}|$ and circumference $|\mathbf{C}|$ which may be repeated along the tube axis to generate the CNT, where $\mathbf{T}$ is to be found in order to prove the existence of this unitcell. In order to show that such a unitcell exists, we only need to prove the existence of a lattice vector $\mathbf{T}$ which is perpendicular to $\mathbf{C}$ - this vector will be mapped onto the CNT along the tube axis, and will thus satisfy the condition of connecting two cylinder segments. However the proof of the existence of this vector is rather trivial, since if we define t_1 and t_2 so that $\mathbf{T} = t_1\mathbf{a_1} + t_2\mathbf{a_2}$ we have, using $a_i \cdot a_j = \begin{cases} 1 & \text{for } i = j \\ \frac{1}{2} & \text{for } i \neq j \end{cases}$, that for $\mathbf{C}$ and $\mathbf{T}$ to be perpendicular,

$$0 = 2\mathbf{T} \cdot \mathbf{C} = 2t_1 m + 2t_2 n + t_1 m + t_2 n \implies t_1(2m+n) = -t_2(2n+m) \tag{3.6}$$

In order for $\mathbf{T}$ to be a lattice vector, t_1 and t_2 must be integers, and we see, that such integers exists, and we may also find smallest possible translatory unitcell by setting

$$t_1 = -\frac{2m+n}{\gcd(2m+n, 2n+m)} \qquad t_2 = \frac{2n+m}{\gcd(2m+n, 2n+m)} \tag{3.7}$$

It is of interest to note that the area of the translatoric compared to the primitive unitcell is

$$N = \frac{|\mathbf{C} \times \mathbf{T}|}{|\mathbf{a_1} \times \mathbf{a_2}|} = \frac{|nt_2 - mt_1||\mathbf{a_1} \times \mathbf{a_2}|}{|\mathbf{a_1} \times \mathbf{a_2}|} = \frac{2(n^2 + m^2 + nm)}{\gcd(2n+m, 2m+n)} \tag{3.8}$$

For example the translatoric unitcell of a (10,9) CNT is 542 times larger than the primitive unitcell!

We may now divide the $\mathbf{k}$ vector of the blochwave into a part along reciprocal basis vector $\mathbf{b_T}$ of $\mathbf{T}$, and a part along the reciprocal basis vector $\mathbf{b_C}$ of $\mathbf{C}$, ie.

$$\mathbf{k} \equiv k_t \frac{\mathbf{b_T}}{|\mathbf{b_T}|} + k_c \frac{\mathbf{b_C}}{|\mathbf{b_C}|} = k_t \hat{\mathbf{b}_T} + k_C \hat{\mathbf{b}_C} \tag{3.9}$$

Given the definition of the reciprocal basis vector, ie. $\mathbf{A} \cdot \mathbf{b_B} = 2\pi\delta_{\mathbf{A},\mathbf{B}}$, we find that

$$\mathbf{b_C} = \frac{-t_2\mathbf{b_1} + t_1\mathbf{b_2}}{N} \qquad \mathbf{b_T} = \frac{m\mathbf{b_1} - n\mathbf{b_2}}{N} \tag{3.10}$$

3.1.3 Comparing the unitcells

The two unitcells are of cause in principle equivalent, but whereas the translatory unitcell is well suited for the numerical experiments, and, as we shall see in the following section, to describe the effect of cyclic boundary conditions (since only k_C will be effected), the larger size of the unitcell is an insurmountable drawback when doing analytical calculations, since the amount of basis functions in eg. a tight-binding model is of cause proportional to the number of atoms considered, and thus to the size of the unitcell. Therefore we shall use either unitcell when convenient throughout this thesis.

3.2 Cyclic boundary conditions. Metallic and semiconducting nanotubes

Having established the basic structure of the CNT, we now turn to the first of the two effects of curling up the nanotube, namely the simple fact that the phase of the wavefunctions available to the electrons must be single valued, and so the phase change when $\mathbf{r}$ is changed by one circumference ($|\mathbf{C}|$) must be an integer multiplum of 2π, or, if we choose to work with the translational unitcell from section 3.1, we have the constraint that, since the blochcondition (2.6) for $\mathbf{r} = \mathbf{C}$ now states $\Psi_{n\mathbf{k}}(\mathbf{r} + \mathbf{C}) = e^{i\mathbf{k}\cdot\mathbf{C}}\Psi_{n\mathbf{k}}(\mathbf{r}) = \Psi_{n\mathbf{k}}(\mathbf{r})$, we must have that, if we recall (3.9)

$$l_C 2\pi = \mathbf{k}\cdot\mathbf{C} = k_C \frac{\mathbf{C}\cdot\mathbf{b_C}}{|\mathbf{b_C}|} = k_C|\mathbf{C}| \implies k_C = \frac{l_C 2\pi}{|\mathbf{C}|} \tag{3.11}$$

where the third equality follows from the fact that $\mathbf{b_C}$ is parallel to $\mathbf{C}$ which in turn follows from the fact that $\mathbf{T}$ and $\mathbf{C}$ are perpendicular, and where we have defined the integer l_C, which must be restricted in order to insure that $\mathbf{k}$ cannot be written as some shorter vector plus a reciprocal lattice vector. Using (3.9) and (3.10) and the above definition of l_C, we find

$$\mathbf{k} = k_t\hat{\mathbf{b}}_\mathbf{T} + k_C\hat{\mathbf{b}}_\mathbf{C} = k_t\hat{\mathbf{b}}_\mathbf{T} + \frac{l_C 2\pi \mathbf{b_C}}{|\mathbf{C}||\mathbf{b_C}|} = k_t\hat{\mathbf{b}}_\mathbf{T} + \frac{l_C}{N}(-t_2\mathbf{b_1} + t_1\mathbf{b_2}) \tag{3.12}$$

Now, using that pr. construction of t_1 and t_2, $\gcd(t_1, t_2) = 1$, we see that if $l_C < N$, $\frac{-t_2 l_C}{N}$ and $\frac{t_1 l_c}{N}$ cannot both be integers so $l_C(-t_2\mathbf{b_1} + t_1\mathbf{b_2})$ is not a reciprocal lattice vector, and thus we have our constraint:

$$0 \leq l_C \leq N - 1 \tag{3.13}$$

Turning now to the effects of this constraint on the bandstructure, we see that this is the (main) reason why some CNTs are semiconducting and others are metallic: If the condition excludes the K and K' points, there are no allowed k-values for which the bands touch the fermisurface, and thus the CNT will be semiconducting, and conversely, if the K and K' points are allowed values of k_C, the CNT will be metallic - in figure 3.2 this is illustrated for an example of either group.

In order to understand the results from the Hückel code shown later in the thesis, it is important to note that we can now see the dispersion relation as being one dimensional (ie. along the k_T direction) and then using a zone folding scheme to include all the N possible values of k_C as different bands - this is of cause the "natural" Brillouin zone to use when we start out with the translational unitcell, rather than the (constrained) 2D unitcell from figure 3.2 which, as is readily seen from its size, corresponds to the diatomic, helical unitcell. In figure 3.2 we see the 1 dimensional bands corresponding to the two chiralities, one metallic, the other semiconducting.

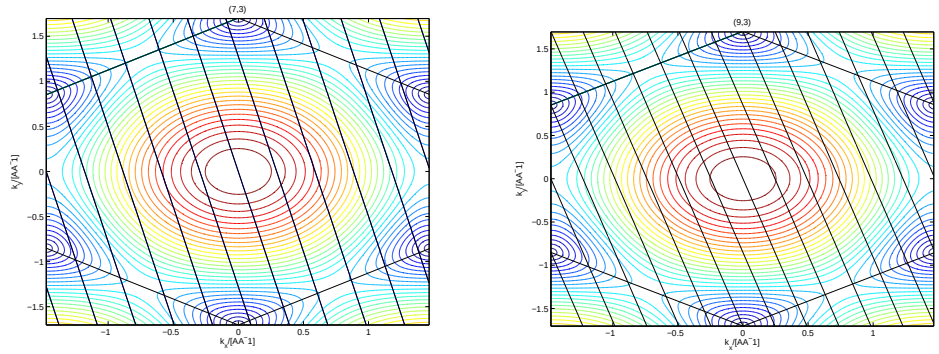

Figure 3.2: The allowed k values are shown as black lines for a semiconducting (7,3) CNT (left) and a metallic (9,3) CNT (right), where we can see explicitly that the lines in the (9,3) CNT touch the diracpoints, while they do not in the (7,3) CNT - the hexagon denotes the first Brillouin zone of graphene.

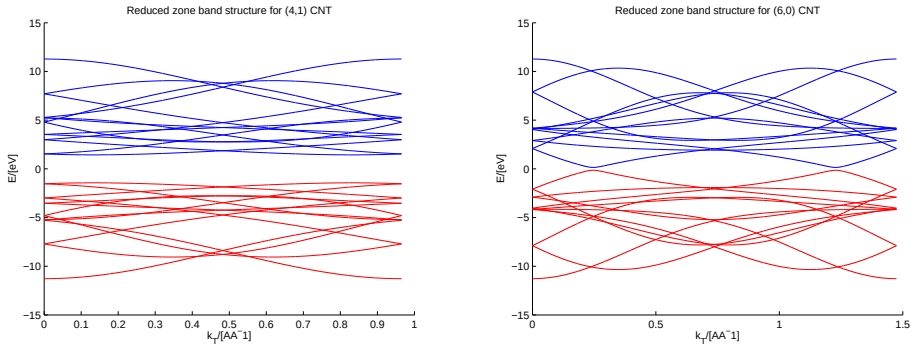

Figure 3.3: Reduced zone bandstructures for two different chiralities: left is the semiconducting (4,1) CNT, and right is the metallic (6,0) CNT. Occupied bands are shown in red, unoccupied are shown in blue. Note that the small gap in the (6,0) spectrum is due to imprecision in the numerical code, and not curvature effects.

For completeness, we shall now derive the condition for metallic vs. semiconducting nanotubes from the numbers (n, m) specifying the chirality (see 3.1). Since $\mathbf{K}(') = \frac{2\pi}{a}(\frac{1}{\sqrt{3}}, \frac{\tau}{3})$, where $\tau = \pm 1$ distinguishes K from K', we find that

$$2\pi l_C = \mathbf{K}(') \cdot \mathbf{C} = \pi(n + m + \tau\frac{n-m}{3}) \implies \begin{cases} \text{for } \tau = 1 : l_C = \frac{2n+m}{3} \\ \text{for } \tau = -1 : l_C = \frac{2m+n}{3} \end{cases} \tag{3.14}$$

Observing that, since $\frac{3m}{3}$ is always an integer, $\frac{2m+n}{3} \in \mathbb{Z} \Leftrightarrow \frac{n-m}{3} \in \mathbb{Z}$, and from that we know that $\frac{2m+n}{3} + \frac{n-m}{3} = \frac{2n+m}{3} \in \mathbb{Z}$, so if K_C is an "allowed" value, then so is K'_C, and thus we have

A CNT is metallic if and only if $\frac{2n+m}{3}$ is an integer.

It is also instructive to derive the effective hamiltonian, and thus the energies close the the K(') point, which is easily done by building on the effective hamiltonian description from last section (2.20), and for simplicity ignore overlap (ie. $s_0 = 0$) and furthermore set the fermilevel so that $\epsilon_0 = 0$. First of all, we now see the logic behind the naming convention in (2.19): For the zigzag case, ie. $\theta = 0$, we have precisely that $k_C = k_C^0$ and $k_T = k_T^0$. From studying figure 3.1 we see that, in general, $k_C^0 = \cos\theta k_C + \sin\theta k_T$ and $k_T^0 = -\sin\theta k_C + \cos\theta k_T$, leading to

$$\tau k_C^0 + i k_T^0 = \tau\cos\theta k_C + \tau\sin\theta k_T - i\sin\theta k_C + i\cos\theta k_T = e^{-i\tau\theta}(\tau k_C + i k_T) \tag{3.15}$$

where we use that $\tau^2 = 1$. This can then be inserted into (2.20), following the spirit of [13], [18], and others but I have used a slightly non-standard coordinatesystem and definition of the chiral angle, so care should be taken when comparing the results. We find

$$\begin{pmatrix} -E_n & \gamma_0\frac{-a_0\sqrt{3}}{2}(\tau k_C^0 + i k_T^0) \\ \gamma_0\frac{-a_0\sqrt{3}}{2}(\tau k_C^0 - i k_T^0) & -E_n \end{pmatrix}\begin{pmatrix} a \\ b \end{pmatrix} = \\ \begin{pmatrix} -E_n & \gamma_0\frac{-a_0\sqrt{3}}{2}(\tau k_C + i k_T)e^{-i\tau\theta} \\ \gamma_0\frac{-a_0\sqrt{3}}{2}(\tau k_C - i k_T)e^{i\tau\theta} & -E_n \end{pmatrix}\begin{pmatrix} a \\ b \end{pmatrix} = \begin{pmatrix} 0 \\ 0 \end{pmatrix} \tag{3.16}$$

Now we must take the constraint of k_C into account. Here we need to remember that it is of cause the *total* vector that has to fulfill the constrain, ie. $(\mathbf{k} + \mathbf{K}(')) \cdot \mathbf{C} = 2\pi l_c$. Therefore, using (3.14) and the fact that $|\mathbf{C}| = 2R\pi$ where R is the radius of the CNT, we have

$$\begin{aligned} 2\pi l_C = (\mathbf{k} + \mathbf{K}(')) \cdot \mathbf{C} &= k_C 2R\pi + \pi(n + m + \tau\frac{n-m}{3}) \\ \implies k_C &= \frac{l_c}{R} - \frac{n + m + \tau\frac{n-m}{3}}{2R} \end{aligned} \tag{3.17}$$

From this, we find the energy to be (recalling (2.20))

$$E^{\pm} = \mp\frac{\gamma_0 a_0\sqrt{3}}{2}\sqrt{|\tau k_C + i k_T|^2} = \mp\gamma_0\frac{a_0\sqrt{3}}{2R}\sqrt{(Rk_T)^2 + (l_c + \frac{\tau(3m-3n) + n - m}{6})^2} \tag{3.18}$$

It is of cause important to remember, that this is the result of an expansion, so the formula is only accurate for the l_C values closest to the Dirac-points, ie.

$$l_c + \frac{\tau(3m-3n)+n-m}{6} = \begin{cases} 0 \text{ for metallic tubes} \\ \pm\frac{1}{3} \text{ for semiconducting tubes} \end{cases} \tag{3.19}$$

Since we can choose k_T freely (due to the infinitely long tube), it is now clear that the energy gap between the HOMO and the LUMO band in semiconducting CNTs should be inversely proportional to the radius, irrespective of the details of the chirality.

When we alter (2.20) with our restriction on $\mathbf{k}$ we end up with the effective hamiltonian

$$\begin{pmatrix} -E_n & \gamma_0\frac{-a_0\sqrt{3}}{2R}(\frac{\nu}{3}+iRk_T))e^{-i\tau\theta} \\ \gamma_0\frac{-a_0\sqrt{3}}{2R}(\frac{\nu}{3}-iRk_T)e^{i\tau\theta} & -E_n \end{pmatrix}\begin{pmatrix} a \\ b \end{pmatrix} = \begin{pmatrix} 0 \\ 0 \end{pmatrix} \tag{3.20}$$

where ν is the "family number" of the CNT chirality, which is 0 for metallic tubes, or ± 1 for semiconducting tubes, depending on whether the smallest numeric value of k_C is + or $-\frac{1}{3}$ in (3.19) off, compared to the Dirac points - later we shall see that ν plays an important role for the understanding of spin-orbit coupling. One final manipulation of this hamiltonian is to realize that we may rotate it to get rid of the phases in the off-diagonal elements, by evaluating $\hat{H}^{eff}_{CNT} = \mathbf{U}\hat{\tilde{H}}^{eff}_{CNT}\mathbf{U}^{-1}$ with $\mathbf{U} = \begin{pmatrix} e^{i\tau\theta} & 0 \\ 0 & 1 \end{pmatrix}$, so we finally have

$$\hat{H}^{eff}_{CNT} = \begin{pmatrix} -E_n & \gamma_0\frac{-a_0\sqrt{3}}{2R}(\frac{\nu}{3}+iRk_T)) \\ \gamma_0\frac{-a_0\sqrt{3}}{2R}(\frac{\nu}{3}-iRk_T) & -E_n \end{pmatrix}\begin{pmatrix} a \\ b \end{pmatrix} = \begin{pmatrix} 0 \\ 0 \end{pmatrix} \tag{3.21}$$

This hamiltonian finally yields the following expressions for the eigenenergies near the K(') point:

$$E_n^{\pm} = \mp\frac{\gamma_0 a_0\sqrt{3}}{2R}\sqrt{(\frac{\nu}{3})^2 + R^2k_T^2} \tag{3.22}$$

3.3 σ/π band mixing

We now turn to the other major effect of curling up the nanotube, namely the breaking of the mirror symmetry that allowed us to ignore the σ bands in the case of graphene. The first important observation is now that the π bands on neighbouring sites now tilt towards one another - secondly we shall find that the matrix elements between the σ orbitals and the π orbitals are no longer zero. In order to parametrize these effects, we shall first study the geometry of the coupling between the $n = 2$ shells on two neighbouring atoms, and due to symmetry reasons we shall find that in principle only 4 different parameters are necessary, when we make the assumption that the hamiltonian matrix element is zero if the orbital overlap is zero.

In table 3.1 we see the fundamentally different pairs of orbitals around two neighbouring carbon atoms (denoted A and B) separated by a_{cc} along the x axis (notice, that the matrix elements we seek are of cause the same if we exchange the A and B orbital, except for a complex conjugation,

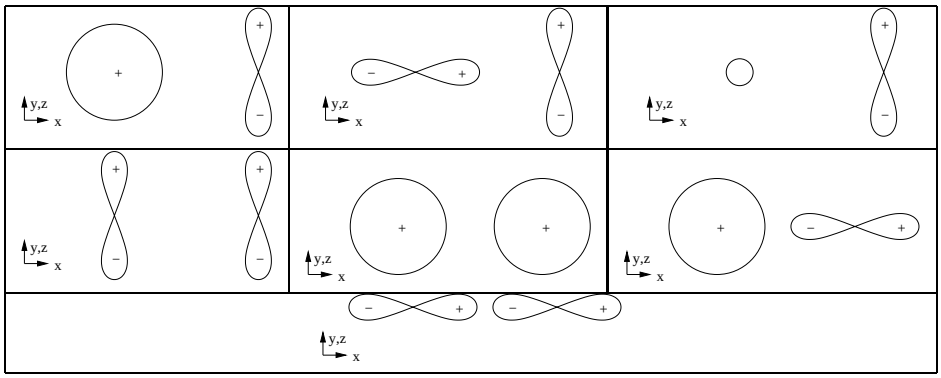

Table 3.1: The seven inequivalent orbit pairs at two neighbouring carbon atoms. The upper row is shown in the text to have no overlap, and then by assumption no hamiltonian, matrix elements. In 3.23 the overlap and hamiltonian elements for the remaining combinations is denoted, for the second row, left to right, $V^{\pi}_{pp}/s^{\pi}_{pp}$,$V^{\sigma}_{ss}/s^{\sigma}_{ss}$,$V^{\sigma}_{sp}/s^{\sigma}_{sp}$, and the coupling shown in the third row is denoted $V^{\sigma}_{pp}/s^{\sigma}_{pp}$.

stemming from the hermiticity of the hamiltonian). From these figures, and from the wellknown property of the real p-orbitals that p_i is an odd function along the i axis, and even along the two other axises, plus the fact that s-orbitals are even along all Cartesian coordinates, it is easy to see that overlap between the $p_{x,A}$ and $p_{(y,z),B}$ (the y and z axises are indistinguishable in this case) is 0, since the integrant $p^*_{x,A}p_{(y,z),B}$ is odd along either the y or z axis respectively. Likewise, the overlap between $p_{y,A}$ and $p_{z,B}$ is zero (since the integrant is then odd along both the y and z axis), and finally the overlap between S_A and $p_{(y,z),B}$ is zero, since again the integrant is odd along either the y or the z direction - as mentioned, we then assume that the hamiltonian matrix elements between these orbitals are also 0.

This leaves four pairs of orbitals have non-zero overlap/hamiltonian matrix elements, and, using the numerical values from [10], we have

$$\begin{aligned}
\int d\mathbf{r} p^*_{(y,z),A}\hat{H}p_{(y,z),B} = V^{\pi}_{pp} = -3.033eV, \int d\mathbf{r} p^*_{(y,z),A}p_{(y,z),B} = s^{\pi}_{pp} = 0.129 \\
\int d\mathbf{r} p^*_{x,A}\hat{H}p_{x,B} = V^{\sigma}_{pp} = -5.037eV, \int d\mathbf{r} p^*_{x,A}p_{x,B} = s^{\sigma}_{pp} = 0.146 \\
\int d\mathbf{r} S^*_{A}\hat{H}p_{x,B} = V^{\sigma}_{sp} = -5.580eV, \int d\mathbf{r} S^*_{A}p_{x,B} = s^{\sigma}_{pp} = 0.102 \\
\int d\mathbf{r} S^*_{A}\hat{H}S_{B} = V^{\sigma}_{ss} = -6.769eV, \int d\mathbf{r} S^*_{A}S_{B} = s^{\sigma}_{ss} = 0.212
\end{aligned} \tag{3.23}$$

We need one final parameter to describe the entire $n = 2$ shell: In the previous sections, we have only dealt with one "self-energy", ϵ_0, being the diagonal element of the hamiltonian of a 2p orbital. We now have to include an energy corresponding to the 2S orbital, $\epsilon_S = -8.868eV$. We choose, following [14] to define the π orbitals on the CNT as the ones perpendicular to the cylinder surface and we also "choose" to call the other three $n = 2$ orbitals, formed in the "three-clover"

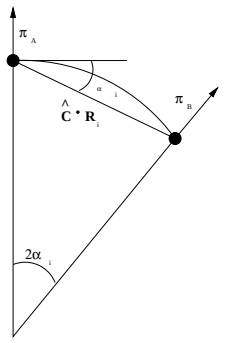

Figure 3.4: The geometry of two neighbouring atoms, projected onto the endface of the cylinder, ie. $\mathbf{T}$ is perpendicular to the paper. Shown is the definition of α_i and the directions of the π orbitals at the two atom positions, A and B, $\mathbf{R_i}$ vector projected onto the plane of the paper, perpendicular to the tube axis.

form as in graphene, and perpendicular to the radial, "π" direction, "σ" orbitals, although of cause the symmetry that lead us to employ the sp^2 is now broken.

Now we make some observations and definitions concerning the geometrical effects of curvature. In figure 3.4 we define the angle α to parametrise the curvature effect between two neighbouring atoms. We wish to couple this angle to the chirality of a CNT, and to this end, we know the radius as seen in section 3.1, either as one of the parameters that define the chirality, or as $\frac{|\mathbf{C}|}{2\pi}$, and thus for a given pair of carbon atoms, we need the length of the vector between them ("R_i", where the i subscript denotes the bond) projected onto the face perpendicular to the tube axis (which is of cause not just a_{cc}, since the bond between neighbours will usually be partly along the tube axis direction as well) - ie. we need the length $\mathbf{R_i} \cdot \hat{\mathbf{C}}$. However, if one studies the honeycomb lattice, it is clear that only three *different* $\mathbf{R_i}$'s exists, as we still restrict ourselves to nearest neighbour interaction and only the *direction* of the bonds (compared to $\mathbf{C}$) plays any role in the calculation of α. Rigorously, if we define the angle between $\mathbf{R_i}$ and $\mathbf{C}$ as β_i, we find that

$$\beta_i = cos^{-1}(\frac{\mathbf{R_i} \cdot \hat{\mathbf{C}}}{a_{cc}}) \implies sin(\alpha_i) = \frac{\mathbf{R_i} \cdot \hat{\mathbf{C}}}{2R} = \frac{cos(\beta_i)a_{cc}}{2R} \equiv \eta cos(\beta_i) \tag{3.24}$$

We should note here, that there is actually an assumption hidden in this calculation, since it is not clear whether $\mathbf{R_i} \cdot \hat{\mathbf{C}}$ (which is well defined in flat graphene) is, after rolling up the CNT, the length along the straight line in figure 3.4 - we could also have chosen it to be the length along the curved line, ie. the surface of the cylinder. There are a few things to say about this

- The difference between the two is minute for anything but the smallest CNTs (of the order of femtometers).
- The bondlength (a_{cc}) should be the length of the vector connecting the two atoms, regardless of the cylindrical form we imagine for the tube.

The procedure for including the σ orbitals into the hamiltonian can be divided it three steps: First, we shall derive the angle dependent hamiltonian between the π orbitals on neighbouring

sites, then the hamiltonian connecting π orbitals to σ orbitals, and finally the coupling between σ orbitals on neighbouring sites.

3.3.1 $\pi - \pi$ orbital coupling

It turns out to be convenient to use the coordinate system $\{\hat{\mathbf{C}}, \hat{\mathbf{T}}, \hat{\mathbf{z}}\}$, where $\hat{\mathbf{C}}$ and $\hat{\mathbf{z}}$ is defined as the circumferential and radial direction *at the A atoms position*, respectively. Now, following [14], we can see the coupling between two neighbouring π orbitals as being composed of a coupling of the V_{pp}^{σ} type along the R_{ij} vector plus a coupling of the V_{pp}^{π} type perpendicular to the R_{ij} vector - this can be done since a p-type orbital in an arbitrary direction, can be expressed as a weighted sum of any three linearly independent p orbitals, as they comprise a complete set for the $n = 2, l = 1$ orbitals around a given atom. Furthermore from studying the real p orbitals, it is easy to see that they transform as simple vectors under rotation, ie. with the usual definition of θ and ϕ in a spherical coordinate system, a p orbital pointing in the (θ, ϕ) direction can be written as

$$p_{\theta,\phi} = sin(\theta)cos(\phi)p_x + sin(\theta)sin(\phi)p_y + cos(\theta)p_z \tag{3.25}$$

This implies that we can write the hamiltonian integrals for the $\pi - \pi$ coupling as[14]

$$\begin{aligned}\langle \pi_A | \hat{H} | \pi_B \rangle &= ((\pi_{\mathbf{A}} \cdot \hat{\mathbf{R}}_{\mathbf{i}})\hat{\mathbf{R}}_{\mathbf{i}} \cdot (\pi_{\mathbf{B}} \cdot \hat{\mathbf{R}}_{\mathbf{i}})\hat{\mathbf{R}}_{\mathbf{i}})V_{pp}^{\sigma} + (\pi_{\mathbf{A}} - (\pi_{\mathbf{A}} \cdot \hat{\mathbf{R}}_{\mathbf{i}})\hat{\mathbf{R}}_{\mathbf{i}}) \cdot (\pi_{\mathbf{B}} - (\pi_{\mathbf{B}}\hat{\mathbf{R}}_{\mathbf{i}})\hat{\mathbf{R}}_{\mathbf{i}})V_{pp}^{\pi} \cdot \\ &= (\pi_{\mathbf{A}} \cdot \hat{\mathbf{R}}_{\mathbf{i}})(\pi_{\mathbf{B}} \cdot \hat{\mathbf{R}}_{\mathbf{i}})V_{pp}^{\sigma} + (\pi_{\mathbf{A}} \cdot \pi_{\mathbf{B}} - 2(\pi_{\mathbf{A}} \cdot \hat{\mathbf{R}}_{\mathbf{i}})(\pi_{\mathbf{B}} \cdot \hat{\mathbf{R}}_{\mathbf{i}}) + (\pi_{\mathbf{A}} \cdot \hat{\mathbf{R}}_{\mathbf{i}})(\pi_{\mathbf{B}} \cdot \hat{\mathbf{R}}_{\mathbf{i}}))V_{pp}^{\pi} \\ &= (\pi_{\mathbf{A}} \cdot \hat{\mathbf{R}}_{\mathbf{i}})(\pi_{\mathbf{B}} \cdot \hat{\mathbf{R}}_{\mathbf{i}})(V_{pp}^{\sigma} - V_{pp}^{\pi}) + (\pi_{\mathbf{A}} \cdot \pi_{\mathbf{B}})V_{pp}^{\pi}\end{aligned} \tag{3.26}$$

where $\pi_{\mathbf{A}}$ and $\pi_{\mathbf{B}}$ are unitvectors in the direction of the π orbitals at the origo site (A) and the neighbouring site we are considering (B). All that remains then, is to describe the vectors $\pi_{\mathbf{A}}$,$\pi_{\mathbf{B}}$ and $\hat{\mathbf{R}}_{\mathbf{i}}$ in terms of the chirality, or equivalently (as we have seen) in terms of the angles β_i and α_i. However, remembering the definition of our $\{\hat{\mathbf{C}}, \hat{\mathbf{T}}, \hat{\mathbf{z}}\}$ coordinate system, we clearly have $\pi_{\mathbf{A}} = (0, 0, 1)$ and from figure 3.4, and from the fact that no π orbital has any component along the tube axis, we see that $\pi_{\mathbf{B}} = (sin(2\alpha_i), 0, cos(2\alpha_i))$. The remaining vector in (3.26), $\hat{\mathbf{R}}_{\mathbf{i}}$, is determined by noting that before we curve the graphene sheet, the vector is given by the definition of the β_i angles as $(cos(\beta_i), sin(\beta_i), 0)$, and from figure 3.4 we see that, since only the $\mathbf{C}$ and $\mathbf{z}$ directions are involved in the curving (since obviously $\mathbf{T}$ along the tube axis direction is along the direction of the axis around which we curve the graphene sheet), we have that $\hat{\mathbf{R}}_{\mathbf{i}} = (cos(\alpha_i)cos(\beta_i), sin(\beta_i), -sin(\alpha_i)cos(\beta_i))$. Thus we may write

$$\pi_{\mathbf{A}} \cdot \pi_{\mathbf{B}} = cos(2\alpha_i) \tag{3.27}$$

$$\pi_{\mathbf{A}} \cdot \hat{\mathbf{R}}_{\mathbf{i}} = -sin(\alpha_i)cos(\beta_i) \tag{3.28}$$

$$\begin{aligned}\pi_{\mathbf{B}} \cdot \hat{\mathbf{R}}_{\mathbf{i}} &= sin(2\alpha_i)cos(\alpha_i)cos(\beta_i) - cos(2\alpha_i)sin(\alpha_i)cos(\beta_i)) \\ &= -\pi_{\mathbf{A}} \cdot \hat{\mathbf{R}}_{\mathbf{i}} = sin(\alpha_i)cos(\beta_i)\end{aligned} \tag{3.29}$$

and, inserting into (3.26),

$$\begin{aligned}&\langle \pi_{\mathbf{A}} | \hat{H} | \pi_{\mathbf{B}} \rangle = -sin(\alpha_i)cos(\beta_i)(sin(2\alpha_i)cos(\beta_i)cos(\alpha_i) - \\ &cos(2\alpha_i)sin(\alpha_i)cos(\beta_i))(V_{pp}^{\sigma} - V_{pp}^{\pi}) + cos(2\alpha_i)V_{pp}^{\pi} = \\ &\eta^2 cos^4(\beta_i)(V_{pp}^{\pi} - V_{pp}^{\sigma}) + (1 - 2\eta^2 cos^2(\beta_i))V_{pp}^{\pi}\end{aligned} \tag{3.30}$$

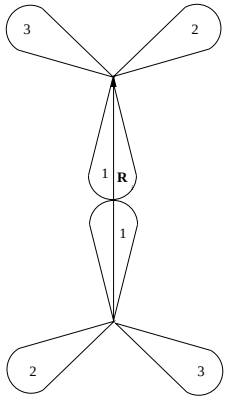

Figure 3.5: The σ orbitals of two neighbouring atoms shown schematically, along with the enumeration used in this thesis of them.

where we have used (3.24), in order to transform all dependency on α_i into dependency on β_i - the reason for this is that the parameter η now enters explicitly as the only parameter for the radius: the β_is depend *only* on the chiral angle from section 3.1, while η depends *only* on the radius, which will help us in later sections, were we shall want to do perturbation theory in $\frac{a_0}{R} \propto \eta$, ie. construct solutions for large radius CNTs.

3.3.2 $\sigma - \pi$ orbital coupling

We now turn to calculating the hamiltonian elements between the π and σ orbital. As we know from (2.4), there are three σ orbitals pr. atom, illustrated in figure 3.3.2.

Now, as we now from (2.4), the σ orbitals consists of part s orbital, and part p orbital (that we shall treat using a unitvector pointing in the direction of this orbital, denoted $p_{\sigma_{l,A}}$ for the lth σ orbital in the following), directed towards the neighbouring atoms, but tangential to the cylinder surface, rather than along the appropriate $\mathbf{R_i}$, and so, given the definitions in (3.23) and table 3.1, we see that the matrix element from the jth σ orbital to the π orbital at the atom that σ_1 points towards, is given as

$$\langle \sigma_{\mathbf{l,A}} | \hat{H} | \pi_{\mathbf{B}} \rangle = \frac{1}{\sqrt{3}} \langle \mathbf{S_i} | \hat{H} | \pi_{\mathbf{B}} \rangle + \sqrt{\frac{2}{3}} \langle \mathbf{p}_{\sigma_{\mathbf{l,A}}} | \hat{H} | \pi_{\mathbf{B}} \rangle \tag{3.31}$$

where we see that the term involving $\mathbf{p}_{\sigma_{\mathbf{l,A}}}$ is similar to the $\pi - \pi$ term, except $\pi_{\mathbf{A}}$ has been exchanged with $\mathbf{p}_{\sigma_{\mathbf{l,A}}}$, and thus we reach by analogy with (3.26) and from the fact at the integral depicted in table 3.1 upper left is zero, that

$$\langle \sigma_{\mathbf{l,A}} | \hat{H} | \pi_{\mathbf{B}} \rangle = -\frac{1}{\sqrt{3}} \pi_{\mathbf{B}} \cdot \hat{\mathbf{R}}_{\mathbf{i}} V_{sp}^{\sigma} + \sqrt{\frac{2}{3}} ((\mathbf{p}_{\sigma_{\mathbf{l,A}}} \cdot \hat{\mathbf{R}}_{\mathbf{i}})(\pi_{\mathbf{B}} \cdot \hat{\mathbf{R}}_{\mathbf{i}})(V_{pp}^{\sigma} - V_{pp}^{\pi}) + (\pi_{\mathbf{B}} \cdot \mathbf{p}_{\sigma_{\mathbf{l,A}}}) V_{pp}^{\pi}) \tag{3.32}$$

where the minus on the first term is due to the fact that the definition in (3.23) of V_{sp}^{σ} was for the situation where the positive part of the p orbital pointed towards the s orbital, and here $\mathbf{R_i}$ points away from it. From this, it is obvious that we need a describing of the $\mathbf{p}_{\sigma_{\mathbf{l,A}}}$'s in terms of

the chirality, just as above for the other vectors, and we shall treat the $\mathbf{p}_{\sigma_{\mathbf{1,A}}}$ orbital separately from the others, as it turns out that the difference between $\sigma_{2,A}$ and $\sigma_{3,A}$ is a simple sign change, reminiscent of the sign change on the $|y\rangle$ part that separates them in (2.4). $\mathbf{p}_{\sigma_{\mathbf{1,A}}}$ is easily found, as it pr. definition of the σ orbitals has no radial component, and the tangential direction is along the bond to the target atom, and so, from the definition of β we have $\mathbf{p}_{\sigma_{\mathbf{1,A}}} = (cos(\beta_i), sin(\beta_i), 0)$. As we already know $\hat{\mathbf{R}}_\mathbf{i} \cdot \pi_\mathbf{B} = \cos\beta_i \sin\alpha_i$ from (3.29), we need only calculate the two remaining factors in (3.32):

$$\mathbf{p}_{\sigma_{\mathbf{1,A}}} \cdot \hat{\mathbf{R}}_\mathbf{i} = cos(\alpha_i)cos^2(\beta_i) + sin^2(\beta_i) \approx 1 - \frac{\alpha_i^2}{2}cos^2(\beta_i) \approx 1 - \frac{sin^2(\alpha_i)}{2}cos^2\beta_i \tag{3.33}$$

$$\mathbf{p}_{\sigma_{\mathbf{1,A}}} \cdot \pi_\mathbf{B} = cos(\beta_i)sin(2\alpha_i) = 2cos(\beta_i)sin(\alpha_i)cos(\alpha_i) \approx 2cos(\beta_i)sin(\alpha_i) \tag{3.34}$$

where the approximations are due to $\alpha \ll 1$. We therefore find, inserting into (3.32) and using $sin(\alpha_i) = \eta cos(\beta_i)$,

$$\langle\sigma_{\mathbf{1,A}}|\hat{H}|\pi_\mathbf{B}\rangle \approx \eta cos^2(\beta_i)(-\frac{1}{\sqrt{3}}V_{sp}^\sigma + \sqrt{\frac{2}{3}}(V_{pp}^\sigma + V_{pp}^\pi)) \tag{3.35}$$

We then turn to the 2 other σ orbitals - from (2.4) it is clear that the only difference we are going to encounter compared to σ_1 is, that the p-part of the σ orbital have been rotated ± 120 degrees around the radial axis, and so we have that

$$\mathbf{p}_{\sigma_\mathbf{2}} = \begin{pmatrix} cos(\frac{2\pi}{3}) & -sin(\frac{2\pi}{3}) & 0 \\ sin(\frac{2\pi}{3}) & cos(\frac{2\pi}{3}) & 0 \\ 0 & 0 & 1 \end{pmatrix} \begin{pmatrix} -sin(\beta_i) \\ cos(\beta_i) \\ 0 \end{pmatrix} = \begin{pmatrix} \frac{1}{2}(-cos(\beta_i) - \sqrt{3}sin(\beta_i)) \\ \frac{1}{2}(\sqrt{3}cos(\beta_i) - sin(\beta_i)) \\ 0 \end{pmatrix}$$

$$\mathbf{p}_{\sigma_\mathbf{3}} = \begin{pmatrix} cos(-\frac{2\pi}{3}) & -sin(-\frac{2\pi}{3}) & 0 \\ sin(-\frac{2\pi}{3}) & cos(-\frac{2\pi}{3}) & 0 \\ 0 & 0 & 1 \end{pmatrix} \begin{pmatrix} -sin(\beta_i) \\ cos(\beta_i) \\ 0 \end{pmatrix} = \begin{pmatrix} \frac{1}{2}(-cos(\beta_i) + \sqrt{3}sin(\beta_i)) \\ \frac{1}{2}(\sqrt{3}cos(\beta_i) + sin(\beta_i)) \\ 0 \end{pmatrix} \tag{3.36}$$

or, if we define a parameter $\zeta = \pm 1$ as 1 for σ_2 and -1 for σ_3, $\mathbf{p}_{\sigma_\mathbf{l}} = (\frac{1}{2}(-cos(\beta_i) - \zeta\sqrt{3}sin(\beta_i)), \frac{1}{2}(\sqrt{3}cos(\beta_i) - \zeta sin(\beta_i)), 0)$ where the subscript l is either 2 or 3, distinguished by ζ. Completely analogously with (3.33), we now need $\mathbf{p}_{\sigma_\mathbf{l}} \cdot \hat{\mathbf{R}}_\mathbf{i}$ and $\mathbf{p}_{\sigma_\mathbf{l}} \cdot \pi_\mathbf{B}$ in order to evaluate (3.32):

$$\mathbf{p}_{\sigma_\mathbf{l}} \cdot \hat{\mathbf{R}}_\mathbf{i} = \frac{1}{2}\begin{pmatrix} -cos(\beta_i) - \zeta\sqrt{3}sin(\beta_i) \\ \zeta\sqrt{3}cos(\beta_i) - sin(\beta_i) \\ 0 \end{pmatrix} \cdot \begin{pmatrix} cos(\alpha_i)cos(\beta_i) \\ sin(\beta_i) \\ -sin(\alpha_i)cos(\beta_i) \end{pmatrix} =$$

$$\frac{1}{2}(-cos^2(\beta_i)cos(\alpha_i) - sin^2(\beta_i)) + \frac{\sqrt{3}\zeta}{2}(-sin(\beta_i)cos(\beta_i)cos(\alpha_i) + cos(\beta_i)sin(\beta_i)) \approx$$

$$(-\frac{1}{2} + \frac{eta^2cos^2(\beta_i)}{4}) + \frac{\sqrt{3}\eta^2cos^2(\beta_i)sin(2\beta_i)\zeta}{2} \tag{3.37}$$

$$\mathbf{p}_{\sigma_\mathbf{l}} \cdot \pi_\mathbf{B} = \frac{1}{2}\begin{pmatrix} -cos(\beta_i) - \zeta\sqrt{3}sin(\beta_i) \\ \zeta\sqrt{3}cos(\beta_i) - sin(\beta_i) \\ 0 \end{pmatrix} \cdot \begin{pmatrix} sin(2\alpha_i) \\ 0 \\ cos(2\alpha_i) \end{pmatrix} =$$

$$-\eta(cos^2(\beta_i)cos(\alpha_i) - \zeta\sqrt{3}sin(\beta_i)cos(\beta_i)cos(\alpha_i)) \approx -\eta(cos^2(\beta_i) + \frac{\zeta\sqrt{3}sin(2\beta_i)}{2}) \tag{3.38}$$

where again we have used $\sin(\alpha_i) = \eta cos(\beta_i)$, and the approximations are due to $\alpha_i \ll 1$. We may now evaluate (3.32) for the last two σ orbitals, where we have also recalled the definition of ζ:

$$\langle \sigma_2 | H | \pi_B \rangle \approx \frac{-\eta cos^2(\beta_i)}{\sqrt{3}} (V_{sp}^{\sigma} + \frac{1}{\sqrt{2}}(V_{pp}^{\sigma} + V_{pp}^{\pi})) + \frac{1}{\sqrt{2}} sin(2\beta_i) V_{pp}^{\pi} \tag{3.39}$$

$$\langle \sigma_3 | H | \pi_B \rangle \approx \frac{-\eta cos^2(\beta_i)}{\sqrt{3}} (V_{sp}^{\sigma} + \frac{1}{\sqrt{2}}(V_{pp}^{\sigma} + V_{pp}^{\pi})) - \frac{1}{\sqrt{2}} sin(2\beta_i) V_{pp}^{\pi} \tag{3.40}$$

This concludes the derivations necessary for calculating the coupling between π and σ bands.

3.3.3 $\sigma - \sigma$ orbital coupling

Finally we turn to calculating the hamiltonian elements internally in the σ bands. The derivations proceed much as above, except of cause that we now have two σ orbitals instead. Thus, analogous to (3.32), we find

$$\begin{aligned} \langle \sigma_{\mathbf{l,i}} | H | \sigma_{\mathbf{l',B}} \rangle &= \frac{1}{3} V_{ss}^{\sigma} + \frac{\sqrt{2}}{3} (\mathbf{p}_{\sigma_{\mathbf{l,A}}} - \mathbf{p}_{\sigma_{\mathbf{l'},\mathbf{B}}}) \cdot \hat{\mathbf{R}}_{\mathbf{i}} V_{sp}^{\sigma} \\ &+ \frac{2}{3} ((\mathbf{p}_{\sigma_{\mathbf{l,A}}} \cdot \hat{\mathbf{R}}_{\mathbf{i}})(\mathbf{p}_{\sigma_{\mathbf{l'},\mathbf{B}}} \cdot \hat{\mathbf{R}}_{\mathbf{i}})(V_{pp}^{\sigma} - V_{pp}^{\pi}) + (\mathbf{p}_{\sigma_{\mathbf{l'},\mathbf{B}}} \cdot \mathbf{p}_{\sigma_{\mathbf{l,A}}}) V_{pp}^{\pi}) \end{aligned} \tag{3.41}$$

where $\mathbf{p}_{\sigma_{\mathbf{l'},\mathbf{B}}}$ is the unit vector pointing in the direction of the l'th sigma orbital at the target atom, and where we have used the same trick as in (3.32) and (3.26) to rewrite the term involving the p-parts of the orbitals. The sign on the V_{sp}^{σ} parts differ, since $\hat{\mathbf{R}}_{\mathbf{i}}$ is directed *from* the origo atom *to* the target atom, and thus the situation is the same as presented in table 3.1 for one when evaluating between the p part on the origo atom, and inverted when evaluating the term dealing with the p part from the target atom.

From (3.41) we see that we now need two new inner products, namely $\mathbf{p}_{\sigma_{\mathbf{l'},\mathbf{B}}} \cdot \mathbf{p}_{\sigma_{\mathbf{l,A}}}$ and $\mathbf{p}_{\sigma_{\mathbf{l'},\mathbf{B}}} \cdot \hat{\mathbf{R}}_{\mathbf{i}}$, which is actually 9+3 new numbers, as both l and l' can take 3 different values, and we need all possible combinations. The derivations of these are straightforward but tedious, and so I have placed them in the appendices - the main difficulty lies in determining the $\mathbf{p}_{\sigma_{\mathbf{l'},\mathbf{B}}}$s, but these can be done by first noting that the orbital pointing toward the origo atom must be in the opposite direction of $\hat{\mathbf{R}}_{\mathbf{i}}$, except tilted α_i clockwise to make it tangential to the cylinder. After this is done, the other p orbitals can be determined as done above for the origo atom, ie. by rotating the first p orbital 120 degrees clockwise and anticlockwise using the $\pi_{\mathbf{B}}$ direction as the axis - refer to appendix A for the details of the calculation.

3.3.4 Selfenergy of the σ orbitals

In order to construct a full hamiltonian for the CNT including the σ orbitals, we need one last ingredient, namely the matrix elements between the σ orbitals internally on a single atom - the following calculation of this matrix is almost the same as the one in the appendix of [16], except for our correction of an error made by them. They are of cause independent of which atom we deal with, and the easiest way to find these elements is to use (2.4) directly, and one finds, using that

the p-orbitals at the same atom are orthogonal, and the standard assumption that zero overlap between two orbitals implies that the coupling between them is also zero, we find

$$\langle\sigma_1|H|\sigma_1\rangle = \langle\sigma_2|H|\sigma_2\rangle = \langle\sigma_3|H|\sigma_3\rangle = \frac{\epsilon_s + 2\epsilon_p}{3} \tag{3.42}$$

$$\langle\sigma_1|H|\sigma_2\rangle = \langle\sigma_2|H|\sigma_3\rangle = \langle\sigma_3|H|\sigma_1\rangle = \frac{\epsilon_s - \epsilon_p}{3} \tag{3.43}$$

where as usual $\epsilon_s = \langle S|H|S\rangle$ and $\epsilon_p = \langle p_i|H|p_i\rangle$ with $i = x, y, z$, and as discussed below (3.23) we set this to zero, but unlike [16] we do not conclude from this that the diagonal elements must then be zero, indeed we have that

$$\hat{H}_{\sigma_A,\sigma_A} = \frac{\epsilon_s}{3}\begin{pmatrix} 1 & 1 & 1 \\ 1 & 1 & 1 \\ 1 & 1 & 1 \end{pmatrix} \tag{3.44}$$

In this case the overlap matrix is of cause the identity matrix, since the sp^2 basis set is orthonormal.

3.3.5 Solving the full CNT hamiltonian

Although we do not go into the same detail in the $\sigma - \sigma$ case as for the $\pi - \pi$ and the $\sigma - \pi$ orbital coupling, it should be clear that we can now produce all the matrix elements of the hamiltonian for the CNT including the σ orbitals - of cause the overlap matrix elements follow the exact same procedure as above, except we use the overlap parameters from (3.23). We now write a schematic form of these matrices, in which we have used the coordinatesystem $(\pi_A, \pi_B, \sigma_A, \sigma_B)$, the σs of cause consisting of 3 coordinates each:

$$\mathbf{H}_i = \begin{pmatrix} & & & 0 & 0 & 0 & \mathbf{H}_{\sigma_B\to\pi_A} \\ & \mathbf{H}_{\pi_A\to\pi_B} & & & \mathbf{H}_{\sigma_A\to\pi_B} & & \\ 0 & & & 0 & 0 & 0 & \\ 0 & \mathbf{H}_{\pi_\mathbf{B}\to\sigma_\mathbf{A}} & & \mathbf{H}_{\sigma_A\to\sigma_A} & & \mathbf{H}_{\sigma_B\to\sigma_A} & \\ 0 & & & & & & \\ & & 0 & & & & \\ \mathbf{H}_{\pi_\mathbf{A}\to\sigma_\mathbf{B}} & & 0 & \mathbf{H}_{\sigma_A\to\sigma_B} & & \mathbf{H}_{\sigma_B\to\sigma_B} & \\ & & 0 & & & & \end{pmatrix} \quad \mathbf{S_i} = \begin{pmatrix} & & & 0 & 0 & 0 & \mathbf{S}_{\sigma_B\to\pi_A} \\ & \mathbf{S}_{\pi_A\to\pi_B} & & & \mathbf{S}_{\sigma_A\to\pi_B} & & \\ 0 & & & 1 & 0 & 0 & \\ 0 & \mathbf{S}_{\pi_\mathbf{B}\to\sigma_\mathbf{A}} & & 0 & 1 & 0 & \mathbf{S}_{\sigma_B\to\sigma_A} \\ 0 & & & 0 & 0 & 1 & \\ & & 0 & & & & \\ \mathbf{S}_{\pi_\mathbf{A}\to\sigma_\mathbf{B}} & & 0 & \mathbf{S}_{\sigma_A\to\sigma_B} & & \mathbf{S}_{\sigma_B\to\sigma_B} & \\ & & 0 & & & & \end{pmatrix} \tag{3.45}$$

Notice that eg. the $\hat{H}_{\pi\to\sigma}$ matrix, that we haven't calculated directly can by found using the hermiticity of the hamiltonian: as always, only the upper triangle is needed for a complete specification. Also, we subscript the matrices with the bond index i, since of cause there are different matrices for each of the three bond directions, as both α_i,β_i,$\mathbf{R_i}$ and the relative blochphase to the unitcell being connected to, is dependent on the bond number. We are now ready to insert these matrices into the machinery of the blochwaves, ie. we must now, in analogy with the case for graphene above, solve the generalized eigenvalue problem

$$(\sum_{\mathbf{R_i}} e^{-i\mathbf{k}\cdot\mathbf{R_i}}\mathbf{H_i} - E_n\mathbf{S_i})\Psi_{n,\mathbf{k}} = 0 \tag{3.46}$$

Once this is solved, we then have to apply the same restrictions to the **k** value as were done in section 3.2 - since the algebra is formidable, we shall not do this explicitly, but it should be clear how one calculates the band structure of the CNT including all effects of curvature. In the later parts of the thesis, we shall take a pertubative approach to curvature and spin-orbit coupling, rather than the full method described here, but we shall still need the matrices presented above.

Chapter 4

Spin orbit interaction in CNTs

In this chapter, we shall derive the effects of the spin-orbit interaction on the electrons in a CNT. We shall start out by briefly reminding ourselves of the general effect of the spin-orbit interaction along with the simplifying assumptions we shall make in order to include it in both an analytic and a numerical manner, and then derive the hamiltonian that shall form the basis of the effective description of the CNT with spin-orbit coupling in the next chapter.

4.1 Basics of the spin-orbit coupling

The spin-orbit coupling originally comes from deriving the first order relativistic corrections to the Pauli equation (that is, the scrödinger (non-relativistic) equation for spin-$\frac{1}{2}$ particles)[17]. However, we shall state that the physical origin of the effect is that in the restframe of the electrons, the electrical field (primarily from the nuclei) in the restframe of the nuclei (the laboratory frame) gives rise to a magnetic field given as $\mathbf{B_{rel}} = \frac{\mathbf{E}\times\mathbf{p}}{mc^2}$, where $\mathbf{p}$ is the momentum of the electron, and m is the electron mass. This couples to the spin of the of the electron through the standard (Zeeman-like) coupling, ie. $H_{so} = -\frac{1}{2}\mathbf{m}\cdot\mathbf{B_{rel}}$ where the $\frac{1}{2}$ is the Thomas-factor, stemming from the fact that the electron restframe is not an inertial frame. The magnetic moment of the electron *in its restframe* is due only to its intrinsic spin orbital momentum, so we have that $\mathbf{m} = -g\mu_B\frac{s}{2} = -\frac{ge\hbar}{4m}s \approx -\frac{e\hbar}{2m}s$ where s is the vector of pauli matrices, ie. $s \equiv s_x\hat{\mathbf{x}} + s_y\hat{\mathbf{y}} + s_z\hat{\mathbf{z}}$, and we have used the fact that the gyromagnetic constant for the electron spin moment is ≈ 2[31]. Also from the definition of the *electrostatic* potential ϕ, namely $\mathbf{E} = -\nabla\phi$, and from the fact that the *energy* potential V in an electrostatic field is given as $V = q\phi = -e\phi$, where e is the elementary charge, we find that $\mathbf{E} = \frac{\nabla V}{e}$. We insert this into the expression for $\mathbf{B_{rel}}$ to obtain $\mathbf{B_{rel}} = \frac{\nabla V\times\mathbf{p}}{emc^2}$, and so we reach (in agreement with [14])

$$H_{so} = -\frac{1}{2}\mathbf{m}\cdot\mathbf{B_{rel}} = -\frac{1}{2}(-\frac{e\hbar}{2m}s)\cdot(\frac{\nabla V\times\mathbf{p}}{emc^2}) = \frac{\hbar}{4m^2c^2}(\nabla V\times\mathbf{p})\cdot\mathbf{s} \tag{4.1}$$

This new part of the Hamiltonian has the immediate consequence that the states of our system now also have to include a spin degree of freedom, which we shall denote by s in this thesis, eg. $|p_z, s\rangle$.

Finding the exact electric potential of a manybody system such as the CNT is in itself a formidable problem, so we shall adopt the same assumption as [14], namely that the spin-orbit coupling is purely intra atomic ie. H_{so} couples only the orbitals on the same atom, and that the only relevant potential for these couplings is the centro-symmetric field originating from the nuclei and the inner electrons, ie. $V = V(r)$ - NB: the r used in this equation is of cause the distance to the nucleus, *not* the distance to the CNT axis. This is the first example of an ambiguity that is a source of many misunderstandings between quantities concerning the individual atoms, and quantities concerning the CNT as a whole: I shall be as specific as necessary in order to counter these ambiguities. The two assumptions above will allow us to produce a specific hamiltonian in accordance with the technique used in [14], but note that we are somewhat more ambitious: While Ando merely derives the spin-orbit coupling for the π bands, we aim to find the intra-atomic hamiltonian for the entire atom, ie. also couplings between the π and σ orbitals, which, when coupled with the σ/π curvature induced coupling from section 3.3 gives a previously unknown term to the effective hamiltonian, first presented in [28]. Before this can be seen, however, we must derive the intra atomic spin-orbit hamiltonian in full detail:

4.2 The atomic hamiltonian

The assumption of triatomic interaction allows us to specify one coordinate system for each atom, ie. since we shall consider no effects concerning the other atoms in the CNT, we have the situation of a free atom in vacuum for each carbon atom, and the various geometrical properties of the CNT therefore yields no "natural" coordinate system for us to use. In light of the second assumption, $V = V(r)$, one might be tempted to use a spherical system with the atom in the origo - however, in order to couple the following discussion to the previous sections, I shall instead choose a Cartesian system in which the z direction is in the radial direction *of the CNT*, the y direction is in the tube axis direction, and the x axis is along the circumference - this is precisely the same system as is used in [14], and has the useful property that the p_z orbital in the following can be immediately identified as the π orbitals in the CNT, while the p_x and p_y orbitals[1] are easy to geometrically transform into the σ orbitals of the previous sections.

Now, we see that if we for the moment neglect the constant in (4.1), we have

$$(\nabla V \times \mathbf{p}) \cdot \mathbf{s} = -i\hbar \begin{pmatrix} \frac{dV}{dy}\frac{d}{dz} - \frac{dV}{dz}\frac{d}{dy} \\ \frac{dV}{dz}\frac{d}{dx} - \frac{dV}{dx}\frac{d}{dz} \\ \frac{dV}{dx}\frac{d}{dy} - \frac{dV}{dy}\frac{d}{dx} \end{pmatrix} \cdot \mathbf{s} \tag{4.2}$$

where we have simply inserted the definition of $\mathbf{p}$. Our goal in this section is to evaluate the matrix elements of H_{so} between the $n = 2$ shells, and we shall use the lemma given explicitly in lemma in appendix C, which proves that the derivative function with respect to a coordinate j (e.g. x,y or z) is odd in j.

Now, given the assumption $V = V(r)$ we see that the the potential is even in any of the Cartesian coordinates. Furthermore, we remember that s is diagonal in the spatial part of the

[1] along with the 2s orbital of the atom

Pauli equation, so we see from (4.2) that each term of the scalar product in the spatial part of H_{so} is odd in two coordinates and even in the last coordinate. This means that, since we are considering coupling between the p_j ($j = x, y, z$) which is odd in the j coordinate and even in the two others, and the s shell, which is even in all coordinates, we find that for the matrix element of H_{so} not to be zero by symmetry, the two vectors being coupled must be $|p_j\rangle$ and $|p_k\rangle$ leading to

$$\langle p_j, s'|H_{so}|p_k, s\rangle = \langle p_j, s'|\epsilon_{jkl}\frac{-i\hbar^2}{4m^2c^2}(\frac{dV}{dj}\frac{d}{dk} - \frac{dV}{dk}\frac{d}{dj})s_l|p_k, s\rangle \tag{4.3}$$

where j,k and l are all coordinates, ie. x, y or z, and ϵ_{jkl} is the Levi-Civita symbol, which takes care of two things: First, it insures that the sign of the operator is unchanged under exchange of p_j and p_k, and second, it insures that the symmetry properties of (4.3) are correct, by insuring that j and k are different from each other. Now, remembering that $V = V(r)$, we have that $\frac{dV}{dj} = \frac{dV}{dr}\frac{dr}{dj} = \frac{dV}{dr}\frac{j}{r}$. With this identity (4.3) becomes

$$\langle p_j, s'|H_{so}|p_k, s\rangle = \langle p_j, s'|\epsilon_{jkl}\frac{-i\hbar^2}{r4m^2c^2}\frac{dV}{dr}(j\frac{d}{dk} - k\frac{d}{dj})s_l|p_k, s\rangle = \langle p_j, s'|\frac{\hbar^2}{r4m^2c^2}\frac{dV}{dr}L_l s_l|p_k, s\rangle \tag{4.4}$$

where we have introduced the angular momentum of the electrons along the l axis, $L_l = -i\epsilon_{jkl}(j\frac{d}{dk} - k\frac{d}{dj})$ - note that this definition has been made dimensionless. Three things may be said about this equation: First, the spin part of the integral separates totally, ie. we have that

$$\langle p_j, s'|H_{so}|p_k, s\rangle = \langle p_j|\frac{\hbar}{r4m^2c^2}\frac{dV}{dr}L_l|p_k\rangle\langle s'|s_l|s\rangle \tag{4.5}$$

Second, we have that

$$L_z|p_x\rangle = L_z\frac{1}{\sqrt{2}}(-|211\rangle + |21-1\rangle) = i\frac{i}{\sqrt{2}}(|211\rangle + |21-1\rangle) = i|p_y\rangle \tag{4.6}$$

$$L_z|p_y\rangle = L_z\frac{i}{\sqrt{2}}(|211\rangle + |21-1\rangle) = -i\frac{1}{\sqrt{2}}(-|211\rangle + |21-1\rangle) = -i|p_x\rangle \tag{4.7}$$

$$L_z|p_z\rangle = L_z|210\rangle = 0 \tag{4.8}$$

where we have used (2.4). From this follows the statement

$$L_l|p_k\rangle = -i\epsilon_{jkl}|p_j\rangle \tag{4.9}$$

since the other 6 equations contained in (4.9) is obtained by rotating the coordinates cyclically in equations (4.6), (4.7) and (4.8) once and twice. Third, if we, for a moment, consider the spatial integral in a spherical coordinate system, we see that if we remember that the radial part of the $|nlm\rangle$ orbitals depends only on $n-l$ and since the $|p_i\rangle$ all have $n-l = 1$ and the quantity $\frac{\hbar^2}{2rm^2c^2}\frac{dV}{dr}$ in (4.5) only depends on r (as opposed to ϕ and θ in the spatial integral), we may rewrite (4.5)

$$\begin{aligned}\langle p_j, s'|H_{so}|p_k, s\rangle &= \langle p_j|\frac{-i\epsilon_{jkl}\hbar^2}{r4m^2c^2}\frac{dV}{dr}|p_j\rangle\langle s'|s_l|s\rangle \\ &= \langle p_{j,\theta\phi}(\phi,\theta)|p_{j,\theta\phi}(\phi,\theta)\rangle\langle s'|s_l|s\rangle\int dr|p_{j,r}(r)|^2\frac{-i\epsilon_{jkl}\hbar^2}{r4m^2c^2}\frac{dV}{dr}\end{aligned} \tag{4.10}$$

where we have also used (4.9) in the first equality, and we have separated the real function $p_j(\mathbf{r}) = p_{j,\theta\phi}(\theta,\phi)p_{j,r}(r)$ and the spatial bracket in the final expression is understood to be the integral over the angular dependence only, which furthermore is independent on j, since changing j from eg. x to y simply corresponds to renaming the axises of the coordinatesystem . We can now use the fact that $\langle p_{j,\theta\phi}(\phi,\theta)|p_{j,\theta\phi}(\phi,\theta)\rangle = 1$, easily seen from (2.4) using that for the spherical harmonics $\langle Y_{lm}|Y_{l'm'}\rangle = \delta_{l,l'}\delta_{m,m'}$ to finally define the (real and positive) constant α_{so},as

$$\alpha_{so} = \int dr|p_{j,r}(r)|^2 2\frac{\hbar^2}{r4m^2c^2}\frac{dV}{dr} \tag{4.11}$$

which is approximately 12 meV for the 2p orbitals of carbon[29] (the factor two is there to insure that we get the same value as is conventional in the literature), and thus allows us to write

$$\langle p_j, s'|H_{so}|p_k, s\rangle = -\frac{\alpha_{so}}{2}i\epsilon_{jkl}\langle s'|s_l|s\rangle \tag{4.12}$$

Now, all that remains is to be done is to determine the result of the spin-space integral. In (4.12) we have not yet chosen a spin quantization axis, but if we, along with [14], choose the z direction, we find that for we have

$$\langle\downarrow_z|s_k|\downarrow_z\rangle = \begin{cases} 0 \text{ for k=x} \\ 0 \text{ for k=y} \\ -1 \text{ for k=z} \end{cases} \qquad \langle\downarrow_z|s_k|\uparrow_z\rangle = \begin{cases} 1 \text{ for k=x} \\ i \text{ for k=y} \\ 0 \text{ for k=z} \end{cases}$$
$$\langle\uparrow_z|s_k|\downarrow_z\rangle = \begin{cases} 1 \text{ for k=x} \\ -i \text{ for k=y} \\ 0 \text{ for k=z} \end{cases} \qquad \langle\uparrow_z|s_k|\uparrow_z\rangle = \begin{cases} 0 \text{ for k=x} \\ 0 \text{ for k=y} \\ 1 \text{ for k=z} \end{cases} \tag{4.13}$$

Now, remembering that the 2s shells are not affected by $\hat{H}_{so}$ due to symmetry, we can now write the $\hat{H}_{so}$ in a matrixform, where we use the basis $\{|s,\uparrow_z\rangle, |p_x,\uparrow_z\rangle, |p_y,\uparrow_z\rangle, |p_z,\uparrow_z\rangle, |s,\downarrow_z\rangle, |p_x,\downarrow_z\rangle, |p_y,\downarrow_z\rangle, |p_z,\downarrow_z\rangle\}$,

$$\hat{H}_{so} = \frac{\alpha_{so}}{2}\begin{pmatrix} 0 & 0 & 0 & 0 & 0 & 0 & 0 & 0 \\ 0 & 0 & -i & 0 & 0 & 0 & 0 & -1 \\ 0 & i & 0 & 0 & 0 & 0 & 0 & -i \\ 0 & 0 & 0 & 0 & 0 & 1 & i & 0 \\ 0 & 0 & 0 & 0 & 0 & 0 & 0 & 0 \\ 0 & 0 & 0 & 1 & 0 & 0 & i & 0 \\ 0 & 0 & 0 & -i & 0 & -i & 0 & 0 \\ 0 & -1 & i & 0 & 0 & 0 & 0 & 0 \end{pmatrix} \tag{4.14}$$

and, since we shall need the $\hat{H}_{so}$ in the basis of σ and π orbitals, we can use the fact that the $|p_z\rangle$ orbitals are by definition the same as the π shells, and furthermore, we have that the $|p_x\rangle$ orbitals are in the direction of the chiral vector, we know, that in order to go from the $\{|s\rangle, |p_x\rangle, |p_y\rangle, |p_z\rangle\}$ to the $\{s, x, y, \pi\}$ coordinates used in (2.4), we need to employ β_1 from the previous section (defined above eqn. (3.24)) which is the angle between the chiral vector and the x orbital from (2.4). Now we may switch to the $\{|\sigma_1,\uparrow_z\rangle, |\sigma_2,\uparrow_z\rangle, |\sigma_3,\uparrow_z\rangle, |\pi,\uparrow_z\rangle, |\sigma_1,\downarrow_z\rangle, |\sigma_2,\downarrow_z\rangle, |\sigma_3,\downarrow_z\rangle, |\pi,\downarrow_z\rangle\}$, orbital by

two consecutive transformations (note that since the transformations are purely spatial, there is no difference between spin-↑ and spin-↓, and to be concise, we show only the 4x4 transformation matrix which may be used for either spin direction)

$$\tilde{\mathbf{T}} = \begin{pmatrix} \frac{1}{\sqrt{3}} & \frac{\sqrt{2}}{\sqrt{3}} & 0 & 0 \\ \frac{1}{\sqrt{3}} & -\frac{1}{\sqrt{6}} & \frac{1}{\sqrt{2}} & 0 \\ \frac{1}{\sqrt{3}} & -\frac{1}{\sqrt{6}} & -\frac{1}{\sqrt{2}} & 0 \\ 0 & 0 & 0 & 1 \end{pmatrix} \begin{pmatrix} 1 & 0 & 0 & 0 \\ 0 & \cos\beta_1 & \sin\beta_1 & 0 \\ 0 & -\sin\beta_1 & \cos\beta_1 & 0 \\ 0 & 0 & 0 & 1 \end{pmatrix} \tag{4.15}$$

$$= \begin{pmatrix} \frac{1}{\sqrt{3}} & \sqrt{\frac{2}{3}}\cos\beta_1 & \sqrt{\frac{2}{3}}\sin\beta_1 & 0 \\ \frac{1}{\sqrt{3}} & -\frac{\cos\beta_1}{\sqrt{6}} - \frac{\sin\beta_1}{\sqrt{2}} & \frac{\cos\beta_1}{\sqrt{2}} - \frac{\sin\beta_1}{\sqrt{6}} & 0 \\ \frac{1}{\sqrt{3}} & -\frac{\cos\beta_1}{\sqrt{6}} + \frac{\sin\beta_1}{\sqrt{2}} & -\frac{\cos\beta_1}{\sqrt{2}} - \frac{\sin\beta_1}{\sqrt{6}} & 0 \\ 0 & 0 & 0 & 1 \end{pmatrix} \tag{4.16}$$

and so, if we define $\mathbf{T} = \begin{pmatrix} \tilde{\mathbf{T}} & 0 \\ 0 & \tilde{\mathbf{T}} \end{pmatrix}$, we may formally write

$$\hat{H}_{so,\{\sigma,\pi\}} = \mathbf{T}\hat{H}_{so,\{|s\rangle,|p_j\rangle\}}\mathbf{T}^{-1} \tag{4.17}$$

where the extra subscripts on the $\hat{H}_{so}$ denotes the coordinatesystem. Due to its size, I have put the explicit expression of the matrix in appendix B.1.

In principle we are now done with the intra atomic spin-orbit coupling hamiltonian, however, for later use we shall also need the spin-orbit hamiltonian in another system which will be global rather than a local system defined with respect to the individual atom, as the above: We shall use the cylindrical axis of the nanotube as the y axis, just as above, but the x-axis and z-axis shall be defined with respect to some arbitrary, but fixed, atom position. In other words, if we define an angular coordinate, ϕ, as the angular difference between the starting point and a given atom, and rename the atomic coordinates from above for this atom x' and z', we have

$$|p_z\rangle = \cos(\phi)|p_{z'}\rangle - \sin(\phi)|p_{x'}\rangle \qquad |p_x\rangle = \sin(\phi)|p_{z'}\rangle + \cos(\phi)|p_{x'}\rangle \tag{4.18}$$

This is the same coordinate system as is used in [28], fig. 2. Furthermore, we shall choose to use the y axis, ie. the tube axis, as spin quantization axis, both because it is the quantization used by the numerical code used in this project, and because it will later be seen that the spin in the axis direction is conserved to the lowest order perturbation theory in $\hat{H}_{so}$, in contrast to the other directions.

Now, of cause we could simply use the above results, and geometrically transform them to the new system, however, we shall use a slightly different approach, the one probably most common in the literature, both to present it in this thesis, and because it is quite easy to apply given the above calculations. The method diverges from the above at the point of (4.2), where we now immediately insert the specific form of $\nabla V(r)$, ie.

$$\hat{H}_{so} = \frac{\hbar}{4m^2c^2}(\nabla V(r) \times \mathbf{p}) \cdot \hat{s} = \frac{\hbar}{4rm^2c^2}\frac{dV}{dr}(\mathbf{r} \times \mathbf{p}) \cdot \hat{s} = \frac{\hbar^2}{4rm^2c^2}\frac{dV}{dr}\hat{L} \cdot \hat{s} \tag{4.19}$$

where the extra $\hbar$ in the last equality comes from the use of a dimensionless angular momentum. This formula reminds us of the Heisenberg interaction, or exchange interaction, from basic quantum magnetism, and in particular it reminds us of the rewriting we may make, using $\hat{J}^j_\pm = \hat{J}_k \pm i\hat{J}_l$, where j,k and l are Cartesian axis denominators, fulfilling $\epsilon_{jkl} = 1$, namely (using the trick of separating the radial part of the integral and inserting α_{so} from (4.11), thus implicitly changing $\hat{H}_{so}$ from an operator on the full spatial+spin Hilbert space to an operator on the angular dependencies+spin, since α_{so} contains the radial integral):

$$\hat{H}_{so} = \alpha_{so}(\hat{L}_y\hat{s}_y + \frac{1}{2}(\hat{L}^y_+\hat{s}^y_- + \hat{L}^y_-\hat{s}^y_+) \tag{4.20}$$

where we use the definition of $\hat{J}^j_\pm$ of j being y, instead of the usual case where the quantization axis is defined as z. Now, by reinserting the definitions for $\hat{J}^y_\pm$ into this expression, we find

$$\hat{H}_{so} = \alpha_{so}(\hat{L}_y\hat{s}_y + \frac{1}{2}((\hat{L}_{z'} + i\hat{L}_{x'})\hat{s}^y_- + (\hat{L}_{z'} - i\hat{L}_{x'})\hat{s}^y_+)) \tag{4.21}$$

the matrix elements of which can easily be calculated, using (4.9). We present a derivation of all the non-zero matrix elements, where we implicitly use that (4.9) contains a Levi-Civita symbol, and that $S^y_{+(-)}|\uparrow_y(\downarrow_y)\rangle = 0$:

$$\hat{H}_{so}|p_{x'},\uparrow_y\rangle = \frac{\alpha_{so}}{2}(-i|p_{z'},\uparrow_y\rangle + i|p_y,\downarrow_y\rangle) \tag{4.22}$$

$$\hat{H}_{so}|p_y,\uparrow_y\rangle = \frac{\alpha_{so}}{2}(-i|p_{x'},\downarrow_y\rangle - |p_{z'},\downarrow_y\rangle) \tag{4.23}$$

$$\hat{H}_{so}|p_{z'},\uparrow_y\rangle = \frac{\alpha_{so}}{2}(i|p_{x'},\uparrow_y\rangle + |p_y,\downarrow_y\rangle) \tag{4.24}$$

$$\hat{H}_{so}|p_{x'},\downarrow_y\rangle = \frac{\alpha_{so}}{2}(i|p_{z'},\downarrow_y\rangle + i|p_y,\uparrow_y\rangle) \tag{4.25}$$

$$\hat{H}_{so}|p_y,\downarrow_y\rangle = \frac{\alpha_{so}}{2}(-i|p_{x'},\uparrow_y\rangle + |p_{z'},\uparrow_y\rangle) \tag{4.26}$$

$$\hat{H}_{so}|p_{z'},\downarrow_y\rangle = \frac{\alpha_{so}}{2}(-i|p_{x'},\downarrow_y\rangle - |p_y,\uparrow_y\rangle) \tag{4.27}$$

Of cause we find that the $|2s\rangle$ orbitals have no non-zero elements in this matrix, since $\hat{L}_j|2s\rangle = 0$ for $j = x, y, z$. This hamiltonian is still defined with respect to a local coordinatesystem, but this is of cause easily remedied using (4.18), such that, if we decide to use the basis

$$\{|2s_\uparrow\rangle, |p_{x,\uparrow}\rangle, |p_{y,\uparrow}\rangle, |p_{z,\uparrow}\rangle, |2s_\downarrow\rangle, |p_{x,\downarrow}\rangle, |p_{y,\downarrow}\rangle, |p_{z,\downarrow}\rangle\} \tag{4.28}$$

and the corresponding one for the atomic coordinatesystem (ie. with $x(z)$ exchanged to $x'(z')$), we have the transformation matrix *from* the global *to* the local system $\tilde{\mathbf{T}_{\mathbf{g,l}}} = \begin{pmatrix} 1 & 0 & 0 & 0 \\ 0 & \cos\phi & 0 & -\sin\phi \\ 0 & 0 & 1 & 0 \\ 0 & \sin\phi & 0 & \cos\phi \end{pmatrix}$

for both spin-up and down, we have

$$\hat{H}_{so,g} = \begin{pmatrix} \tilde{\mathbf{T}}_{\mathbf{g,l}} & 0 \\ 0 & \tilde{\mathbf{T}}_{\mathbf{g,l}} \end{pmatrix}^{-1} \hat{H}_{so} \begin{pmatrix} \tilde{\mathbf{T}}_{\mathbf{g,l}} & 0 \\ 0 & \tilde{\mathbf{T}}_{\mathbf{g,l}} \end{pmatrix} = \frac{\alpha_{so}}{2} \begin{pmatrix} 0 & 0 & 0 & 0 & 0 & 0 & 0 & 0 \\ 0 & 0 & 0 & i & 0 & 0 & -ie^{-i\phi} & 0 \\ 0 & 0 & 0 & 0 & 0 & ie^{-i\phi} & 0 & -e^{-i\phi} \\ 0 & -i & 0 & 0 & 0 & 0 & e^{-i\phi} & 0 \\ 0 & 0 & 0 & 0 & 0 & 0 & 0 & 0 \\ 0 & 0 & -ie^{i\phi} & 0 & 0 & 0 & 0 & -i \\ 0 & ie^{i\phi} & 0 & e^{i\phi} & 0 & 0 & 0 & 0 \\ 0 & 0 & -e^{i\phi} & 0 & 0 & i & 0 & 0 \end{pmatrix} \tag{4.29}$$

Chapter 5

The pertubative hamiltonian

5.1 The basic problem

We are now in a position to understand the basic problem that we shall attempt to solve in this thesis: First, we observe, that since all the terms of the hamiltonian presented so far are invariant under time-reversal, we should expect Kramer doublets in the energy spectrum, ie. each energylevel should have (at least) a degeneracy of 2. In terms of the quantum numbers so far used to describe the states, and for the lowest energy states (where $k_t = 0$) the effect of time reversal is to change $\tau \to -\tau$ and $s_y \to -s_y$, the first replacement owing to the fact that the state closest to the K point will the same absolute value of k_C as the one closest to K', but with opposite sign, ie. under time-reversal, where $k_C \to -k_C$, K and K' is exchanged, and the spin sign change is seen from its identity as intrinsic angular momentum, since angular momenta always changes sign under time-reversal. An instructive way to think of these states is to identify τ with the direction of the (crystal) momentum along the circumference, and thus a (crystal) angular momentum of the electrons parallel to the tube axis. Thus one may interpret the Kramer doublets as states having either parallel or antiparallel orbital[1] and spin angular momentum. It is possible, and indeed as we shall see actually the case, that spin-orbit coupling and curvature effects leads to an energysplitting between these Kramer doublets: We shall call this difference in energy between the Kramer doublets Δ_{so}.

Due to the curvature dependency it was expected that Δ_{so} would be inversely proportional to the radius of the CNT. However when we investigated this quantity as a function of chirality in zigzag CNTs we found the mystifying functional dependence shown in figure 5.1: Something is significantly different for the $\nu = -1$ family of semiconducting CNTs.

Furthermore, the non-perturbed system has electron-hole symmetry for the low energy states, as seen in the energy expression (3.22). However, when we studied the chirality dependence of Δ_{so} for zigzag nanotubes in figure 5.2, we see that this is broken by curvature and spin-orbit coupling: When Δ_{so} is large in the conduction band, it is small in the valence band, and vice versa.

These two effects can be explained by the pertubative hamiltonian that includes first order curvature perturbation and first order spin-orbit coupling, ie. an effective 2nd order perturbation.

[1] crystal, *not* atomic

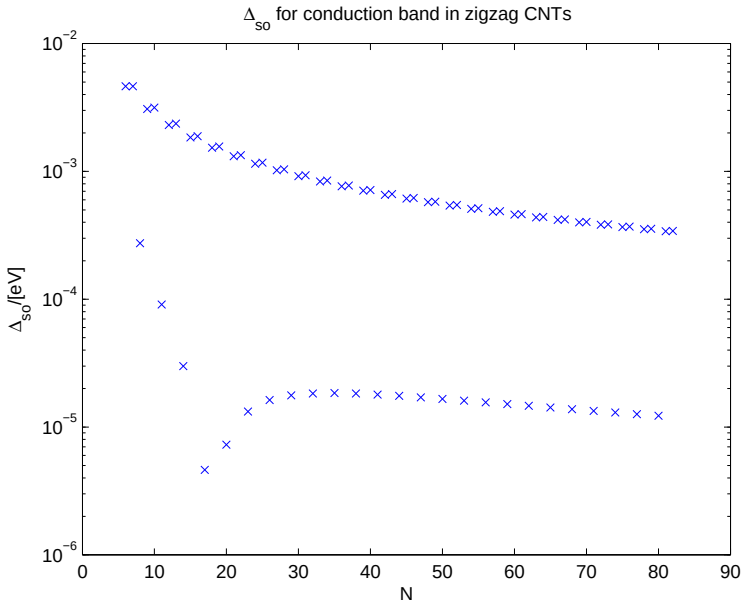

Figure 5.1: Spin-orbit splitting for the conduction band in zigzag nanotubes. Note the logarithmic y-axis, and that n on the x-axis is proportional to R, ie. $R = \frac{a_0}{2\pi}n$. The first few chiralities have abnormal values due to higher order effects, and have been omitted.

The goal of this chapter is to derive and interpret this hamiltonian using the results of the two previous chapters.

The reason why we call this splitting Δ_{so} is, that in the experiments where we first saw the data illustrated in figures 5.1 and 5.2, the gap opened only when we enabled the spin-orbit coupling. There are reasons why only a spin dependent term could open this gap, but we shall choose to see it as an experimental fact, to be explained by the following theory.

These data was obtained independently by me in the autumn of 2008, but was published first in [35] - however, the explanation for the data given by [35] is not the one found by us, and by [19] and [28].

5.2 The effective spin-orbit/curvature perturbation

Having established the atomic effect of the spin-orbit coupling in the previous chapter, we now turn to the task of determining what the effect on the full eigenstates close to the K(') points, ie. formulating an effective hamiltonian. While this has been done in [28] and [19], it was also done independently by me and the Copenhagen group. Since the spin-orbit effect involves the σ orbitals as well as the π orbitals, we cannot simply augment the previously found effective hamiltonians (which pr. definition only concerns the π orbitals), but we can consider the pertubative expansion of the effective hamiltonian where, in the beginning, we consider the $\hat{H}_{so}$ as the perturbation. Now, the first thing we notice, from appendix B.1 is, that there is no coupling between the

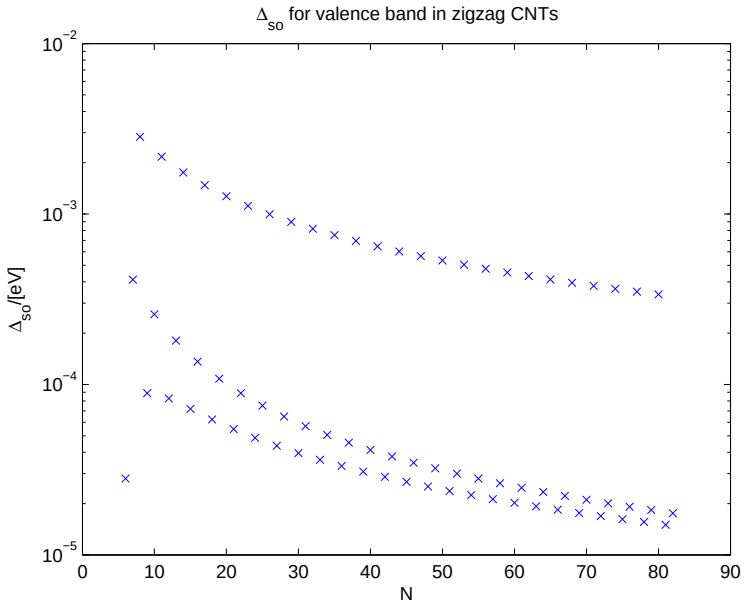

Figure 5.2: Spin-orbit splitting for the valence band in zigzag nanotubes. This is opposite figure 5.1, in the sense that the $\nu = -1$ family of the conduction band and the $\nu = 0, +1$ family of the valence band have similar values of Δ_{so} for similar chiralities, and likewise for $\nu = 0, +1$ of the conduction band and $\nu = -1$ of the valence band spin-orbit gaps. Again, the first few chiralities are omitted

π orbitals (neither between spin-$\uparrow$/spin-$\downarrow$ or between the sublattices, as $\hat{H}_{so}$ is intra atomic by assumption). Therefore, there is no 1st order contribution from the spin-orbit coupling to the effective hamiltonian, and so we may think to immediately proceed to second order perturbation in $\hat{H}_{so}$. However, as stated above, we shall instead treat both the $\hat{H}_{so}$ and the hamiltonian describing the curvature induced coupling (in the following denoted $\hat{H}_{cv}$). We have to remember though, that the states we are perturbing are degenerate at the K(') points, wherefore we need the projection operator that takes us out of the subspace spanned by the π bands, $\hat{P}_\pi \equiv 1 - \sum_{\{n:E_n=\epsilon_f\}} |\Psi_{n\mathbf{k}}\rangle\langle\Psi_{n\mathbf{k}}|$ where $|\Psi_{n\mathbf{k}}\rangle$ is the solution to the effective hamiltonian without curvature induced mixing and spin-orbit coupling, found by diagonalizing (3.21). So, using the standard methods of perturbation theory (eg. [32] chapter 5), we wish to evaluate the matrix element of

$$\hat{H}_{pert} = \hat{H}_{so} \frac{\hat{P}_\pi}{\epsilon_f - \hat{H}_0} \hat{H}_{cv} + H.C. \tag{5.1}$$

on the states $|\Psi_{n\mathbf{k}}, s\rangle$ from (3.21), where we have now included the spin degree of freedom. First, we see that we may ignore the curvature induced coupling between $\pi - \pi$ and $\sigma - \sigma$ orbitals: since the $\hat{P}_\pi$ operator eliminates all contributions from the π orbitals, $\hat{P}_\pi \hat{H}_{c,(\pi,\pi)} = \hat{H}_{c,(\pi,\pi)} \hat{P}_\pi = 0$ (there *is* a first order effect of this part of the curvature hamiltonian as seen in section 3.3.1, but that is spin independent, and so not interesting for us). On the other hand, the $|\Psi_{n\mathbf{k}}, s\rangle$ states contain no

σ orbitals, so $H_{c,(\sigma,\sigma)}|\Psi_{n\mathbf{k}}, s\rangle = 0$, wherefore the 1+1 order perturbation due to these two parts of the curvature hamiltonian will vanish and so we may replace $\hat{H}_{cv}$ with $\hat{H}_{c,(\sigma-\pi)}$ ie. the hamiltonian build from (3.35),(3.39) and (3.40).

Similarly, we also see (with an argument very similar to the one employed by [16], although to a different matrix), that if we choose the tube axis, y as our spin-quantization axis, the spin flip part of the $\hat{H}_{so}$ hamiltonian is of no consequence, since all matrix elements in the spin off-diagonal part of (4.29) has a factor of either $e^{i\phi}$ or $e^{-i\phi}$, leading us to the conclusion, that if the bra and ket of the energy shift expression, $\langle\Psi_{n\mathbf{k}}|\hat{H}_{pert}|\Psi_{n\mathbf{k}}\rangle$ have the same dependence on ϕ (which is the case for lowenergy states close to either the K or the K' point respectively, since they all have the same allowed k_c value), the integral around the circumference of the spin-flip part of (4.29) will be zero, using the wellknown expression $\int_0^{2\pi} e^{ix\cdot\phi}d\phi = \delta_{x,0}$ for $x \in \mathbb{N}$. We need to be careful here however: the states that we perturb comes from (close to) *both* the K and K' point, which will have opposite values of the wavenumber in the circumferential direction, k_C, easily seen from figure 3.2 on page 18 when we remember that the difference from neighbouring lines of allowed k-values is exactly $\frac{2\pi}{|\mathbf{C}|}$, since this changes the value of k_C by as little as possible while preserving the cyclic boundary conditions, as seen from (3.11). This shows us why we cannot have a matrix element of H_{so} between a state from near the K point to a state near the K' point: Their k_C value differs by more than one "allowed" step. Actually, this interpretation of the $e^{\pm i\phi}$ as a change in the circumferential k_C value gives us an unsurprising, but reassuring interpretation of the spin off-diagonal elements of (4.29): the exponential functions insures that the total orbital momentum along the y-axis is preserved, although now by adding or subtracting to/from the orbital angular momentum of the blochwave, ie. the (crystal) angular momentum associated with going around the circumference of the CNT, rather than the atomic orbital angular momentum from above. Corresponding to this interpretation, it is also reassuring that the spin diagonal elements of (4.29) doesn't have any exponential functions in them: There would be nowhere for the orbital angular momentum to come from/go to. Note, that the above argument is fundamentally dependent on the fact that we only have one $\hat{H}_{so}$ in $\hat{H}_{pert}$: if we go to higher order in $\hat{H}_{so}$ we will get terms of the perturbation proportional to $(\hat{L}_+\hat{S}_-)(\hat{L}_-\hat{S}_+)$, where $\hat{L}_\pm$ now refers to the orbital angular momentum around the tube axis. As stated, and as observed by [16], this effect is at least an order of magnitude smaller than the effect of $\hat{H}_{pert}$ that we are currently studying, at least for normal sized nanotubes: Since we know that the effect of the $\hat{H}_{cv}$ has an inversely proportional dependence on the radius, for very large CNTs, the so called *intrinsic* spin- orbit coupling effect, ie. the 2nd order effect of $\hat{H}_{so}$ becomes dominant, and indeed it is the only effect detected in graphene, which can be thought of as a nanotube with infinite radius.

Now, similarly to the case for $\hat{H}_{cv}$, we see that we only need the $\sigma - \pi$ part of the $\hat{H}_{so}$ hamiltonian. Using that, from (4.29) and the above argument, we can write (in the language of second quantization)

$$\hat{H}_{so} = is_y(c_x^\dagger c_z - c_z^\dagger c_x) \tag{5.2}$$

Returning to the calculation (5.1) we see that in order to calculate the full perturbed hamiltonian, we also need to have the unperturbed hamiltonian for the system, ie. the graphene-hamiltonian, for the σ states, rather than the π states as were found in chapter 2. This could in principle be found from the derivations in the end of chapter 3, setting the curvature parameter

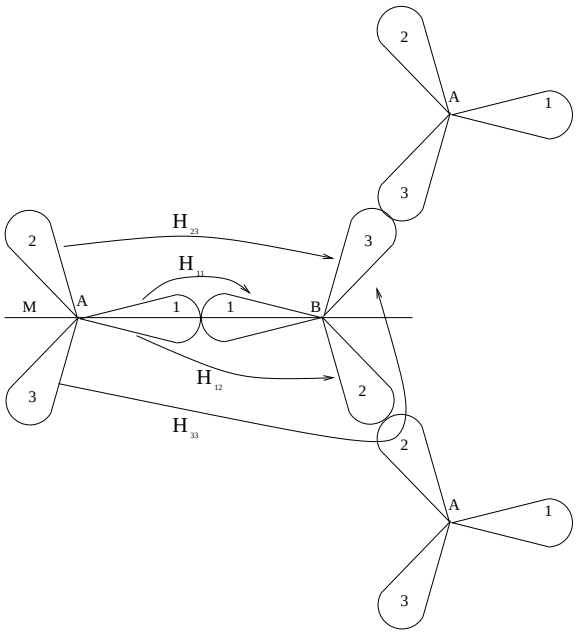

Figure 5.3: The four different couplings between σ orbitals between to neighbouring atoms. The other 5 possibilities can be generated by either the parity operation, ie. by interchanging the A and B atom, or by the mirror symmetry in the line M.

to 0 (this is what [19] does, as we shall see in chapter 6), but some symmetries of graphene make the calculation quite easy, and thus we shall carry it out in detail for the sake of completeness. The principle of this calculation is the same as was used in [16] appendix A, except that we do not employ the approximation that only σ orbitals pointing in the direction of each others host atom couples, but rather, we calculate the entire coupling between all orbitals in the unitcell. Also note that [16] make some untenable assumptions in their calculations, and so our result is different from theirs.

5.2.1 calculation of $\hat{H}_0$

From symmetry we may determine that the number of different couplings is 4, even though there are of cause 9 matrix elements to be determined (9 since there er 3 σ orbitals on either atom). The four couplings are shown in figure 5.3 and the calculation of each uses the same parameters as were defined in table 3.1 and numerically specified in eqn. (3.23) in section 3.3. Remembering that the B atoms σ orbitals are found from the A atoms σ orbitals (2.4) by setting $|x\rangle \rightarrow -|x\rangle$

and $|y\rangle \to -|y\rangle$, we find that (using the definitions of the matrix elements from figure 5.3):

$$\begin{aligned}
H_{11} \equiv \langle \sigma_{A,1}|\sigma_{B,1}\rangle =& \frac{1}{3}V_{ss}^{\sigma} + \frac{2\sqrt{2}}{3}V_{sp}^{\sigma} - \frac{2}{3}V_{pp}^{\sigma} \\
H_{12} \equiv \langle \sigma_{A,1}|\sigma_{B,2}\rangle =& \frac{1}{3}V_{ss}^{\sigma} + \frac{1}{3\sqrt{2}}V_{sp}^{\sigma} + \frac{1}{3}V_{pp}^{\sigma} \\
H_{23} \equiv \langle \sigma_{A,2}|\sigma_{B,3}\rangle =& \frac{1}{3}V_{ss}^{\sigma} - \frac{\sqrt{2}}{3}V_{sp}^{\sigma} - \frac{1}{6}V_{pp}^{\sigma} + \frac{1}{2}V_{pp}^{\pi} \\
H_{33} \equiv \langle \sigma_{A,3}|\sigma_{B,3}\rangle =& \frac{1}{3}V_{ss}^{\sigma} - \frac{\sqrt{2}}{3}V_{sp}^{\sigma} - \frac{1}{6}V_{pp}^{\sigma} - \frac{1}{2}V_{pp}^{\pi}
\end{aligned} \tag{5.3}$$

We then, by symmetry have that

$$H_{31} = H_{21} = H_{13} = H_{12} \qquad H_{32} = H_{23} \qquad H_{22} = H_{33} \tag{5.4}$$

Remembering section 3.3.4 we see that there is a coupling between the σ orbitals on the same atom (unlike the case for the π orbitals, which we set to 0). This energy is

$$H_i \equiv \langle \sigma_A|\hat{H}_0|\sigma_A\rangle = \langle \sigma_B|\hat{H}_0|\sigma_B\rangle = \frac{1}{3}\epsilon_s \tag{5.5}$$

where $|\sigma_{A/B}\rangle$ represents any σ orbital on the specified atom.

There is a point to consider when calculating the H_0, namely the precise form of the other two terms in the Bloch sum, ie. the sum over the neighbours introduced (for the $\pi - \pi$ coupling) in (2.13): We have to remember that the orientation of the σ orbitals for eg. the A position is of cause the same throughout the crystal, so the when specifying the matrix elements of the coupling between the B atom and the A atom in the direction of the B atoms σ_2 orbital, we have to cyclically rotate the orbital numbers in (5.3) and (5.4), and for the last bond we have to rotate cyclically once more - as can be seen from studying figure 5.3.

We furthermore have to consider which blochphase to use in the sum: strictly speaking, it should clearly be $e^{\pm i\mathbf{k}\cdot\tau_{\mathbf{j}}}$ where $\tau_{\mathbf{j}}$ is the vector defined in section 2, the $\pm$ takes care of the difference between going from the A sublattice to the B sublattice and vice versa, and $\mathbf{k} = \mathbf{K}(') + \kappa$, where κ is the small deviation in the $\mathbf{C}$ direction, specified in (3.17) due to the cyclic boundary condition. However, since we see from (3.17) that $\kappa = O(\frac{1}{R})$, and since we wish to study (5.1) to lowest order in $\frac{1}{R}$, we may use $\mathbf{K}(')$ instead of $\mathbf{k}$, because

$$e^{\pm i(\mathbf{K}+\kappa)\cdot\tau_{\mathbf{j}}} = e^{\pm i\mathbf{K}\cdot\tau_{\mathbf{j}}}e^{\pm i\kappa\cdot\tau_{\mathbf{j}}} = e^{\pm i\mathbf{K}\cdot\tau_{\mathbf{j}}}(1 + O(\frac{1}{R})) \approx e^{\pm i\mathbf{K}\cdot\tau_{\mathbf{j}}} \tag{5.6}$$

Thus, we may write $\hat{H}_0$ as

$$\hat{H}_0 = \begin{pmatrix} \hat{H}_{intra} & \sum_{j=1\ldots3} e^{i\tau_{\mathbf{j}}\cdot\mathbf{K}(')}\hat{H}_{0,\sigma,j} \\ \sum_{j=1\ldots3} e^{-i\tau_{\mathbf{j}}\cdot\mathbf{K}(')}\hat{H}_{0,\sigma,j}^{\dagger} & \hat{H}_{intra} \end{pmatrix} \tag{5.7}$$

where

$$\hat{H}_{intra} = \frac{1}{3}\begin{pmatrix} \epsilon_s & \epsilon_s & \epsilon_s \\ \epsilon_s & \epsilon_s & \epsilon_s \\ \epsilon_s & \epsilon_s & \epsilon_s \end{pmatrix} \tag{5.8}$$

and

$$\hat{H}_{0,\sigma,1} = \begin{pmatrix} H_{11} & H_{12} & H_{12} \\ H_{12} & H_{33} & H_{23} \\ H_{12} & H_{23} & H_{33} \end{pmatrix} \quad \hat{H}_{0,\sigma,2} = \begin{pmatrix} H_{33} & H_{12} & H_{23} \\ H_{12} & H_{11} & H_{12} \\ H_{23} & H_{12} & H_{33} \end{pmatrix} \quad \hat{H}_{0,\sigma,1} = \begin{pmatrix} H_{33} & H_{23} & H_{12} \\ H_{23} & H_{33} & H_{12} \\ H_{12} & H_{12} & H_{11} \end{pmatrix} \tag{5.9}$$

5.3 The pertubative hamiltonian

We are now in a position to calculate the (1+1)nd order perturbation of curvature and spin-orbit coupling, using as our basis (5.1), the $\hat{H}^{curv}_{\pi,\sigma}$ hamiltonian from section 3.3.2 as $\hat{H}_{cv}$ and the part of (4.29) that involves p_z orbitals as $\hat{H}_{so}$ and constructing $\hat{H}_0$ from (5.7), (5.8) and (5.9). Using only the parts of the hamiltonians coupling σ and π orbitals implicitly includes the $\hat{P}_\pi$ and insures that we perturb the low energy states [2] of graphene, since these are precisely the π bands.

The actual calculation is extremely involved, but may be carried out symbolically using a computer (ie. mathematica). The only point one might worry about in this context is, that we usually interpret the division by $\hat{H}_0$ in (5.1) as "diagonalize $\hat{H}_0$, insert the outer product of the eigenstates into the numerator and divide each term by the corresponding eigenvalue". But our $\hat{H}_0$ is a 6x6 matrix, and thus cannot (necessarily) be automatically diagonalized, since this would require solving a 6th order polynomial. This is not a major problem however, since we may equally well interpret $\frac{1}{\hat{H}_0}$ as the inverse matrix of $\hat{H}_0$, ie. $\hat{H}_0^{-1}$, which can be calculated for any dimension, thus avoiding the 6th order polynomial altogether.

The result of this calculation is the following:

$$\hat{H}_{pert} = s_y\tau \begin{pmatrix} \frac{-V^\sigma_{pp} a_0 \alpha_{so} \cos 3\theta}{2\sqrt{6}R(V^\pi_{pp} - V^\sigma_{pp})} & \frac{a_0 \alpha_{so} \epsilon_{2s}(V^\pi_{pp} + V^\sigma_{pp})}{6\sqrt{6}(V^\sigma_{sp})^2} \\ \frac{a_0 \alpha_{so} \epsilon_{2s}(V^\pi_{pp} + V^\sigma_{pp})}{6\sqrt{6}(V^\sigma_{sp})^2} & \frac{-V^\sigma_{pp} a_0 \alpha_{so} \cos 3\theta}{2\sqrt{6}R(V^\pi_{pp} - V^\sigma_{pp})} \end{pmatrix} \equiv s_y\tau \begin{pmatrix} A & B \\ B & A \end{pmatrix} \tag{5.10}$$

In order to understand the results presented above, we wish the effect of it on the lowenergy states. Therefore, we should add it to the effective 0th order hamiltonian with cyclic boundary conditions (3.21), and diagonalize. Recalling that the real part of the off diagonal element of (3.21) is k_c , we see that $+s_y\tau\frac{B2R}{a_0\sqrt{3}(-\gamma_0)}$ (which is real) from (5.10) can seen as a pertubative correction to $\frac{\nu}{3}$, and it is therefore easy to augment the energy expression in (3.22) to an expression for the full, perturbed energy, that is, the energy taking the combined effect of the curvature and spin-orbit coupling into account. As mentioned there is another contribution from the second (and first) order perturbation due to curvature alone, similar in size to the one presented here. which we omit in this part of the thesis, as it is naturally spin-independent, and thus, not relevant for the explanation of the spin-orbit gap problem presented in the beginning of this section, and nor does it contain any terms that break the electron-hole symmetry. There is also a quadratic term in the spin-orbit coupling involving spin-flip processes, but the effect of this term is several orders of magnitude smaller than the one presented here. A more complete discussion of these terms is presented in the next chapter.

[2] ie. the states close to the Fermi level

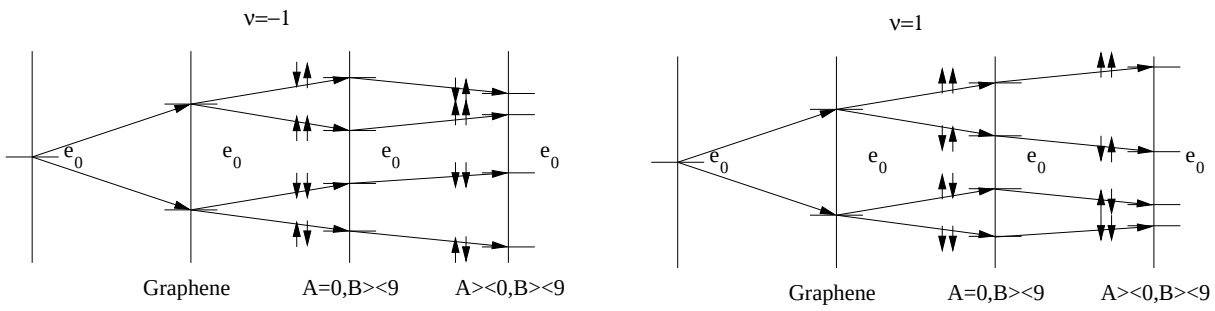

Figure 5.4: The effect of the (1+1)nd order perturbation derived in the text for the two semiconducting families of nanotubes. From left to right in the two diagrams, first the graphene hamiltonian (ie. ν) is introduced, then the B correction from the text is included, and finally the A part is included. The arrows denote in the last two steps denote parallel or antiparallel states.

Thus we find the expression of the perturbed energy

$$E_{eff} = \frac{a_0\sqrt{3}}{2R}(s_y\tau A \mp \gamma_0\sqrt{(\frac{\nu}{3} + \frac{B2R}{\sqrt{3}a_0(-\gamma_0)}s_y\tau)^2 + R^2k_t^2}) \tag{5.11}$$

This expression explains both results presented in the beginning of this chapter: First, recall that we may set $k_t = 0$ due to the assumption of an infinitely long nanotube. so the square root in (5.11) becomes

$$|\frac{\nu}{3} + \frac{B2R}{\sqrt{3}a_0(-\gamma_0)}s_y\tau| \tag{5.12}$$

Thus, if $\frac{\nu}{3}$ and $Bs_y\tau$ have the same sign, there will be a large splitting between the plus and the minus sign on the square root. Now, by inspection of (5.10) we see that B and A are positive numbers (note that for zigzag nanotubes, $\cos 3\theta = 1$), and thus, from the square root alone (ie. ignoring A), we should expect for the "odd" family $\nu = -1$ that the "parallel" states (ie. states with $\tau = s_y$) to be closest to the Fermi level, and the "anti-parallel" states (ie. states where $\tau \neq s_y$) to be farthest away from it. However, since A is a positive number, the parallel states *both* in the conduction and valence bands are shifted upwards, and so, the gap in the conduction band is made narrower, and the gap in the valence band is made wider. For the situation where $\nu = +1$ the situation is the opposite: Here, the parallel states are farthest from the Fermi level and the antiparallel is closest to it, and thus, $s_y\tau A$ widens the gap in the conduction band, and narrows it for the valence band, in agreement with the numerical experiments presented in the beginning of this chapter. I have tried to illustrate this effect in figure 5.4.

Chapter 6

Izumidas derivation

There is a different, perhaps more elegant, way of reaching the effective hamiltonian of a CNT with spin orbit coupling in the literature, namely the one presented by Izumida et al. in [19]. I have chosen not to present it as the main method, mainly to present the (independent) work of me and the Copenhagen group, but I shall still present the calculation in this thesis, which is the subject of this section.

The idea of Izumidas calculation is the same as ours, ie. to attempt to explain the spin-orbit coupling by using perturbation theory of the two perturbations, curvature and spin-orbit interaction using the graphene hamiltonian as the unperturbed system. However, there are several technical differences between the two calculations, and I shall therefore present a relatively thorough derivation of their results.

6.1 Their coordinatesystem

Before going into the derivation of the effective hamiltonian, we must specify the coordinatesystem used by Izumida, and furthermore we shall change the naming convention so as to become similar to ours. The Izumida group, like we, operate with two different coordinate systems, ie. one global and one atomic, defined for each atomic site on the tube. In order to be as close as possible to our own calculation, we rename the axises of [19] so that, for the global coordinate system, the y (not z) axis is along the tube axis, and x and z are in the plane perpendicular to the axis, where the x-coordinate for the (arbitrarily chosen) atom 0 is chosen to be 0, so that the z-direction, for atom 0, is coinciding precisely with the radial direction, and, consequently the x axis is along the circumference at the position of atom 0. Compared to [19] this corresponds to making the transformation $x \to y \to z \to x$ *from* their *to* ours. Similarly, their local coordinate system is defined with origo at a given atom (denoted by subscript l) and having the x axis in the radial direction, the z axis in the tube axis direction and y axis in the circumferential direction. We make the same rotation here as for the global coordinate system, so as to ease comparison between the methods: That is, in the following, the local coordinatesystem has z in the radial direction, x in the circumferential direction and y in the tube axis direction. I have tried to illustrate this in figure 6.1 where I have also included the θ_l angle, which is defined as the angle in a cylindrical

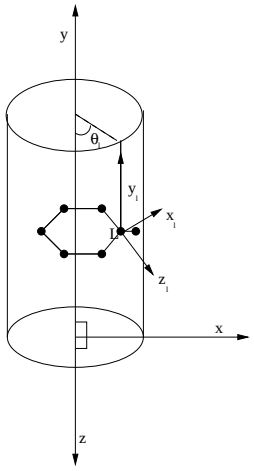

Figure 6.1: The coordinate system used in this thesis to derive the results of Izumida et al.

coordinate system from the 0-atom to the lth atom on the tube, and likewise the y_l coordinate is the cylindrical coordinate along the tube from the 0 atom to the lth atom.

6.2 The effective hamiltonian

The premise, as mentioned, is the same as ours: Consider $\hat{H}_0 = \hat{H}_{graphene}$ from 2 in a perturbation expansion with the perturbation being $\hat{H}' = \hat{H}_{SO} + \hat{H}_{CV}$ being the hamiltonians describing spin-orbit interaction and curvature effects respectively, both of which are assumed to be small in the following calculation, and therefore candidates for perturbation theory. Then, introducing the same nomenclature as in [19], 2nd order perturbation theory (5.1) becomes

$$\langle z\sigma_2 s_2\tau_2|\hat{H}^{(2)}_{eff}|z\sigma_1 s_1\tau_1\rangle = \sum_m \frac{\langle z\sigma_2 s_2\tau_2|\hat{H}'|m\rangle\langle m|\hat{H}'|z\sigma_1 s_1\tau_1\rangle}{-E_m} = \sum_m \frac{\langle z\sigma_2 s_2\tau_2|(\hat{H}_{SO}+\hat{H}_{CV})|m\rangle\langle m|(\hat{H}_{SO}+\hat{H}_{CV})|z\sigma_1 s_1\tau_1\rangle}{-E_m} \tag{6.1}$$

where σ denotes whether a state represents Bloch functions on the A or B atoms, s represents the spin of the state, and τ denotes whether the state is close to the K or the K' point in k-space, and $\langle m|$ and E_m is the state and energy of the σ bands of $\hat{H}_0$ corresponding to one another (thus, the projection operator from (5.1) is implicitly included), and where the Fermi energy has been set to 0. We therefore see that we have in principle three different effective hamiltonians to calculate the matrix elements for, namely one ($\hat{H}^{(2)}_{SOSO}$) that comes from combining the two $\hat{H}_{SO}$s in (6.1), another one ($\hat{H}^{(2)}_{CVCV}$) similarly coming from combining the two $\hat{H}_{CV}$s in (6.1), and one that comes from the two combinations

$$\hat{H}^{(2)}_{SOCV} = \sum_m \frac{\langle z\sigma_2 s_2\tau_2|\hat{H}_{SO}|m\rangle\langle m|\hat{H}_{CV}|z\sigma_1 s_1\tau_1\rangle + \langle z\sigma_2 s_2\tau_2|\hat{H}_{CV}|m\rangle\langle m|\hat{H}_{SO}|z\sigma_1 s_1\tau_1\rangle}{-E_m} \tag{6.2}$$

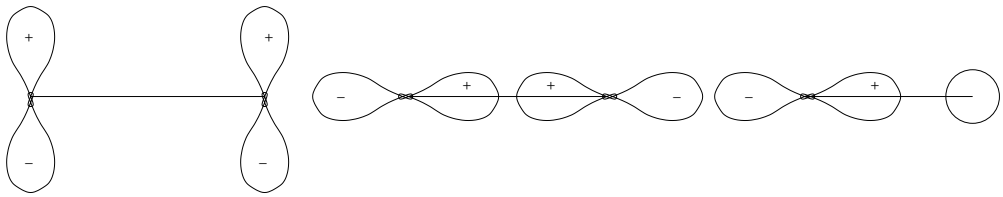

Figure 6.2: The three independent parameters which are not zero by symmetry, denoted H_π, H_σ and H_{sp}, respectively.

describing the process of going into the σ bands (ie. bands composed of the 2s orbitals and the p orbitals lying in the plane of the nanotube) using spin-orbit coupling and then returning to the π bands, which are the states close to the Fermi level, composed of the p orbitals in the radial direction at each atom site, plus the opposite direction, ie. into the σ band by curvature perturbation and back to the π band by spin-orbit coupling. In this section we shall mostly concern ourselves with the $\hat{H}^{(2)}_{SOCV}$ and $\hat{H}^{(2)}_{CVCV}$ (where we shall also include a first order contribution from $\hat{H}_{CV}$) and briefly note that the energy shift from $\hat{H}^{(2)}_{SOSO}$ is of the order of μeV and can thus be safely ignored.

Just as in our own derivation, three things are necessary to evaluate (6.1):

1. The matrix elements from the $|z\sigma s\tau\rangle$ states to all the other states via curvature, ie. the $\langle j\sigma_2 s_2\tau_2|\hat{H}_{CV}|z\sigma s\tau\rangle$ matrix elements, where j represents an atomic $n = 2$ orbital, ie. $2s$, p_x, p_y or p_z.

2. The corresponding matrix elements for $\hat{H}_{SO}$, ie. $\langle j\sigma_2 s_2\tau_2|\hat{H}_{SO}|z\sigma s\tau\rangle$.

3. The energies and eigenstates of the σ bands of $\hat{H}_0$, ie. of graphene.

6.2.1 The $\hat{H}_{CV}$ hamiltonian

The curvature hamiltonian is in principle determined the same way as in chapter 3, ie. we start by calculating the matrix elements for the orbitals on 2 neighbouring atoms (only nearest neighbour hopping is considered in the analytics of [19], just as in our own calculations), and then, differing from our calculation, a trick is used to generalize to the (spin-independent) Bloch-functions, from which the generalization to the (spin-dependent) matrix elements we need is trivial, since curvature effects are spin-independent (so we may simply add another index for spin without considering spin-quantization axis). Now, the fundamental assumption of their derivation is the same as for our calculations, namely that for any hopping element of all the hamiltonians considered, we have

$$\langle j_2\sigma_2|\hat{H}|j_1\sigma_1\rangle \propto \langle j_2\sigma_2|j_1\sigma_1\rangle \tag{6.3}$$

This assumption allows us to parametrize the matrix elements using only 3 parameters, as already seen in chapter 3 - note, that although 4 different couplings was seen in table 3.1, we

shall see that only the three depicted in figure 6.2 are necessary in this derivation. Since we are considering curvature, we need to consider hopping elements from 2p or 2s orbitals to neighbouring 2s or 2p orbitals, where the 2p orbitals is not necessarily perpendicular or parallel to the vector between the two atoms. Here [19] use the same decomposition as we did in 3.25 to obtain the same equation as our 3.26:

$$\begin{aligned}\langle jA0|\hat{H}_{cv}|j'Bl\rangle &= ((\hat{\mathbf{n}}_{\mathbf{0j}} - \frac{\hat{\mathbf{n}}_{\mathbf{0j}}\cdot\mathbf{R_l}}{|\mathbf{R_l}|^2}\mathbf{R_l})\cdot(\hat{\mathbf{n}}_{\mathbf{lj'}} - \frac{\hat{\mathbf{n}}_{\mathbf{lj'}}\cdot\mathbf{R_l}}{|\mathbf{R_l}|^2}\mathbf{R_l}))H_\pi + (\frac{\hat{\mathbf{n}}_{\mathbf{0j}}\cdot\mathbf{R_l}}{|\mathbf{R_l}|}\cdot\frac{-\hat{\mathbf{n}}_{\mathbf{lj'}}\cdot\mathbf{R_l}}{|\mathbf{R_l}|})H_\sigma \\ &= (\hat{\mathbf{n}}_{\mathbf{0j}}\cdot\hat{\mathbf{n}}_{\mathbf{lj'}} - 2\frac{(\hat{\mathbf{n}}_{\mathbf{0j}}\cdot\mathbf{R_l})(\hat{\mathbf{n}}_{\mathbf{lj'}}\cdot\mathbf{R_l})}{|\mathbf{R_l}|^2} + \frac{(\hat{\mathbf{n}}_{\mathbf{0j}}\cdot\mathbf{R_l})(\hat{\mathbf{n}}_{\mathbf{lj'}}\cdot\mathbf{R_l})(\mathbf{R_l}\cdot\mathbf{R_l})}{|\mathbf{R_l}|^4})H_\pi - (\frac{\hat{\mathbf{n}}_{\mathbf{0j}}\cdot\mathbf{R_l}}{|\mathbf{R_l}|}\cdot\frac{\hat{\mathbf{n}}_{\mathbf{lj'}}\cdot\mathbf{R_l}}{|\mathbf{R_l}|})H_\sigma \\ &= (\hat{\mathbf{n}}_{\mathbf{0j}}\cdot\hat{\mathbf{n}}_{\mathbf{lj'}})H_\pi - (\frac{\hat{\mathbf{n}}_{\mathbf{0j}}\cdot\mathbf{R_l}}{|\mathbf{R_l}|}\cdot\frac{\hat{\mathbf{n}}_{\mathbf{lj'}}\cdot\mathbf{R_l}}{|\mathbf{R_l}|})(H_\pi + H_\sigma) \end{aligned} \tag{6.4}$$

where we use [19]s names for the basic hamiltonian overlaps from (3.23) to remind ourselves that there is a sign difference between H_σ and V_{pp}^σ in (3.23). Besides of this difference however, H_π and H_{sp} are the same as V_{pp}^π and H_{sp}^σ, respectively.

Similarly, we desire the overlap between a tilted 2p shell, and a neighbouring 2s shell and, referring to figure 6.2, we see that we need only find the part of the 2p orbital lying along the $\mathbf{R_l}$:

$$\langle jA0|\hat{H}_{cv}|2sBl\rangle = \frac{\hat{\mathbf{n}}_{\mathbf{0j}}\cdot\mathbf{R_l}}{|\mathbf{R_l}|}H_{sp} \tag{6.5}$$

The next step is to relate these matrix elements to the geometry of the CNT. In order for us to explain Izumida et al.s ideas, we choose to remain faithful to the definitions given in the appendix of [19]. First, as noted before, in graphene, and indeed on the nanotube, there are only three different nearest neighbour bonds, where "different" refers to different directions, or components along the tube axis and circumferential directions, exemplified by the three bonds between the 0th (A) atom and its three (B) neighbours. We shall, as in [19], define the first of these to be the one closest to the positive circumferential direction and the second to be the one closest to the positive direction of translational unit vector, ie. the tube axis direction. We wish to specify the vectors of these bonds as an angle in the circumference direction and a length in the translatoric direction, which we will call θ_l and T_l respectively, with l denoting the bond number.

In order to couple the results to the chirality of the CNT, we immediately calculate the dependence of θ_l and T_l on the chiral angle, or rather, on $\phi_c = \frac{\pi}{6} - \theta$, where θ (without subscript) is the chiral angle, defined in the same way as we do in our own calculation , so ϕ_c is the angle between the first bond and the circumferential direction. In the following, we shall make the assumption (as we shall in general for the curvature hamiltonian) that $\frac{a_0}{R}$, where a is the lattice parameter and R is the radius of the nanotube, is a small number, and we can therefore find the components of the vectors representing the bonds using the approximation that the CNT close to atom 0 is almost the same as a graphene sheet. Then, in order to maintain correspondence with the article, we may choose to see the vector of bond number 2 as *opposite* the vector of bond number 1 rotated $\frac{\pi}{3}$, and the vector of bond 3 as *opposite* the vector of bond number 1 rotated $\frac{-\pi}{3}$. This, along with

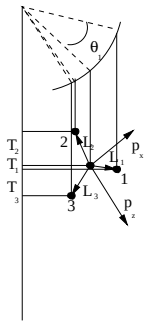

Figure 6.3: The definitions used to calculate $\hat{H}_{so}$ is defined here. Note that only θ_1 is shown, θ_2 and θ_3 follow by obvious extension.

the fact that each bond has the length $\frac{a_0}{\sqrt{3}}$ leads to the following formulas for θ_l and T_l:

$$\theta_l = \gamma_l \frac{a_0}{\sqrt{3}R} \cos(\phi_c + \delta_l) \tag{6.6}$$

$$T_l = -\gamma_l \frac{a_0}{\sqrt{3}} \sin(\phi_c + \delta_l) \tag{6.7}$$

where $\delta_l = (0, \frac{\pi}{3}, -\frac{\pi}{3})$ and $\gamma_l = (1, -1, -1)$. Now from this, it becomes a matter of simple geometry to determine the vectors needed in (6.4) and (6.5) in the global coordinate system, allowing us to start the calculation of the matrix elements: From the definition of the global coordinate system we see, that the unit vectors of the 2p orbitals at atom 0 is simply $\hat{\mathbf{n}}_\mathbf{x} = (1, 0, 0)$, $\hat{\mathbf{n}}_\mathbf{y} = (0, 1, 0)$ and $\hat{\mathbf{n}}_\mathbf{z} = (0, 0, 1)$. The vector $\mathbf{R_l}$ is easily determined from the figure 6.3 as

$$\mathbf{R_l} = (R \sin\theta_l, T_l, R(\cos(\theta_l) - 1)) \tag{6.8}$$

Also shown in figure 6.3 is the two $\hat{\mathbf{n}}_{\mathbf{lj'}}$ in the plane perpendicular to the tube axis. From this we see

$$\hat{\mathbf{n}}_\mathbf{x} = (\cos(\theta_l), 0, -\sin(\theta_l)) \tag{6.9}$$

$$\hat{\mathbf{n}}_\mathbf{z} = (\sin(\theta_l), 0, \cos(\theta_l)) \tag{6.10}$$

Finally, we observe that the unitvector along the tube axis direction is of cause the same for all atoms, regardless of position on the CNT, and therefore we have

$$\hat{\mathbf{n}}_\mathbf{y} = (0, 1, 0) \tag{6.11}$$

Now, calculation of the matrix elements of the atomic curvature hamiltonian proceeds by inserting the relevant equations ((6.6),(6.7),(6.9),(6.11) and (6.10)) into the relevant equations (6.4) and (6.5). The calculations are somewhat tedious but trivial, and so we simply present the results

here:

$$\langle zA0|\hat{H}_{cv}|2sBl\rangle = -\frac{1}{2\sqrt{3}}\frac{a_0}{R}\cos^2(\phi_c+\delta_l)H_{sp} \tag{6.12}$$

$$\langle zA0|\hat{H}_{cv}|xBl\rangle = -\gamma_l\frac{1}{\sqrt{3}}\frac{a_0}{R}\cos(\phi_c+\delta_l)H_\pi - \frac{1}{2}(H_\pi + H_\sigma\cos^2(\phi_c+\delta_l)) \tag{6.13}$$

$$\langle zA0|\hat{H}_{cv}|yBl\rangle = \frac{1}{2\sqrt{3}}\frac{a_0}{R}\gamma_l\sin(\phi_c+\delta_l)\cos^2(\phi_c+\delta_l)(H_\pi+H_\sigma) \tag{6.14}$$

$$\langle zA0|\hat{H}_{cv}|zBl\rangle = -\frac{1}{6}(\frac{a_0}{R})^2\cos^2(\phi_c+\delta_l)(H_\pi - \frac{1}{2}(H_\pi+H_\sigma)\cos^2(\phi_c+\delta_l)) \tag{6.15}$$

The opposite matrix elements, ie. those involving a p_z orbital on the B-atoms, can be determined using a simple symmetry argument: if we consider only two atoms (as we do so far), we may rotate the two nuclei onto one another by a π rotation around an axis going in the radial direction from the tube axis through the point exactly midways between the two nuclei. Such a rotation rotates $|2sA\rangle$ and $|2sB\rangle$ onto one another, and also $|zA\rangle$ and $|zB\rangle$ onto one another, however, $|xA\rangle$ and $|yA\rangle$ is rotated onto $-|xA\rangle$ and $-|yA\rangle$ respectively and thus gives rise to a sign change in the matrix elements, ie.

$$\langle zA0|\hat{H}_{cv}|2sBl\rangle = \langle 2sA0|\hat{H}_{cv}|zBl\rangle \tag{6.16}$$

$$\langle zA0|\hat{H}_{cv}|xBl\rangle = -\langle xA0|\hat{H}_{cv}|zBl\rangle \tag{6.17}$$

$$\langle zA0|\hat{H}_{cv}|yBl\rangle = -\langle yA0|\hat{H}_{cv}|zBl\rangle \tag{6.18}$$

The next step is to determine the matrix elements of $\hat{H}_{cv}$ between various blochfunctions, and since we work with spin independent basis functions in this part, these are naturally defined as

$$|j\sigma\mathbf{k}\rangle = \frac{1}{\sqrt{N_s}}\sum_l e^{i(k_t y_l+\mu\phi_l)}|j\sigma l> \tag{6.19}$$

where N_s is the number of diatomic (primitive) unitcells in the translatoric unitcell, k_t is the k vector component along the tube axis, μ is the (dimensionless) k vector component along the circumference, and y_l and ϕ_l is the position of the σ atom in the lth primitive unitcell, and consequently the sum is over primitive *unitcells*, rather than atoms. Now, before we begin calculating the matrix elements it pays of to make a few general considerations:

First observe that for all the matrix elements we have that

$$\hat{H}_{cv}^{j'A,jB}(\mathbf{k}) \equiv \langle j'A\mathbf{k}|\hat{H}_{cv}|jB\mathbf{k}\rangle = \frac{1}{N_s}\sum_{l,l'} e^{i(k_t(y_l-y_{l'})+\mu(\phi_l-\phi_{l'}))}\langle j'Al'|\hat{H}_{cv}|jBl\rangle =$$

$$\sum_{l=1,3} e^{i(k_tT_l+\mu\theta_l)}\langle j'A0|\hat{H}_{cv}|jBl\rangle = e^{i\frac{a_0}{\sqrt{3}}k_x}\langle j'A0|\hat{H}_{cv}|jB1\rangle +$$

$$e^{i(-\frac{a_0k_x}{2\sqrt{3}}+\frac{a_0k_y}{2})}\langle j'A0|\hat{H}_{cv}|jB2\rangle + e^{i(-\frac{a_0k_x}{2\sqrt{3}}-\frac{a_0k_y}{2})}\langle j'A0|\hat{H}_{cv}|jB3\rangle \tag{6.20}$$

where we have used that the first primitive unitcell (containing atom 0) is pr. definition equivalent to all the other unit cells, and thus, instead of summing over l' we may simply multiply by N_s,

and furthermore, the sum over l can be reduced to three terms, due to the nearest neighbour assumption. In the final equality, we exchange the natural CNT coordinatesystem for the k vector, ie. $\mathbf{k} = (k_t, \frac{\mu}{R})$ with the natural coordinatesystem for graphene, ie. $\mathbf{k} = (k_x, k_y)$ where k_x is the k-vector along the bond we defined above as the first. Since ϕ_c is precisely the angle between the circumferential direction and the first bond, we find the relationship between the coordinatesystems to be

$$\begin{pmatrix} k_x \\ k_y \end{pmatrix} = \begin{pmatrix} \cos\phi_c & -\sin\phi_c \\ \sin\phi_c & \cos\phi_c \end{pmatrix} \begin{pmatrix} \frac{\mu}{R} \\ k_t \end{pmatrix} \tag{6.21}$$

The reason for this change of system is primarily that the K and K' points, where the dispersion relation of graphene and thus possibly also the CNT touches the Fermi level, has a chirality independent definition in the graphene system, and we shall choose the same definitions as Izumida, ie. $K = \frac{2\pi}{a_0}(0, -\frac{2}{3})$ and $K = \frac{2\pi}{a_0}(0, \frac{2}{3})$ which we note is different from the K(') points we have chosen (2.17). They are of cause equivalent, but the final results become superficially different in the end of this chapter: We shall deal with this at that point.

As one further derivation, before finding the actual matrix elements, observe that, if we for brevity denote $A = \langle j'A0|\hat{H}_{cv}|jB1\rangle$, $B = \langle j'A0|\hat{H}_{cv}|jB2\rangle$ and $C = \langle j'A0|\hat{H}_{cv}|jB3\rangle$, we find from (6.20) that

$$\begin{aligned}
&\hat{H}_{cv}^{j'A,jB}(\mathbf{k}) = e^{i\frac{a_0}{\sqrt{3}}k_x}A + e^{i(-\frac{a_0k_x}{2\sqrt{3}}+\frac{a_0k_y}{2})}B + e^{i(-\frac{a_0k_x}{2\sqrt{3}}-\frac{a_0k_y}{2})}C = \\
&e^{i\frac{a_0}{\sqrt{3}}k_x}A + e^{-\frac{ia_0k_x}{2\sqrt{3}}}\frac{1}{2}(e^{\frac{ia_0k_y}{2}}(B+C) + e^{\frac{ia_0k_y}{2}}(B-C) + e^{\frac{-ia_0k_y}{2}}(B+C) - e^{\frac{-ia_0k_y}{2}}(B-C)) = \\
&e^{i\frac{a_0}{\sqrt{3}}k_x}A + e^{-\frac{ia_0k_x}{2\sqrt{3}}}(\cos(\frac{a_0k_y}{2})(B+C) + i\sqrt{3}\sin(\frac{ia_0k_y}{2})\frac{B-C}{\sqrt{3}}) = \\
&e^{i\frac{a_0}{\sqrt{3}}k_x}(\frac{1}{3}(A+B+C) + \frac{1}{3}(2A-B-C)) + e^{-\frac{ia_0k_x}{2\sqrt{3}}}\cos(\frac{a_0k_y}{2})(\frac{2}{3}(A+B+C) \\
&+ \frac{1}{3}(B+C-2A)) + e^{-\frac{ia_0k_x}{2\sqrt{3}}}i\sqrt{3}\sin(\frac{ia_0k_y}{2}\frac{B-C}{\sqrt{3}}) = \\
&\frac{A+B+C}{3}(e^{i\frac{a_0}{\sqrt{3}}k_x} + 2e^{-\frac{ia_0k_x}{2\sqrt{3}}}\cos(\frac{a_0k_y}{2})) + \frac{B+C-2A}{3}(-e^{i\frac{a_0}{\sqrt{3}}k_x} + e^{-\frac{ia_0k_x}{2\sqrt{3}}}\cos(\frac{a_0k_y}{2})) \\
&+ e^{-\frac{ia_0k_x}{2\sqrt{3}}}i\sqrt{3}\sin(\frac{ia_0k_y}{2}\frac{B-C}{\sqrt{3}}) \\
&\equiv \frac{A+B+C}{3}f(\mathbf{k}) + \frac{B+C-2A}{3}g(\mathbf{k}) + \frac{B-C}{\sqrt{3}}h(\mathbf{k})
\end{aligned} \tag{6.22}$$

What is the purpose of this derivation? Our general goal is to determine the effective hamiltonian of the perturbations $\hat{H}_{cv}$ and $\hat{H}_{SO}$ *near the K(K') point.* Therefore, in the end, we wish to find the matrix elements not at general values of $\mathbf{k}$ but specifically at the K and K' points, and one can check that

$$f(K) = f(K') = 0 \tag{6.23}$$

$$g(K) = g(K') = -\frac{3}{2} \tag{6.24}$$

$$h(K) = -h(K') = -i\tau\frac{3}{2} \tag{6.25}$$

where we remember that τ is the valley index, which is 1 for K and -1 for K'. This means that with (6.22) it is now easy to determine the matrix elements between the states at the two valleys: First, we extract the atomic matrix elements from (6.12)-(6.15), then we insert into (6.22) and finally we use the above relations at the K(') point to find the matrix elements at the K(') point. The actual calculation is a rather tedious, repeated application of the 5 wellknown trigonometric relations

$$\cos(\phi_c + \delta_l) = \cos\delta_l \cos\phi_c - \sin\delta_l \sin\phi_c \tag{6.26}$$

$$\sin(\phi_c + \delta_l) = \sin\delta_l \cos\phi_c + \cos\delta_l \sin\phi_c \tag{6.27}$$

$$\sin(\alpha)\cos(\beta) = \frac{1}{2}(\sin(\alpha-\beta) + \sin(\alpha+\beta)) \tag{6.28}$$

$$\cos(\alpha)\cos(\beta) = \frac{1}{2}(\cos(\alpha-\beta) + \cos(\alpha+\beta)) \tag{6.29}$$

$$\sin(\alpha)\sin(\beta) = \frac{1}{2}(\cos(\alpha-\beta) - \cos(\alpha+\beta)) \tag{6.30}$$

However, the calculation is essentially trivial, and so we simply present the results:

$$\langle zA\mathbf{k}|\hat{H}_{cv}|2sB\mathbf{k}\rangle = -\frac{1}{4\sqrt{3}}\frac{a_0}{R}H_{sp}(f(\mathbf{k}) - \cos 2\phi_c g(\mathbf{k}) - \sin 2\phi_c h(\mathbf{k})) \tag{6.31}$$

$$\langle zA\mathbf{k}|\hat{H}_{cv}|xB\mathbf{k}\rangle = \frac{1}{8\sqrt{3}}\frac{a_0}{R}(H_\pi + H_\sigma)f(\mathbf{k})\cos 3\phi_c + (5H_\pi - 3H_\sigma)(\cos\phi_c g(\mathbf{k}) - \sin\phi_c h(\mathbf{k})) \tag{6.32}$$

$$\langle zA\mathbf{k}|\hat{H}_{cv}|yB\mathbf{k}\rangle = \frac{1}{8\sqrt{3}}\frac{a_0}{R}(H_\pi + H_\sigma)(-f(\mathbf{k})\sin 3\phi_c + \sin\phi_c g(\mathbf{k}) + \cos\phi_c h(\mathbf{k})) \tag{6.33}$$

$$\begin{aligned}\langle zA\mathbf{k}|\hat{H}_{cv}|zB\mathbf{k}\rangle = H_\pi f(\mathbf{k}) - \frac{1}{96}(\frac{a_0}{R})^2(f(\mathbf{k})(5H_\pi - 3H_\sigma) - 4(H_\pi - H_\sigma)(\cos 2\phi_c g(\mathbf{k}) + \sin 2\phi_c h(\mathbf{k}))\\ + (H_\pi + H_\sigma)(\cos 4\phi_c g(\mathbf{k}) - \sin 4\phi_c h(\mathbf{k})))\end{aligned} \tag{6.34}$$

note that in (6.34) we have actually included the graphene hopping element ($f(\mathbf{k})H_\pi$), and so, as far as the p_z orbitals are concerned, the above equations actually the full hamiltonian, except for spin-orbit coupling. This is the reason why Izumida et al. calls them $\hat{H}_0$ rather than, as we have chosen, $\hat{H}_{cv}$, but note, that the $\sigma - \sigma$ curvature coupling is not included: We shall not need this part of the hamiltonian (just as, in fact, we did not need it in our own calculation - it was included in chapter 3 only for completeness)

The final step in the derivation of $\hat{H}_{cv}$ is to find the matrix elements for any valley and any A-B subspace states. The valley part is easily accomplished, since it simply consists of using (6.23) to (6.25) in (6.31) to (6.34). The subspace part of the calculation is essentially based on two things:

First, (6.3) means that there is always a factor $\delta_{\sigma,-\sigma'}$ in this matrix: orbitals at the same atom are orthogonal and we also use the nearest neighbour assumption.

Second, observe, that since (6.31)-(6.34) are essentially linear combinations of each of the matrix elements (6.12)-(6.15), they transform the same way under exchange of the sublattices, ie. we can use the symmetries presented in (6.16)-(6.18), along with the general property of inner products that

$$\langle\Psi_1|\hat{H}|\Psi_2\rangle = \langle\Psi_2|\hat{H}|\Psi_1\rangle^* \tag{6.35}$$

to find the effect of exchanging the sublattices, and thus expressing a general formula of the form desired.

These calculations are in principle trivial, but for clarity we shall present the full calculation for one of the matrix elements, namely $\langle y\sigma'\tau|\hat{H}_{cv}|z\sigma\tau\rangle$:

$$\langle zA\mathbf{k}|\hat{H}_{cv}|yB\mathbf{k}\rangle[\text{from (6.33)}] = \frac{1}{8\sqrt{3}}\frac{a_0}{R}(H_\pi + H_\sigma)(-f(\mathbf{k})\sin 3\phi_c + \sin\phi_c g(\mathbf{k}) + \cos\phi_c h(\mathbf{k}))$$

$\Downarrow$ [from (6.23)-(6.25)]

$$\langle zA\tau|\hat{H}_{cv}|yB\tau\rangle = -\frac{\sqrt{3}}{16}\frac{a_0}{R}(H_\pi + H_\sigma)(\sin\phi_c + i\tau\cos\phi_c) = -i\tau\frac{\sqrt{3}}{16}\frac{a_0}{R}(H_\pi + H_\sigma)e^{-i\tau\phi_c} \tag{6.36}$$

$$\langle zB\tau|\hat{H}_{cv}|yA\tau\rangle = [\text{from (6.35)}]\langle yA\tau|\hat{H}_{cv}|zB\tau\rangle^* = [\text{from (6.18)}] - \langle zA\tau|\hat{H}_{cv}|yB\tau\rangle^* =$$

$$-i\tau\frac{\sqrt{3}}{16}\frac{a_0}{R}(H_\pi + H_\sigma)e^{i\tau\phi_c} \tag{6.37}$$

By inspection of (6.36) and (6.37), we see that we, remembering the delta-kornecher function mentioned above, may write

$$\langle z\sigma\tau|\hat{H}_{cv}|y\sigma'\tau\rangle = -i\tau\frac{\sqrt{3}}{16}\frac{a_0}{R}(H_\pi + H_\sigma)e^{-i\sigma\tau\phi_c}\delta_{\sigma,-\sigma'} \tag{6.38}$$

The other four elements of $\hat{H}_{cv}$ are found in the same manner, and here we only present the results of the calculations:

$$\langle z\sigma\tau|\hat{H}_{cv}|2s\sigma'\tau\rangle = -\frac{\sqrt{3}}{8}\frac{a_0}{R}H_{sp}e^{i2\sigma\tau\phi_c}\delta_{\sigma,-\sigma'} \tag{6.39}$$

$$\langle z\sigma\tau|\hat{H}_{cv}|x\sigma'\tau\rangle = -\sigma\frac{\sqrt{3}}{16}\frac{a_0}{R}(5H_\pi - 3H_\sigma)e^{-i\sigma\tau\phi_c}\delta_{\sigma,-\sigma'} \tag{6.40}$$

$$\langle z\sigma\tau|\hat{H}_{cv}|z\sigma'\tau\rangle = -\frac{1}{64}(\frac{a_0}{R})^2(4(H_\pi - H_\sigma)e^{i2\sigma\tau\phi_c} - (H_\pi + H_\sigma)e^{i4\sigma\tau\phi_c})\delta_{\sigma,-\sigma'} \tag{6.41}$$

Eqns. (6.38)-(6.41) finishes our derivation of the curvature hamiltonian - next is the derivation of the spin-orbit hamiltonian.

6.2.2 $\hat{H}_{SO}$

Izumida et al makes the same simplifying assumption as we do, namely that the spin-orbit hamiltonian is intra atomic, due to the assumption that the only electric field strong enough to make a noticeable contribution to spin-orbit coupling is due to the nuclei, and then only in the close vicinity of the nuclei, so as to only couple orbitals around that same atom. Thus, along with [19] we may write, remembering (4.20)

$$\hat{H}_{SO,l} = \frac{\alpha_{so}}{2}\hat{\mathbf{L}}_\mathbf{l}\cdot\hat{\mathbf{s}}_\mathbf{l} \tag{6.42}$$

where l is the subscript for the atom and the $\hat{\mathbf{L}}_\mathbf{l}$ and $\hat{\mathbf{s}}_\mathbf{l}$ operators are the orbital and spin angular momentum operators, *defined in the local coordinatesystem of the lth atom*, a fact that we shall

see later is of crucial importance. Now, below we shall see that the only good quantization axis for the spin is the y-direction, and thus we choose to write

$$\hat{H}_{SO,l} = \frac{\alpha_{so}}{2}(\hat{L_{y,l}} \cdot \hat{s_{y,l}} + \hat{L}_{+,y,l}\hat{s}_{-,y,l} + \hat{L}_{-,y,l}\hat{s}_{+,y,l}) \tag{6.43}$$

where $\hat{L}(\hat{s})_{+(-),y,l}$ is the ladder operators for the orbital and spin angular momentum in the y direction. We see that this is exactly the same as our expression (4.20), and so we can use the matrix elements evaluated in (4.27).

This is a good point to elaborate on the symmetry adapted blochfunctions that Izumida et al introduces in section 2 of their article, and which shall have a crucial importance in chapter 8: The first guess for a symmetry adapted (ie. invariant under the CNT symmetries) blochfunction would be simply to stick a *global* spin quantum number into the $|j\sigma k_t\mu\rangle$ spin-independent blochstates, giving us

$$|j\sigma k_t\mu s\rangle = \frac{1}{\sqrt{N_s}}\sum_l e^{i(k_t z_l + \mu\theta_l)}|j\sigma z_l\theta_l\rangle|s\rangle \tag{6.44}$$

From this expression it is obvious that we should choose y as the spin-quantization axis, since any other direction wouldn't be preserved under the screw symmetry operation. However, even if we do this, we still have a problem: Since the coordinate system of the spin part of the Bloch states is global, it doesn't remain invariant under the screw symmetry, even if the $|s_y\rangle$ states do: To make this particular point obvious, remember that we should also demand that linear combinations of the Bloch states be invariant under the symmetry operations. One such linear combination could be

$$|j\sigma k_t\mu s_y\rangle + |j\sigma k_t\mu - s_y\rangle = |j\sigma k_t\mu\downarrow_z\rangle \tag{6.45}$$

and clearly, the global coordinatesystems z axis is *not* preserved under the screw symmetry. In order to fix this, Izumida et al chooses to use the *local* coordinate system to represent the spin at any given atom by rotating the spin coordinatesystem around our y-axis (their z-axis) giving a factor of $e^{-i\frac{\theta_l}{2}s_y}$, since the local coordinatesystem at atom l is rotated θ_l compared to the coordinatesystem of the spin-functions, ie. we have

$$|s_{l,y}\rangle = e^{-i\frac{\theta_l}{2}s_y}|s\rangle \tag{6.46}$$

So, for example we may calculate $\langle j\sigma'\tau's'_l|\hat{H}_{so}|z\sigma\tau s_l\rangle$ in the global spin-coordinatesystem:

$$\begin{aligned}
&\langle j\sigma'\tau's'_l|\hat{H}_{SO}|z\sigma\tau s_l\rangle = \langle j\sigma'\tau's'_l|\frac{\alpha_{so}}{2}(s_l|p_y\sigma\tau,-s_l\rangle + is_l|p_x\sigma\tau,s_l\rangle) = \\
&\langle j\sigma'\tau's|e^{i\frac{\theta_l}{2}s}\frac{\alpha_{so}}{2}(se^{i\frac{\theta_l}{2}s}|p_y\sigma\tau,-s\rangle + ise^{-i\frac{\theta_l}{2}s}|p_x\sigma\tau,s\rangle) = \\
&\langle j\sigma'\tau's|\frac{\alpha_{so}}{2}(se^{i\theta_l s}|p_y\sigma\tau,-s\rangle + is|p_x\sigma\tau,s\rangle) = \\
&\frac{V_s o}{2}(e^{is\theta_l}s\delta_{\sigma',\sigma}\delta_{\tau',\tau}\delta_{-s',s}\delta_{j,p_y} + is\delta_{\sigma',\sigma}\delta_{\tau',\tau}\delta_{s',s}\delta_{j,p_x})
\end{aligned} \tag{6.47}$$

Note, that we can freely exchange the eigen*values* of the spin, due to the fact that we chose the y axis as quantization axis. We see the same encouraging fact that was also seen in section 5.2:the

first, spin-altering term of (6.47) has a factor of $e^{is\theta_l}$, which, when combined with the other, spin-independent phase of the blochstates from (6.44), alters the orbital angular part of the blochphase to insure conservation of total angular moment. That this is in fact so is seen from the fact that, if we find $|s\rangle$ from (6.46) and insert it into (6.44) we get Izumida et als symmetry adapted blochfunctions:

$$|j\sigma\tilde{s}\mathbf{k}_J\rangle = \frac{1}{\sqrt{N_s}}\sum_l e^{i(k_t z_l + J\theta_l)}|j\sigma z_l\theta_l s_l\rangle \tag{6.48}$$

where $J = \mu + \frac{1}{2}$ and the over s in the ket signifies that the spin is measured in the linear combination of local spin-coordinatesystems, rather than in the global coordinatesystem. Note that two states of the form (6.44) goes into a single value of J, namely (taking only the angular quantum numbers) $|\mu\uparrow\rangle$ and $|\mu{+}1\downarrow\rangle$. This makes it evident that the new, total angular momentum quantum number J is invariant under $\hat{H}_{so}$, since it couples only states with both the same μ and s, or states with $\mu' = \mu \pm 1$ and corresponding $s' = s \mp 1$, all of which have the same J value.

The final note on the spin-orbit hamiltonian has to do with the relative relevance of the two terms in (6.47) to second order perturbation theory, hinted at in the previous chapter: Since the curvature hamiltonian is angular momentum preserving, we see that the spin altering term would only enter into a second order perturbation of $\hat{H}_{so}$, and so we see that the prefactor for this effect is

$$\hat{H}^{(2)}_{SOSO} \propto \frac{\alpha^2_{so}}{E_{\mu\pm1}} \tag{6.49}$$

The other, spin preserving term on the other hand, couples the π bands to states that can be "sent back" to the π bands by $\hat{H}_{CV}$, and so the prefactor for these terms will be

$$\hat{H}^{(2)}_{SOCV} \propto \frac{\alpha_{so}a_0}{RE_\mu} \tag{6.50}$$

We shall (as Izumida et al.) assume that we are dealing with tubes with sufficiently small radii that we can neglect the spin altering terms from here on, but it is of cause important to realize that for sufficiently large nanotubes there is another effect that comes into play (indeed, the $\hat{H}^{(2)}_{SOSO}$, also called the *intrinsic* spin-orbit coupling, is the only term in graphene, which may be thought of as an infinitely large CNT [13]).

6.2.3 The graphene hamiltonian $\hat{H}_0$

The last "ingredient" for the second order perturbation theory is the eigenfunctions and energies of the graphene hamiltonian $\hat{H}_0$. One can of cause do what we did in previous chapters and use the standard, real 2p orbitals in-plane (ie. the "σ" orbitals), geometrically calculate the overlap in essentially the same way as we did above for the curvature hamiltonian, and then solve it to yield the desired eigenfunctions and energies. However, Izumida et al. have a symmetry to blockdiagonalize the hamiltonian into three 2x2 matrices:

Notice, that we need only calculate the hamiltonian at the K and K' point. Now, we can calculate what the Bloch phase on the atoms surrounding the zeroth atom (on the A sublattice),

as done in e.g. [13], using the convention $K(') = (0, -\tau\frac{2\pi}{a_0}\frac{2}{3})$:

$$\phi_{Bloch,1} = K(') \cdot \mathbf{l_1} = \begin{pmatrix} 0 \\ -\tau\frac{2\pi}{a_0}\frac{2}{3} \end{pmatrix} \cdot \begin{pmatrix} \frac{a_0}{\sqrt{3}} \\ 0 \end{pmatrix} = 0 \tag{6.51}$$

$$\phi_{Bloch,2} = K(') \cdot \mathbf{l_1} = \begin{pmatrix} 0 \\ -\tau\frac{2\pi}{a_0}\frac{2}{3} \end{pmatrix} \cdot \begin{pmatrix} -\frac{a_0}{2\sqrt{3}} \\ \frac{a_0}{2} \end{pmatrix} = -\tau\frac{2\pi}{3} \tag{6.52}$$

$$\phi_{Bloch,3} = K(') \cdot \mathbf{l_1} = \begin{pmatrix} 0 \\ -\tau\frac{2\pi}{a_0}\frac{2}{3} \end{pmatrix} \cdot \begin{pmatrix} -\frac{a_0}{2\sqrt{3}} \\ -\frac{a_0}{2} \end{pmatrix} = \tau\frac{2\pi}{3} \tag{6.53}$$

Notice, that it is important that we define the zeroth atom to be on the A sublattice: If we were to find the relative blochphase of the atoms surrounding a B atom, the $\mathbf{l_l}$ vectors direction would be inverted, ie. we would have $-\mathbf{l_l}$ at all places of the above calculations, giving us an opposite sign in the results, since scalar product is linear. This can be conveniently expressed as

$$\phi_{Bloch,1} = 0 \quad \phi_{Bloch,2} = -\sigma\tau\frac{2\pi}{3} \quad \phi_{Bloch,3} = \sigma\tau\frac{2\pi}{3} \tag{6.54}$$

where σ stands for the sublattice of the implied zeroth atom.

Already here, we glimpse the outline of the technique used to blockdiagonalize the hamiltonian: Let us try to calculate $\langle 2sA\tau|\hat{H}|2sB\tau\rangle$:

$$\begin{aligned}
&\langle 2sA\tau|\hat{H}|2sB\tau\rangle = \frac{1}{N_s}\sum_{l,l'} e^{i(\mathbf{l_l}-\mathbf{l_{l'}})\cdot(0,-\tau\frac{2\pi}{a_0}\frac{2}{3})}\langle 2sAl'|\hat{H}|2sBl\rangle = \\
&\sum_{l=1..3} e^{i\mathbf{l_1}\cdot(0,-\tau\frac{2\pi}{a_0}\frac{2}{3})}\langle 2sA0|\hat{H}|2sBl_l\rangle = \langle 2sA0|\hat{H}|2sBl_1\rangle \sum_{l=1..3} e^{i\phi_{Bloch}} = \\
&\langle 2sA0|\hat{H}|2sBl_l\rangle \times 0 = 0
\end{aligned} \tag{6.55}$$

In the second equality we used the nearest neighbour assumption, and in the third, we used the fact that the 2s orbitals are rotationally invariant, and so the only difference when calculating the matrix elements to B atom 1, 2 and three is the different blochphases on these atoms. Now, for the other components of the σ orbitals, p_x and p_y, the rotational dependence is not so easy to include in our calculation, since it would be some trigonometric dependence on the angle between the bonds from the A atom. There is, however another set of orbitals more suited for precisely this sort of thing, namely the spherical harmonics we originally used to construct the real 2p orbitals. Recall that

$$|nlm\rangle = F(n,l)e^{im\phi} \tag{6.56}$$

and also that

$$|21\chi\rangle = \frac{1}{\sqrt{2}}(-\chi|p_x\rangle - i|p_y\rangle) \tag{6.57}$$

where $\chi = \pm 1$ has been introduced as a parameter denoting which one of the spherical harmonics we are referring to. Now, in analogy with derivation (6.55), we wish to express $\langle (21\chi)A0|\hat{H}|2sB_l\rangle$ for $l = 2, 3$ as a multiplum of a phase factor and $\langle (21\chi)A0|\hat{H}|2sB_1\rangle$. Of cause, the part of the

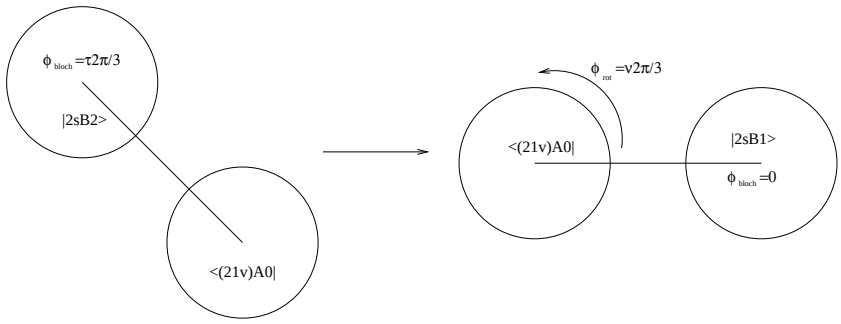

Figure 6.4: The rotational symmetry of the (21χ) at the K(') points relevance for matrix element calculation is seen here for an example of $\langle(21\chi)A0|\hat{H}|2sB2\rangle$: In order to make $\langle(21\chi)A0|\hat{H}|2sB2\rangle$ look like$\langle(21\chi)A0|\hat{H}|2sB1\rangle$, we have to rotate the orbital on the A atom $\frac{2\pi}{3}$. We also remember the blochphase, and the fact that we rotate the bra, not the ket, which gives us an extra minus sign in the calculation in the text.

phase that comes from the Bloch nature of the functions is the same as it was in derivation (6.55), but there is now an extra phase stemming from the fact, that the direction towards e.g. B atom 2 ($\mathbf{l_2}$) is rotated $\frac{2\pi}{3}$ around the z-axis compared to the bond towards $\mathbf{l_1}$, and so, due to the rotational dependence of the $|21\chi\rangle$ functions (6.56), if we imagine looking at the $|21\chi A\rangle$ orbital from B atom 2, compared to the same function "seen" from B atom 1, the only difference will be a phase factor of $\chi\frac{2\pi}{3}$. However, we must also remember that we wish to find the complex conjugate of this rotation, since we need $\langle 21\chi|$, rather than $|21\chi\rangle$. Therefore, we finally find, we may write

$$\langle(21\chi)A0|\hat{H}|2sB_2\rangle = e^{i\frac{2\pi}{3}(-\chi-\tau)}\langle(21\chi)A0|\hat{H}|2sB_1\rangle \tag{6.58}$$

This is illustrated in figure 6.4

For the last bond we see that both the rotation and the blochphase changes sign, and we therefore get

$$\langle(21\chi)A0|\hat{H}|2sB_3\rangle = e^{i\frac{2\pi}{3}(\chi+\tau)}\langle(21\chi)A0|\hat{H}|2sB_1\rangle \tag{6.59}$$

Now calculating $\langle(21\chi)A\tau|\hat{H}|2sB\tau\rangle$ is simple:

$$\begin{aligned}\langle(21\chi)A\tau|\hat{H}|2sB\tau\rangle &= \sum_{l=1..3} e^{i\mathbf{l_1}\cdot(0,-\tau\frac{2\pi}{a_0}\frac{2}{3})}\langle(21\chi)A0|\hat{H}|2sBl_l\rangle = \langle(21\chi)A0|\hat{H}|2sB1\rangle \\ (1+e^{i\frac{2\pi}{3}(-\tau-\chi)}+e^{i\frac{2\pi}{3}(\tau+\chi)}) &= 3\delta_{\tau,-\chi}\langle(21\chi)A0|\hat{H}|2sB1\rangle \end{aligned} \tag{6.60}$$

where the final delta-kornecher is derived from the fact that if τ and χ are the same, the phase factors becomes $1+e^{i\frac{2\pi}{3}}+e^{-i\frac{2\pi}{3}}=0$. An equivalent calculation for $\langle(21\chi)B\tau|\hat{H}|2sA\tau\rangle$ gives

$$\begin{aligned}\langle(21\chi)B\tau|\hat{H}|2sA\tau\rangle &= \sum_{l=1..3} e^{i\mathbf{l_1}\cdot(0,-\tau\frac{2\pi}{a_0}\frac{2}{3})}\langle(21\chi)B0|\hat{H}|2sAl_l\rangle = \langle(21\chi)B0|\hat{H}|2sA1\rangle \\ (1+e^{i\frac{2\pi}{3}(-\tau+\chi)}+e^{i\frac{2\pi}{3}(\tau-\chi)}) &= 3\delta_{\tau,\chi}\langle(21\chi)B0|\hat{H}|2sA1\rangle \end{aligned} \tag{6.61}$$

where the sign change on χ in the last line comes from the σ dependence of (6.54). Notice that from (6.60) and (6.61) we may write

$$\begin{aligned}&\langle(21\chi)\sigma\tau|\hat{H}|2s\sigma'\tau\rangle = 3\delta_{-\sigma\tau,\chi}\langle(21\chi)\sigma 0|\hat{H}|2s\sigma' 1\rangle\delta_{\sigma,-\sigma'} = \\ &3\langle(21-\sigma\tau)\sigma 0|\hat{H}|2s\sigma' 1\rangle\delta_{\sigma,-\sigma'}\end{aligned} \tag{6.62}$$

The last thing to calculate is the overlap between two $|(21\chi)\rangle$ orbitals on neighbouring sites. If, in figure 6.4 we replace the 2s orbital with another $|(21\chi')\rangle$ orbital, we see, that in order to get from the bond $\mathbf{l_2}$ to the bond $\mathbf{l_1}$, we need to rotate the $|(21\chi')\rangle$ on the B atom as well, in the same direction as the A atom, on top of the phase factors already found above. Specifically, we find the matrixelement is

$$\begin{aligned}&\langle(21\chi)A\tau|\hat{H}|(21\chi')B\tau\rangle = \sum_{l=1..3} e^{i\mathbf{l_1}\cdot(0,-\tau\frac{2\pi}{a_0}\frac{2}{3})}\langle(21\chi)A0|\hat{H}|(21\chi')Bl_l\rangle = \\ &\langle(21\chi)A0|\hat{H}|(21\chi')B1\rangle(1+e^{i\frac{2\pi}{3}(-\tau-\chi+\chi')}+e^{i\frac{2\pi}{3}(\tau+\chi-\chi')}) = \\ &3\delta_{\tau,\chi}\delta_{\chi,-\chi'}\langle(21\chi)A0|\hat{H}|(21\chi')B1\rangle = 3\langle(21\tau)A0|\hat{H}|(21-\tau)B1\rangle\end{aligned} \tag{6.63}$$

By carefully inspecting the results (6.60), (6.61) and (6.63), we find, that we have in fact found a good basis in which the hamiltonian is composed of 3 2x2 blockdiagonal matrices, since the $|21\chi\rangle$ orbitals combine with either another $|21\chi\rangle$ orbital or a 2s on the other sublattice, but not both.

In order to calculate the actual eigenfunctions and energies, we need the atomic overlaps, but that is simple using (6.57) and using the formulas (6.4) and (6.5) with the two simplifications that there is no curvature, and we need only consider $\mathbf{R_1}$. Note however, that for the calculation arising from (6.62), we need to have both $\mathbf{R_1}$, going from the A to the B sublattice, and $-\mathbf{R_1}$ going from the B to the A sublattice. This we shall take into account by using $\sigma\mathbf{R_1}$, since this will exactly take care of this issue. From the fact that there is no curvature, we see that $\hat{\mathbf{n_{x,1}}} = (1,0,0)$ and $\hat{\mathbf{n_{y,1}}} = (0,1,0)$, and also $\sigma\mathbf{R_1} = \sigma\frac{a_0}{\sqrt{3}}(\cos\phi_c, -\sin\phi_c, 0)$. We thus find

$$\begin{aligned}&3\langle(21-\sigma\tau)\sigma 0|\hat{H}|2s\sigma' 1\rangle\delta_{\sigma,-\sigma'} = \frac{3}{\sqrt{2}}(\sigma\tau\langle x\sigma 0|\hat{H}|2s\sigma' 1\rangle + i\langle y\sigma 0|\hat{H}|2s\sigma' 0\rangle) = \\ &\frac{3H_{sp}}{\sqrt{2}}(\sigma\tau\frac{\sigma\mathbf{R_1}\cdot\hat{\mathbf{n_x}}}{|\mathbf{R_1}|}+i\frac{\sigma\mathbf{R_1}\cdot\hat{\mathbf{n_y}}}{|\mathbf{R_1}|}) = \frac{3H_{sp}}{\sqrt{2}}(\sigma\tau\frac{\sigma a/\sqrt{3}\cos\phi_c}{a/\sqrt{3}}+i\frac{-\sigma a_0/\sqrt{3}\sin\phi_c}{a_0/\sqrt{3}}) = \\ &\frac{3H_{sp}}{\sqrt{2}}\tau(\cos\phi_c - i\sigma\tau\sin\phi_c) = \frac{3H_{sp}}{\sqrt{2}}\tau e^{-i\sigma\tau\phi_c}\end{aligned} \tag{6.64}$$

and

$$
\begin{aligned}
&3\langle(21\tau)A0|\hat{H}|(21-\tau)B1\rangle = \frac{3}{2}((-\tau\langle xA0| + i\langle yA0|)\hat{H}(\tau|xB0\rangle - i|yB0\rangle)) = \\
&\frac{3}{2}(-\langle xA0|\hat{H}|xB0\rangle + \langle yA0|\hat{H}|yB0\rangle + i\tau(\langle yA0|\hat{H}|xB0\rangle + \langle xA0|\hat{H}|yB0\rangle)) = \\
&\frac{3}{2}(-(H_\pi \mathbf{n}_{\mathbf{x},\mathbf{0}}\hat{} \cdot \mathbf{n}_{\mathbf{x},\mathbf{1}}\hat{} - (H_\pi + H_\sigma)\frac{(\mathbf{R_1}\cdot \mathbf{n}_{\mathbf{x},\mathbf{0}}\hat{})(\mathbf{R_1}\cdot \mathbf{n}_{\mathbf{x},\mathbf{1}}\hat{})}{|\mathbf{R_1}|^2})+ \\
&(H_\pi \mathbf{n}_{\mathbf{y},\mathbf{0}}\hat{} \cdot \mathbf{n}_{\mathbf{y},\mathbf{1}}\hat{} - (H_\pi + H_\sigma)\frac{(\mathbf{R_1}\cdot \mathbf{n}_{\mathbf{y},\mathbf{0}}\hat{})(\mathbf{R_1}\cdot \mathbf{n}_{\mathbf{y},\mathbf{1}}\hat{})}{|\mathbf{R_1}|^2}) \\
&+ i\tau((H_\pi \mathbf{n}_{\mathbf{x},\mathbf{0}}\hat{} \cdot \mathbf{n}_{\mathbf{y},\mathbf{1}}\hat{} - (H_\pi + H_\sigma)\frac{(\mathbf{R_1}\cdot \mathbf{n}_{\mathbf{x},\mathbf{0}}\hat{})(\mathbf{R_1}\cdot \mathbf{n}_{\mathbf{y},\mathbf{1}}\hat{})}{|\mathbf{R_1}|^2})+ \\
&(H_\pi \mathbf{n}_{\mathbf{y},\mathbf{0}}\hat{} \cdot \mathbf{n}_{\mathbf{x},\mathbf{1}}\hat{} - (H_\pi + H_\sigma)\frac{(\mathbf{R_1}\cdot \mathbf{n}_{\mathbf{y},\mathbf{0}}\hat{})(\mathbf{R_1}\cdot \mathbf{n}_{\mathbf{x},\mathbf{1}}\hat{})}{|\mathbf{R_1}|^2}))) = \\
&\frac{3}{2}(H_\pi - (H_\pi + H_\sigma)\cos^2\phi_c - H_\pi + (H_\pi - H_\sigma)\sin^2\phi_c + i\tau 2(H_\pi + H_\sigma)\sin\phi_c\cos\phi_c) = \\
&\frac{3}{2}(H_\pi + H_\sigma)(\cos 2\phi_c + i\tau\sin 2\phi_c) = \frac{3}{2}(H_\pi + H_\sigma)e^{i2\phi_c\tau}
\end{aligned}
\tag{6.65}
$$

This establishes the off-diagonal elements of the graphene hamiltonian. The diagonal elements fall into two categories: Those between 2s orbitals and those between 2p orbitals (Izumida et al. also makes the assumption that the energy of any 2p shell is the same as any other 2p shell). Along with [19] we set $\langle 2p\sigma|\hat{H}|2p\sigma\rangle = 0$ and define $\epsilon_{2s} = \langle 2s\sigma|\hat{H}|2s\sigma\rangle$, as in our own calculation.

With the graphene hamiltonian established, we can find the eigenvalues and eigenfunctions that we need for the perturbation. This calculation is simple but tedious, and so we shall simply present the results here:

For the two block matrices coming from overlap between $|2s\rangle$ and $|21\chi\rangle$ orbitals we get the same two eigenvalues for both:

$$E_{(2s,21\chi),\eta} = \frac{1}{2}(\epsilon_{2s} + \eta\sqrt{\epsilon_{2s}^2 + 18H_{sp}}) \tag{6.66}$$

and, defining $c_\eta = \sqrt{\frac{\eta E_{(2s,21\chi),\eta}}{E_{(2s,21\chi),+1} - E_{(2s,21\chi),-1}}}$, the eigenfunctions

$$|m_{(2s,21\chi)}, \eta\sigma\tau\rangle = -\eta\tau c_\eta|2s - \sigma\tau\rangle + c_{-\eta}e^{-i\sigma\tau\phi_c}|(21-\sigma\tau)\sigma\tau\rangle \tag{6.67}$$

where $\eta = \pm 1$ denotes conduction/valence band. Note that there are 4 eigenfunctions for a given point in k-space (ie. a given τ): 2 possible η values times 2 possible values of σ.

For the third blockmatrix we find the eigenvalues

$$E_{(21\chi,21\chi),\eta} = \frac{3}{2}\eta(H_\pi + H_\sigma) \tag{6.68}$$

and the eigenfunctions

$$|m_{(21\chi,21\chi),\eta\tau}\rangle = \frac{1}{\sqrt{2}}\sum_\sigma (-1)^{\frac{1-\eta}{2}\frac{1-\sigma}{2}}e^{i\sigma\tau\phi_c}|(21\sigma\tau)\sigma\tau\rangle \tag{6.69}$$

At last, we are now ready to derive the effective hamiltonian: Using (6.38)-(6.40) for $\hat{H}_{CV}$, (6.47) for $\hat{H}_{so}$ (or in fact, only the spin preserving part of (6.47), since we are interested only in intra-subband processes) and (6.66),(6.67),(6.68) and (6.69) for $|m\rangle$ and E_m in equation (6.2) for the perturbation theory, we may finally derive the matrices we set out to find.

6.2.4 $\hat{H}^{(2)}_{SOCV}$ and $\hat{H}^{(2)}_{CVCV}$

The derivation leading to the two desired hamiltonians are now in principle trivial, but rather involved: For completeness we shall go through them here. It is a good idea to find the 4 matrix elements that shall be needed, as done in [19], namely the matrixelement between $|z\sigma s\tau\rangle$ and the two eigenfunctions (6.67) and (6.69), respectively, for the two perturbation hamiltonians, $\hat{H}_{CV}$ and $\hat{H}_{SO}$, respectively: First we find the elements of $\hat{H}_{CV}$ from (6.67), (6.69), (6.38)-(6.40) and of cause employing the definition in (6.57). Since there is no spin dependency in $\hat{H}_{CV}$, we may simply add the s index, and multiply the result of the spin-independent matrix elements by $\delta_{s,s'}$ to insure spin conservation:

$$\begin{aligned}
&\langle z\sigma s\tau|\hat{H}_{CV}|m_{(2s,21\chi),\eta\sigma' s'\tau'}\rangle = \delta_{s,s'}(-\eta\tau' c_\eta|z\sigma s\tau\rangle\hat{H}_{CV}|2s-\sigma' s'\tau'\rangle + \frac{c_{-\eta}}{\sqrt{2}}e^{-i\sigma'\tau'\phi_c}\\
&(\sigma'\tau'\langle z\sigma s\tau|\hat{H}_{CV}|x\sigma' s'\tau'\rangle - i\langle z\sigma s\tau|\hat{H}_{CV}|y\sigma' s'\tau'\rangle)) = \delta_{s,s'}\delta_{\tau,\tau'}(\delta_{\sigma,-(-\sigma')}\frac{\eta\tau c_\eta\sqrt{3}a_0}{8R}\\
&e^{i2\phi_c\sigma\tau}H_{sp} + \delta_{\sigma,-\sigma'}\frac{c_{-\eta}}{\sqrt{2}}e^{i\sigma\tau\phi_c}(-\sigma\tau(-\sigma)\frac{\sqrt{3}a_0}{16R}(5H_\pi - 3H_\sigma)e^{-i\sigma\tau\phi_c} - \tau\frac{\sqrt{3}a_0}{16R}(H_\pi + H_\sigma)e^{-i\sigma\tau\phi_c})) =\\
&\delta_{s,s'}\delta_{\tau,\tau'}\tau\frac{\sqrt{3}a_0}{8R}(\delta_{\sigma,\sigma'}\eta c_\eta e^{i2\sigma\tau\phi_c}H_{sp} + \delta_{\sigma,-\sigma'}\sqrt{2}c_{-\eta}(H_\pi - H_\sigma))
\end{aligned} \tag{6.70}$$

and

$$\begin{aligned}
&\langle z\sigma s\tau|\hat{H}_{CV}|m_{(21\chi,21\chi),\eta s'\tau'}\rangle = \frac{1}{2}\delta_{s,s'}\sum_{\sigma'}(-1)^{\frac{1-\eta}{2}\frac{1-\sigma'}{2}}e^{i\phi_c\tau'\sigma'}(-\sigma'\tau'\langle z\sigma s\tau|\hat{H}_{CV}|x\sigma'\tau' s'\rangle\\
&- i\langle z\sigma s\tau|\hat{H}_{CV}|y\sigma' s'\tau'\rangle) = \frac{1}{2}\delta_{\tau,\tau'}\delta_{s,s'}(-1)^{\frac{1-\eta}{2}\frac{1+\sigma}{2}}e^{-i\phi_c\sigma\tau}(\sigma\tau(-\sigma\frac{\sqrt{3}}{16}\frac{a_0}{R}(5H_\pi - H_\sigma)e^{-i\phi_c\tau\sigma})\\
&- \tau\frac{\sqrt{3}}{16}\frac{a_0}{R}(H_\pi + H_\sigma)e^{-i\sigma\tau\phi_c}) = \delta_{s,s'}\delta_{\tau,\tau'}\tau(-1)^{\frac{1-\eta}{2}\frac{1+\sigma}{2}+1}e^{-i2\phi_c\tau\sigma}\frac{\sqrt{3}}{16}\frac{a_0}{R}(3H_\pi - H_\sigma)
\end{aligned} \tag{6.71}$$

Next, we calculate the corresponding matrix elements of $\hat{H}_{SO}$, using (6.47). Notice, that due to the way (6.47) was derived, we unfortunately need the complex conjugate of it. However, all parameters (α_{so} in particular) are real, so complex conjugating is a simple matter. Recall also, that since we are not dealing linear combinations of states, we can freely exchange s_l with s in the

bra and ket of (6.47):

$$\begin{aligned}
&\langle z\sigma s\tau|\hat{H}_{SO}|m_{(2s,21\chi),\eta\sigma' s'\tau'}\rangle = \\
&-\eta\tau' c_\eta \langle z\sigma s\tau|\hat{H}_{SO}|2s\sigma' s'\tau'\rangle + \frac{c_{-\eta}}{\sqrt{2}}\frac{\alpha_{so}}{2}e^{-i\sigma'\tau'\phi_c}(\sigma'\tau'\langle z\sigma s\tau|\hat{H}_{SO}|x\sigma' s'\tau'\rangle - i\langle z\sigma s\tau|\hat{H}_{SO}|y\sigma' s'\tau'\rangle) = \\
&\frac{\alpha_{so}c_{-\eta}}{2\sqrt{2}}e^{-i\sigma'\tau'\phi_c}(-is\sigma'\tau'\delta_{\tau,\tau'}\delta_{\sigma,\sigma'}\delta_{s,s'} - is\delta_{\mu,\mu'-s}\delta_{s,-s'}\delta_{\tau,\tau'}\delta_{\sigma,\sigma'}) = \\
&-is\frac{\alpha_{so}c_{-\eta}}{2\sqrt{2}}e^{-i\sigma\tau\phi_c}(\sigma\tau\delta_{s,s'} + \delta_{\mu,\mu'-s}\delta_{s,-s'})\delta_{\tau,\tau'}\delta_{\sigma,\sigma'}
\end{aligned} \tag{6.72}$$

Where we remember from section 6.2.2 that the μ quantum number is the quantum number for the circumferential part of the $\mathbf{k}$ vector. The final matrix element needed is

$$\begin{aligned}
&\langle z\sigma s\tau|\hat{H}_{SO}|m_{(21\chi,21\chi),\eta s'\tau'}\rangle = \\
&\frac{1}{2}\sum_{\sigma'}(-1)^{\frac{1-\eta}{2}\frac{1-\sigma'}{2}}e^{i\sigma'\tau'\phi_c}(\sigma'\tau'\langle z\sigma s\tau|\hat{H}_{SO}|x\sigma' s'\tau'\rangle - i\langle z\sigma s\tau|\hat{H}_{SO}|y\sigma' s'\tau'\rangle) = \\
&\frac{V_{SO}}{4}\sum_{\sigma'}(-1)^{\frac{1-\eta}{2}\frac{1-\sigma'}{2}}e^{i\sigma'\tau'\phi_c}(is\sigma'\tau'\delta_{s,s'}\delta_{\sigma,\sigma'}\delta_{\tau,\tau'} - is\delta_{s,-s'}\delta_{\mu,\mu'-s}\delta_{\sigma,\sigma'}\delta_{\tau,\tau'}) = \\
&\frac{i\alpha_{so}s}{4}(-1)^{\frac{1-\eta}{2}\frac{1-\sigma}{2}}e^{i\sigma\tau\phi_c}\delta_{\tau,\tau'}(\sigma\tau\delta_{s,s'} - \delta_{\mu,\mu'-s}\delta_{s,-s'})
\end{aligned} \tag{6.73}$$

In the following derivation, it will turn out to be useful to know three quantities, which we shall therefore derive first. Since only the eigenvalues from (6.66) shall be involved, we abbreviate $E_{(2s,21\chi),\eta}$ to E_η:

$$\sum_\eta \frac{c_\eta^2}{E_\eta} = \sum_\eta \frac{\eta E_\eta}{E_\eta(E_1 - E_{-1})} = \sum_\eta \frac{\eta}{(E_1 - E_{-1})} = 0 \tag{6.74}$$

$$\begin{aligned}
&\sum_\eta \frac{c_{-\eta}^2}{E_\eta} = \frac{c_{-1}^2}{E_1} + \frac{c_1^2}{E_{-1}} = \frac{E_{-1}c_{-1}^2 + E_1 c_1^2}{E_1 E_{-1}} = \frac{-E_{-1}^2 + E_1^2}{E_1 E_{-1}(E_1 - E_{-1})} = \\
&\frac{E_1 + E_{-1}}{E_1 E_{-1}} = \frac{\epsilon_{2s}}{\frac{1}{4}\epsilon_{2s} - \frac{1}{4}(\epsilon_{2s} + 18H_{sp}^2)} = -\frac{2\epsilon_{2s}}{9H_{sp}^2}
\end{aligned} \tag{6.75}$$

$$\begin{aligned}
&\sum_\eta \frac{c_{-\eta}c_\eta\eta}{E_\eta} = \frac{c_{-1}c_1}{E_1} - \frac{c_1 c_{-1}}{E_{-1}} = \frac{E_{-1}\sqrt{-E_1E_{-1}}}{E_1E_{-1}(E_1 - E_{-1})} - \frac{E_1\sqrt{-E_1E_{-1}}}{E_1E_{-1}(E_1 - E_{-1})} = \\
&-\frac{E_1 - E_{-1}}{\sqrt{-E_1E_{-1}}(E_1 - E_{-1})} = \frac{-1}{\sqrt{-E_1E_{-1}}} = \frac{-1}{\sqrt{-\frac{1}{4}(\epsilon_{2s} - \epsilon_{2s} - 18H_{sp}^2)}} = -\frac{\sqrt{2}}{3H_{sp}}
\end{aligned} \tag{6.76}$$

As stated in section 6.2.2 we shall ignore the inter-subband terms, ie. the terms containing $\delta_{\mu,\mu'-s}$. We can then derive

$$\sum_{\eta} \frac{\langle z\sigma'' s'' \tau'' | \hat{H}_{CV} | m_{2s,21\chi}, \eta\sigma' s'\tau' \rangle \langle m_{2s,21\chi}, \eta\sigma' s'\tau' | \hat{H}_{SO} | z\sigma s\tau \rangle}{-E_{(2s,21\chi),\eta}} =$$

$$\sum_{\eta} \frac{(\delta_{s'',s'}\delta_{\tau'',\tau'}\tau'' \frac{\sqrt{3}a_0}{8R}(\delta_{\sigma'',\sigma'}\eta c_\eta e^{i2\tau''\sigma''\phi_c} H_{sp} + \delta_{\sigma'',-\sigma'}\sqrt{2}c_{-\eta}(H_\pi - H_\sigma)))(\frac{is\alpha_{so}c_{-\eta}}{2\sqrt{2}} e^{i\sigma\tau\phi_c}\delta_{\tau,\tau'}\delta_{\sigma,\sigma'}\sigma\tau\delta_{s,s'})}{-E_{(2s,21\chi),\eta}} =$$

$$\alpha_{so}\frac{a_0}{R}\delta_{\tau'',\tau}\delta_{s'',s}s\frac{\sqrt{3}i}{16\sqrt{2}}\tau^2(\delta_{\sigma'',\sigma}\sum_{\eta}(\frac{\eta c_\eta c_{-\eta}}{-E_{(2s,21\chi),\eta}})e^{3i\sigma\tau\phi_c}H_{sp}\sigma +$$

$$\delta_{\sigma'',-\sigma}\sqrt{2}\sum_{\eta}(\frac{c_{-\eta}^2}{-E_{(2s,21\chi),\eta}})\sigma(H_\pi - H_\sigma)e^{i\tau\sigma\phi_c}) =$$

$$\frac{\alpha_{so}a_0\sqrt{3}}{16R}\hat{s}_Z\hat{\tau}_I(i\hat{\sigma}_Z\frac{1}{3}e^{i3\sigma\tau\phi_c} + \hat{\sigma}_Y e^{i\sigma\tau\phi_c}\frac{2\epsilon_{2s}(H_\pi - H_\sigma)}{9H_{sp}^2}) \tag{6.77}$$

Where in the last equality we have started to use the subband,valley and spin Pauli matrices, through the identities for the components of a general paulimatrixvector $\hat{\mathbf{\Sigma}}$:

$$\hat{\Sigma}_I = \delta_{\Sigma,\Sigma''} \quad \hat{\Sigma}_X = \delta_{\Sigma,-\Sigma''} \quad \hat{\Sigma}_Y = i\Sigma\delta_{\Sigma,-\Sigma''} \quad \hat{\Sigma}_Z = \Sigma\delta_{\Sigma,\Sigma''} \tag{6.78}$$

Next we calculate the other term of $\hat{H}_{SOCV}^{(2)}$ involving $|m_{2s,21\chi}, \eta\sigma' s'\tau'\rangle$[1]:

$$\sum_{\eta} \frac{\langle z\sigma'' s'' \tau'' | \hat{H}_{SO} | m_{2s,21\chi}, \eta\sigma' s'\tau' \rangle \langle m_{2s,21\chi}, \eta\sigma' s'\tau' | \hat{H}_{CV} | z\sigma s\tau \rangle}{-E_{(2s,21\chi),\eta}} =$$

$$\sum_{\eta} \frac{(-i\sigma''\tau'' s''\delta_{s'',s'}\delta_{\tau''.\tau'}\delta_{\sigma'',\sigma'}\frac{\alpha_{so}c_{-\eta}}{2\sqrt{2}}e^{-i\sigma''\tau''\phi_c})(\delta_{s,s'}\delta_{\tau,\tau'}\tau\frac{\sqrt{3}a_0}{8R}(\delta_{\sigma,\sigma'}\eta c_\eta e^{-i2\phi_c\sigma\tau}H_{sp} + \delta_{\sigma,-\sigma'}\sqrt{2}c_{-\eta}(H_\pi - H_\sigma)))}{-E_{(2s,21\chi),\eta}}$$

$$= -is\delta_{s,s''}\frac{\alpha_{so}a_0\sqrt{3}}{16R}\tau^2\delta_{\tau,\tau''}(\delta_{\sigma,\sigma''}e^{-i3\sigma\tau\phi_c}\sigma\frac{1}{\sqrt{2}}H_{sp}\sum_{\eta}(\frac{\eta c_\eta c_{-\eta}}{-E_{(2s,21\chi)\eta}}) +$$

$$\delta_{\sigma,-\sigma''}e^{i\sigma\tau\phi_c}(H_\pi - H_\sigma)(-\sigma)\sum_{\eta}(\frac{c_{-\eta}^2}{-E_{(2s,21\chi)\eta}}))$$

$$= \frac{\alpha_{so}a_0\sqrt{3}}{16r}\hat{s}_Z\hat{\tau}_I(-i\hat{\sigma}_Z\frac{1}{3}e^{-i3\sigma\tau\phi_c} + \hat{\sigma}_Y e^{i\sigma\tau\phi_c}\frac{2\epsilon_{2s}(H_\pi - H_\sigma)}{9H_{sp}^2}) \tag{6.79}$$

Following this, we need to calculate the contribution to $\hat{H}_{SOCV}^{(2)}$ using the other intermediate states, ie. $|m_{21\chi,21\chi}\eta\tau s\rangle$. There are three observations that shall make the calculation somewhat easier:

[1]This may at first seem as a simple complex conjugation of (6.77) - that is not true however: We also need to exchange the initial and final state after complex conjugation, and it is therefore better to be careful and make a separate calculation.

First, $E_{(21\chi,21\chi),+1} = -E_{(21\chi,21\chi),-1}$. Second, since both σ and η are ± 1, the quantity $2\frac{1-\eta}{2}\frac{1-\sigma}{2}+1$ is always odd, and third $(-1)^{\frac{1-\eta}{2}(\frac{1-\sigma}{2}+\frac{1+\sigma}{2})+1} = -\eta$. So:

$$\sum_\eta \frac{\langle z\sigma'' s'' \tau'' | \hat{H}_{CV} | m_{(21\chi,21\chi),\eta s'\tau'}\rangle \langle m_{(21\chi,21\chi),\eta s'\tau'} | \hat{H}_{SO} | z\sigma s\tau\rangle}{-E_{(21\chi,21\chi),\eta}} =$$
$$\sum_\eta \frac{(\delta_{s'',s'}\delta_{\tau'',\tau'}\tau''(-1)^{\frac{1-\eta}{2}\frac{1+\sigma''}{2}+1} e^{-2i\sigma''\tau''\phi_c}\frac{\sqrt{3}a_0}{16R}(3H_\pi - H_\sigma))(\frac{-i\alpha_{so}s}{4}(-1)^{\frac{1-\eta}{2}\frac{1-\sigma}{2}} e^{-i\sigma\tau\phi_c}\delta_{\tau,\tau'}\sigma\tau\delta_{s,s'})}{-E_\eta} =$$
$$- s\delta_{s'',s}\tau^2\delta_{\tau'',\tau}\frac{(3H_\pi - H_\sigma)\sqrt{3}a_0\alpha_{so}i}{64R}(\delta_{\sigma,\sigma''}\sigma\sum_\eta(\frac{(-1)^{\frac{1-\eta}{2}(\frac{1-\sigma}{2}+\frac{1+\sigma}{2})+1}}{-E_\eta})e^{-i3\phi_c\sigma\tau} -$$
$$\delta_{\sigma,-\sigma''}\sigma\sum_\eta(\frac{(-1)^{\frac{1-\eta}{2}(\frac{1-\sigma}{2}+\frac{1-\sigma}{2})+1}}{-E_\eta})e^{i\sigma\tau\phi_c}) =$$
$$- s\delta_{s'',s}\delta_{\tau'',\tau}\frac{(3H_\pi - H_\sigma)\sqrt{3}a_0\alpha_{so}i}{64R}(\delta_{\sigma,\sigma''}\sigma e^{-i3\phi_c\sigma\tau}(\frac{1}{E_{+1}} - \frac{1}{E_{-1}}) - \delta_{\sigma,-\sigma}\sigma e^{i\sigma\tau\phi_c}(\frac{1}{E_{+1}} + \frac{1}{E_{-1}})) =$$
$$- s\delta_{s,s''}\delta_{\tau,\tau''}\delta_{\sigma,\sigma''}\sigma\frac{(3H_\pi - H_\sigma)a_0\alpha_{so}i}{16\sqrt{3}R(H_\pi + H_\sigma)}e^{-3i\sigma\tau\phi_c} = -\frac{(3H_\pi - H_\sigma)a_0\alpha_{so}i}{16\sqrt{3}R(H_\pi + H_\sigma)}\hat{\sigma}_Z\hat{\tau}_I\hat{s}_Z e^{-3i\sigma\tau\phi_c} \tag{6.80}$$

where we from the second line onwards have abbreviated $E_{(21\chi,21\chi),\eta}$ to E_η for readability. Then the other element from (6.2) involving the functions $|m_{(21\chi,21\chi),\eta s\tau}\rangle$ is evaluated:

$$\sum_\eta \frac{\langle z\sigma'' s'' \tau'' | \hat{H}_{SO} | m_{(21\chi,21\chi),\eta s'\tau'}\rangle \langle m_{(21\chi,21\chi),\eta s'\tau'} | \hat{H}_{CV} | z\sigma s\tau\rangle}{-E_{(21\chi,21\chi),\eta}} =$$
$$\sum_\eta \frac{(\frac{i\alpha_{so}s''}{4}(-1)^{\frac{1-\eta}{2}\frac{1-\sigma''}{2}} e^{i\sigma''\tau''\phi_c}\delta_{\tau'',\tau'}\sigma''\tau''\delta_{s,s''})(\delta_{s,s'}\delta_{\tau,\tau'}\tau(-1)^{\frac{1-\eta}{2}\frac{1+\sigma}{2}+1}e^{2i\phi_c\sigma\tau}\frac{\sqrt{3}a_0}{16R}(3H_\pi - H_\sigma))}{-E_\eta} =$$
$$s\delta_{s,s''}\tau^2\delta_{\tau,\tau''}\frac{i\alpha_{so}\sqrt{3}a_0(3H_\pi - H_\sigma)}{64R}(\delta_{\sigma,\sigma''}\sigma\sum_\eta(\frac{(-1)^{\frac{1-\eta}{2}(\frac{1-\sigma}{2}+\frac{1+\sigma}{2})+1}}{-E_\eta})e^{3i\sigma\tau\phi_c}$$
$$+ \delta_{\sigma,-\sigma''}(-\sigma)\sum_\eta(\frac{(-1)^{\frac{1-\eta}{2}(\frac{1+\sigma}{2}+\frac{1+\sigma}{2})+1}}{-E_\eta})e^{i\sigma\tau\phi_c}) =$$
$$\frac{i\alpha_{so}\sqrt{3}a_0(3H_\pi - H_\sigma)}{64R}s\delta_{s,s''}\delta_{\tau,\tau''}(\delta_{\sigma,\sigma''}\sigma e^{i3\sigma\tau\phi_c}(\frac{1}{E_{-1}} - \frac{1}{E_{+1}}) - \delta_{\sigma,-\sigma''}\sigma e^{i\sigma\tau\phi_c}(\frac{1}{E_{+1}} + \frac{1}{E_{-1}})) =$$
$$s\delta_{s,s''}\delta_{\tau,\tau''}\delta_{\sigma,\sigma''}\sigma\frac{(3H_\pi - H_\sigma)a_0\alpha_{so}i}{16\sqrt{3}R(H_\pi + H_\sigma)}e^{3i\sigma\tau\phi_c} = \frac{(3H_\pi - H_\sigma)a_0\alpha_{so}i}{16\sqrt{3}R(H_\pi + H_\sigma)}\hat{\sigma}_Z\hat{\tau}_I\hat{s}_Z e^{3i\sigma\tau\phi_c} \tag{6.81}$$

where again we have abbreviated $E_{(21\chi,21\chi),\eta}$ to E_η.

Finally we can construct $\hat{H}^{(2)}_{SOCV}$ by adding the contributions from (6.77), (6.79), (6.80) and

(6.81):

$$\hat{H}^{(2)}_{SOCV} = \frac{\alpha_{so}a_0\sqrt{3}}{16R}\hat{s}_Z\hat{\tau}_I(i\hat{\sigma}_Z\frac{1}{3}(e^{i3\sigma\tau\phi_c} - e^{-i3\sigma\tau\phi_c}) + 2\hat{\sigma}_Y e^{i\sigma\tau\phi_c}\frac{2\epsilon_{2s}(H_\pi - H_\sigma)}{9H^2_{sp}})+$$
$$\frac{(3H_\pi - H_\sigma)a_0\alpha_{so}i}{16\sqrt{3}R(H_\pi + H_\sigma)}\hat{\sigma}_Z\hat{\tau}_I\hat{s}_Z(e^{3i\sigma\tau\phi_c} - e^{-3i\sigma\tau\phi_c}) = -(\frac{(3H_\pi - H_\sigma)a_0\alpha_{so}i}{16\sqrt{3}R(H_\pi + H_\sigma)} + \frac{\alpha_{so}a_0\sqrt{3}}{16R})\hat{\sigma}_I\hat{\tau}_Z\hat{s}_Z\sin 3\phi_c+$$
$$\frac{(H_\pi - H_\sigma)\epsilon_{2s}}{12\sqrt{3}H^2_{sp}}\alpha_{so}\frac{a_0}{R}(\hat{\tau}_I\hat{s}_z\hat{\sigma}_y\cos\phi_c + i\hat{\sigma}_Y\hat{\tau}_I\hat{s}_Z\sigma\tau\sin\phi_c) =$$
$$(\frac{-H_\pi}{2\sqrt{3}(H_\pi + H_\sigma)}\hat{\sigma}_I\hat{\tau}_Z\sin 3\phi_c + \frac{(H_\pi - H_\sigma)\epsilon_{2s}}{12\sqrt{3}H^2_{sp}}(\hat{\tau}_I\hat{\sigma}_y\cos\phi_c - \hat{\sigma}_X\hat{\tau}_Z\sin\phi_c))\hat{s}_Z\frac{\alpha_{so}a_0}{R}$$
$$\equiv (A_2\hat{\sigma}_I\hat{\tau}_Z\sin 3\phi_c + A_1(\hat{\sigma}_Y\hat{\tau}_I\cos\phi_c - \hat{\sigma}_X\hat{\tau}_Z\sin\phi_c))\hat{s}_z \tag{6.82}$$

where we have introduced the two parameters $A_1 = \frac{(H_\pi - H_\sigma)\epsilon_{2s}}{12\sqrt{3}H^2_{sp}}\alpha_{so}\frac{a_0}{R}$ and $A_2 = \frac{-H_\pi}{2\sqrt{3}(H_\pi + H_\sigma)}\alpha_{so}\frac{a_0}{R}$.

Similarly the above calculations for $\hat{H}^{(2)}_{SOCV}$, we may find the 2nd order curvature induced perturbation, $\hat{H}^{(2)}_{CVCV}$, arising from hybridization with the σ states, using (6.70) and (6.71) for both perturbation matrices. From (6.1) we see that only one term relevant to this calculation exists, as opposed to the two terms necessary when calculating $\hat{H}^{(2)}_{SOCV}$:

$$\hat{H}^{(2)}_{CVCV} = \sum_{m,\eta}\frac{\langle z\sigma''s''\tau''|\hat{H}_{CV}|m_{\eta s'\tau'\sigma'}\rangle\langle m_{\eta s'\tau'\sigma'}|\hat{H}_{CV}|z\sigma s\tau\rangle}{-E_{m\eta}} \tag{6.83}$$

where the m subscript denotes the two possible types of σ states, ie. $|m_{21\chi,21\chi}, \eta s\tau\rangle$ and $|m_{2s,21\chi}, \eta s\tau\sigma\rangle$ (so obviously the σ' index in (6.83) only applies to the $(2s, 21\chi)$ states). Thus analogous with the calculation above for $\hat{H}^{(2)}_{SOCV}$ we evaluate (6.83) for each m:

$$\sum_\eta \frac{\langle z\sigma''s''\tau''|\hat{H}_{CV}|m_{2s,21\chi}, \eta s'\tau'\sigma'\rangle\langle m_{2s,21\chi}\eta s'\tau'\sigma'|\hat{H}_{CV}|z\sigma s\tau\rangle}{-E_{(2s,21\chi),\eta}}$$
$$= \sum_\eta \frac{1}{-E_{(2s,21\chi),\eta}}(\delta_{\tau'',\tau'}\delta_{s'',s'}\tau''\frac{3a_0^2}{64R^2}(c_{-\eta}(H_\pi - H_\sigma)\sqrt{2}\delta_{\sigma'',\sigma'} + \eta c_\eta e^{i2\sigma''\tau''\phi_c}H_{sp}\delta_{\sigma'',\sigma})$$
$$\cdot\tau(c_{-\eta}(H_\pi - H_\sigma)\sqrt{2}\delta_{\sigma,\sigma'} + \eta c_\eta e^{-i2\sigma\tau\phi_c}H_{sp}\delta_{\sigma,\sigma}))$$

$$= \frac{-3}{64}(\frac{a_0}{R})^2\tau^2\delta_{\tau,\tau''}\delta_{s,s''}(\delta_{\sigma,\sigma''}(2(H_\pi - H_\sigma)^2\sum_\eta(\frac{c^2_{-\eta}}{E_\eta}) + H^2_{sp}\sum_\eta\frac{\eta c^2_\eta}{E_{(2s,21\chi),\eta}})$$
$$+ \delta_{\sigma,-\sigma''}(\sqrt{2}\sum_\eta(\frac{c_{-\eta}c_\eta\eta}{E_{(2s,21\chi),\eta}})(H_\pi - H_\sigma)H_{sp}e^{-i2\sigma\tau\phi_c} + \sqrt{2}\sum_\eta(\frac{c_{-\eta}c_\eta\eta}{E_{(2s,21\chi),\eta}})(H_\pi - H_\sigma)H_{sp}e^{-i2\sigma\tau\phi_c}))$$
$$= \frac{-3}{64}(\frac{a_0}{R})^2\delta_{\tau,\tau''}\delta_{s,s''}(\delta_{\sigma,\sigma''}2(H_\pi - H_\sigma)^2\frac{2\epsilon_{2s}}{9H^2_{sp}} + \delta_{\sigma,-\sigma''}2\sqrt{2}\frac{-\sqrt{2}}{3H_{sp}}(H_\pi - H_\sigma)H_{sp}e^{-2i\sigma\tau\phi_c})$$
$$= -\frac{3}{64}(\frac{a_0}{R})^2(\frac{4(H_\pi - H_\sigma)^2\epsilon_{2s}}{9H^2_{sp}}\hat{\tau}_I\hat{\sigma}_I\hat{s}_I + \frac{-4(H_\pi - H_\sigma)}{3}(\hat{\sigma}_x\hat{\tau}_I\hat{s}_I\cos 2\phi_c - \hat{\sigma}_y\hat{\tau}_z\hat{s}_I\sin 2\phi_c)) \tag{6.84}$$

where we have used (6.74)-(6.76) in the third equality and (6.78) in the last equality. We then calculate (6.83) for the other σ states:

$$\begin{aligned}
&\sum_\eta \frac{\langle z\sigma'' s''\tau''|\hat{H}_{CV}|m_{21\chi,21\chi},\eta s'\tau'\rangle\langle m_{21\chi,21\chi}\eta s'\tau'|\hat{H}_{CV}|z\sigma s\tau\rangle}{-E_{(21\chi,21\chi),\eta}} \\
&= \sum_\eta \frac{\delta_{\tau,\tau''}\delta_{s,s''}\tau''\tau\frac{3}{256}(\frac{a_0}{R})^2(3H_\pi - H_\sigma)^2(-1)^{\frac{1-\eta}{2}\frac{1+\sigma''}{2}+1}e^{-2i\sigma''\tau''\phi_c}(-1)^{\frac{1-\eta}{2}\frac{1+\sigma}{2}+1}e^{2i\sigma\tau\phi_c}}{-E_{(21\chi,21\chi),\eta}} \\
&= -\delta_{\tau,\tau''}\delta_{s,s''}\tau^2\frac{3}{256}(\frac{a_0}{R})^2(3H_\pi - H_\sigma)^2 e^{2i\tau\phi_c(\sigma-\sigma'')}\sum_\eta \frac{(-1)^{\frac{1-\eta}{2}\frac{1+\sigma}{2}+1+\frac{1-\eta}{2}\frac{1+\sigma''}{2}+1}}{E_{(21\chi,21\chi),\eta}} \\
&= -\delta_{\tau'',\tau}\delta_{s'',s}\frac{3}{256}(\frac{a_0}{R})^2(3H_\pi - H_\sigma)^2(\delta_{\sigma,\sigma''}\sum_\eta \frac{(-1)^{(1-\eta)\frac{1+\sigma}{2}}}{E_{(21\chi,21\chi),\eta}} + \delta_{\sigma,-\sigma''}e^{4i\tau\sigma\phi_c}\sum_\eta \frac{(-1)^{\frac{1-\eta}{2}}}{E_{(21\chi,21\chi),\eta}}) \\
&= -\delta_{\tau,\tau''}\delta_{s,s''}\delta_{\sigma,-\sigma''}\frac{3}{256}(3H_\pi - H_\sigma)^2(\frac{a_0}{R})^2 2\frac{2}{3(H_\pi + H_\sigma)}e^{4i\tau\sigma\phi_c} \\
&= -\hat{s}_I\frac{1}{64}(\frac{a_0}{R})^2\frac{(3H_\pi - H_\sigma)^2}{H_\pi + H_\sigma}(\hat{\tau}_I\hat{\sigma}_x\cos 4\phi_c + \hat{\tau}_z\hat{\sigma}_y\sin 4\phi_c)
\end{aligned} \tag{6.85}$$

where we, in the fourth equation, have used that $E_{(21\chi,21\chi),\eta} \propto \eta$ (6.68) and the fact that (since $\eta = \pm 1$ and $\sigma = \pm 1$), $(-1)^{(1-\eta)\frac{1+\sigma}{2}} = 1$.

In contrast to the case for $\hat{H}^{(2)}_{SOCV}$ there is a "first order" contribution $(6.41)^2$ contribution to the effective hamiltonian, that must be added to the above expressions to get the effective curvature hamiltonian to order $(\frac{a_0}{R})^2$. We notice also that the first term of the result of (6.84) has a factor of $\hat{\tau}_I\hat{\sigma}_I\hat{s}_I$ and so simply shifts the energy for all states, and therefore we ignore it (or rather, shift the origin of the energy axis so as to make this term effectively 0). We therefore reach the final result

$$\begin{aligned}
\hat{H}^{(2)}_{CVCV} &= \frac{(H_\pi - H_\sigma)}{16}(\hat{\sigma}_x\hat{\tau}_I\hat{s}_I\cos 2\phi_c - \hat{\sigma}_y\hat{\tau}_z\hat{s}_I\sin 2\phi_c) \\
&\quad - \hat{s}_I\frac{1}{64}(\frac{a_0}{R})^2\frac{(3H_\pi - H_\sigma)^2}{H_\pi + H_\sigma}(\hat{\tau}_I\hat{\sigma}_x\cos 4\phi_c + \hat{\tau}_z\hat{\sigma}_y\sin 4\phi_c) \\
&\quad - \frac{1}{64}(\frac{a_0}{R})^2(4(H_\pi - H_\sigma)(\hat{s}_I\hat{\sigma}_x\hat{\tau}_I\cos 2\phi_c - \hat{s}_I\hat{\sigma}_y\hat{\tau}_z\sin 2\phi_c) \\
&\qquad\qquad + (H_\pi + H_\sigma)\hat{s}_I\hat{\sigma}_x\hat{\tau}_I\cos 4\phi_c + \hat{s}_I\hat{\sigma}_y\hat{\tau}_z\sin 4\phi_c) \\
&= (\frac{a_0}{R})^2\frac{H_\pi(H_\pi + H_\sigma)}{8(H_\pi + H_\sigma)}(\hat{s}_I\hat{\sigma}_x\hat{\tau}_I\cos 4\phi_c + \hat{s}_I\hat{\sigma}_y\hat{\tau}_z\sin 4\phi_c) \\
&\equiv B(\hat{s}_I\hat{\sigma}_X\hat{\tau}_I\cos 4\phi_c + \hat{s}_I\hat{\sigma}_Y\hat{\tau}_Z\sin 4\phi_c)
\end{aligned} \tag{6.86}$$

where we defined $B = (\frac{a_0}{R})^2\frac{H_\pi(H_\pi+H_\sigma)}{8(H_\pi+H_\sigma)}$. Note that this results differ from [19]: They get a non-zero contribution to the $2\phi_c$ dependent part of $\hat{H}^{(2)}_{CVCV}$, probably due to a factor 2 error in their version of (6.84).

[2]It is first order in the sense that there are no intermediate states, but it has the same prefactor $(\frac{a_0}{R})^2$ as the second order contribution

In principle, this ends the derivations made in [19]. However, in order for us to compare to our own results, and to ascertain the physical consequences of this derivation, we wish to rotate these results into the effective hamiltonian formalism used so far in the thesis, ie. we wish to rotate from the k-coordinatesystem k_x and k_y that is natural for graphene (and thus chirality independent), into the coordinatesystem natural to the CNT, ie. $k_c = \frac{\mu}{R}$ and k_t: This is the same procedure as was done in (2.18). This can be done by a unitary transformation very similar to the one used in [13], which can be seen by finding the π band graphene hamiltonian by expanding $\langle zA\mathbf{k}|\hat{H}|zB\mathbf{k}\rangle$ around the K(') point to find

$$\begin{aligned}&\langle zA\mathbf{k}|\hat{H}|zB\mathbf{k}\rangle \approx H_\pi f(\mathbf{k}) \approx \frac{-\sqrt{3}aH_\pi}{2}(-ik_x - \tau k_y) = \\ &\hbar v_f(k_C(-i\cos\phi_C - \tau\sin\phi_C) + k_t(i\sin\phi_C - \tau\cos\phi_C)) = \hbar v_f(-ie^{-i\tau\phi_C}(k_v - i\tau k_t))\end{aligned} \tag{6.87}$$

and so we have (since $(\langle zB\mathbf{k}|\hat{H}|zA\mathbf{k}\rangle)^* = \langle zA\mathbf{k}|\hat{H}|zB\mathbf{k}\rangle$) the effective hamiltonian

$$\hat{\tilde{H}}_\pi^{eff} = \hbar v_f \begin{pmatrix} 0 & -ie^{-i\tau\phi_c}(k_c - i\tau k_t) \\ ie^{i\tau\phi_c}(k_c + i\tau k_t) & 0 \end{pmatrix} \tag{6.88}$$

and from this we see that the unitary transformation from k_x,k_y to k_c,k_t should be $\mathbf{U} = \begin{pmatrix} ie^{i\tau\phi_c} & 0 \\ 0 & 1 \end{pmatrix}$ so

$$\hat{H}_\pi^{eff} = \mathbf{U}\hat{\tilde{H}}_\pi^{eff}\mathbf{U}^{-1} = \hbar v_f \begin{pmatrix} 0 & k_c - i\tau k_t \\ k_c + i\tau k_t & 0 \end{pmatrix} \tag{6.89}$$

also derived in section 2, except for the position of the τ: This is due to the difference in the choice of K(') points, mentioned above.

Observe that (6.86) and (6.82) does not contain $\hat{s}_x$,$\hat{s}_y$,$\hat{\tau}_x$ or $\hat{\tau}_y$, that is, it contains no non-diagonal elements in s or τ. Thus both hamiltonians may be written in the AB-subspace, "effective" basis, since $\hat{s}_z(\hat{\tau}_z)$ can be written as $s\hat{s}_I(\tau\hat{\tau}_I)$, and further, we can transform these using the same unitary transformation as above to obtain the effective hamiltonians:

$$\begin{aligned}&\mathbf{U}\hat{H}_{SOCV}^{eff}\mathbf{U}^{-1} = \\ &\begin{pmatrix} ie^{i\tau\phi_C} & 0 \\ 0 & 1 \end{pmatrix}\begin{pmatrix} s\tau A_2\sin(3\phi) & sA_1(-i\cos\phi_C - \tau\sin\phi_C) \\ sA_1(i\cos\phi_C - \tau\sin\phi_C) & s\tau A_2\sin(3\phi) \end{pmatrix}\begin{pmatrix} -ie^{-i\tau\phi_C} & 0 \\ 0 & 1 \end{pmatrix} = \\ &\begin{pmatrix} A_2 s\tau\sin 3\phi_C & -sA_1 \\ -sA_1 & A_2 s\tau\sin 3\phi_c \end{pmatrix} = \hbar v_f \begin{pmatrix} \frac{A_2}{\hbar v_f}s\tau\cos 3\theta & -s\frac{A_1}{\hbar v_f} \\ -s\frac{A_1}{\hbar v_f} & \frac{A_2}{\hbar v_f}s\tau\cos 3\theta \end{pmatrix}\end{aligned} \tag{6.90}$$

and

$$\begin{aligned}&\mathbf{U}\hat{H}_{CVCV}^{eff}\mathbf{U}^{-1} = \\ &\begin{pmatrix} ie^{i\tau\phi_C} & 0 \\ 0 & 1 \end{pmatrix}\begin{pmatrix} 0 & B(\cos 4\phi_C - i\tau\sin 4\phi_C) \\ B(\cos 4\phi_C + i\tau\sin 4\phi_C) & 0 \end{pmatrix}\begin{pmatrix} -ie^{-i\tau\phi_C} & 0 \\ 0 & 1 \end{pmatrix} = \\ &\begin{pmatrix} 0 & iBe^{-i3\phi_C} \\ -iBe^{i3\phi_C} & 0 \end{pmatrix} = \hbar v_f \begin{pmatrix} 0 & \frac{B}{\hbar v_f}(i\sin 3\theta + \tau\cos 3\theta) \\ \frac{B}{\hbar v_f}(-i\sin 3\theta + \tau\cos 3\theta) & 0 \end{pmatrix}\end{aligned} \tag{6.91}$$

where we have reintroduced the chiral angle $\theta = \frac{\pi}{6} - \phi_C$ and taken a factor $\hbar v_f$ out of the matrices, so the can be immediately compared to the unperturbed hamiltonian, (6.89). We also used that $\sin 3\phi_C = \sin(\frac{\pi}{2} - 3\theta) = \cos 3\theta$, and $\cos 3\phi_C = \cos(\frac{\pi}{2} - 3\theta) = \sin 3\theta$. When we add the three contributions to the full effective hamiltonian, we see that the imaginary part of the off-diagonal element in (6.91) can be interpreted as a shift in k_t, while the real part of the off-diagonal part of (6.90) and (6.91) becomes a shift in k_c. Diagonalizing the full hamiltonian gives us the expression for the energy also found in [19]:

$$E^{\pm}_{eff} = s\tau A_2 \cos 3\theta \pm \sqrt{(\frac{\nu\tau}{3R} - s\frac{A_1}{\hbar v_f} + \tau\frac{B}{\hbar v_f}\cos 3\theta)^2 + (k_t - \frac{B}{\hbar v_f}\sin 3\theta)^2} \tag{6.92}$$

where we used that $\tau^2 = 1$, and where we have only given the energy for the energy band closest to K('), ie. we have set $k_c = \frac{\nu\tau}{3}$, as in (3.21)

This function have all the same qualitative features as the energy function found in the last chapter (5.11) except for the introduction of the $\hat{H}^{(2)}_{CVCV}$ part in this chapter, and for the dependence of τ inside the squareroot. However, one may always multiply the shifted k_c by τ, since $\tau^2 = 1$, and then we see that we get precisely the same dependence on σ and τ as in (5.11). However, it should be admitted that there is a real difference in the value of A_2: [19] have H_π in the nominator, while we found H_σ in the calculation of (5.11). While this is of cause unfortunate, we see that there is no qualitative difference due to this: The properties of (6.92) is the same as those of (5.11), and we shall not restate them here. Izumidas et als calculation, while obviously equivalent to our own, has the nice feature, that it can be solved without appealing to automated derivations, ie. mathematica, thus making each step of the calculation more transparent.

Chapter 7

Magnetic field

We now wish to include a magnetic field into the system. In this thesis we shall constrain ourselves to a field parallel to the tube-axis. Essentially, there are two separate effects of such a field: The Aharonov-Bohm effect and the Zeeman effect. The latter we shall consider as an experimental fact, since deriving it from the Dirac equation (of which it is, like the spin-orbit coupling, a lowenergy approximation consequence) would take us too far of topic. The second, most peculiar effect follow directly from the derivation of the inclusion of an electromagnetic field in the Schrodinger equation, which have been carried out in some detail in appendix D, giving us the basic Schrodinger equation for a particle in a magnetic field:

$$\hat{H} = \frac{1}{2m}(\hat{\mathbf{p}} - q\mathbf{A})^2 + q\phi(\mathbf{x}) = \frac{1}{2m}(-i\hbar\nabla - q\mathbf{A})^2 + q\phi(\mathbf{x}) \tag{7.1}$$

After presenting the two effects, we shall make some quantitative considerations in order to explain the numerical data obtained from the Hückel simulations, discussed in the last section.

7.1 Zeeman effect

The theoretical origin of the Zeeman effect is the Foldy-Wouthuysen approximation of the Dirac equation, but we treat the effect as a basic effect, stating that a spin in a magnetic field will behave as a magnetic dipole moment, described by the spin angular momentum exactly as if though it was a classical, orbital angular momentum, except from the Thomas g-factor equal to 2, ie. there will be a spin dependent term in the hamiltonian

$$\hat{H}_Z = g\mu_B \frac{1}{2}\hat{\sigma}_y B = \mu_B \hat{\sigma_y} B \tag{7.2}$$

where we have introduced the Bohr magneton $\mu_B = \frac{e\hbar}{2m}$ and availed ourselves of the convenient fact that we have chosen the spin-quantization axis in the axial direction, so that the standard energy, $-\mathbf{S}\cdot\mathbf{B}$ reduces to the product of the magnetic field and the spin of the electron (notice, that the minus in the energy is countered by the (unfortunate) convention that the electron has a negative charge).

7.2 The Aharonov-Bohm effect

In order to understand this surprising effect we need to solve the hamiltonian (7.1) in terms of the solutions to the hamiltonian without a magnetic field, ie. the wavefunctions found in the previous sections. Since the difference between the hamiltonians can be viewed as a change of the momentum operator, ie. $-i\hbar\nabla \rightarrow -i\hbar\nabla + e\mathbf{A}$, we should try to "counteract" the $e\mathbf{A}$ correction by changing the phase of the wavefunctions.

Now, the standard derivation of the Aharonov Bohm effect assumes that we have electrons moving in vacuum, ie. the wavefunctions are simple plane waves, travelling through a portion of space with a non-zero $\mathbf{A}$ field but vanishing $\mathbf{B}$ field. Here the correction is obvious, since we can simply multiply the non-corrected wavefunctions with $e^{\int_{x_s}^{x} -i\frac{e}{\hbar}\mathbf{A}(\mathbf{x}')d\mathbf{x}'}$, where x_s is some arbitrary starting point, since we have

$$\begin{aligned}
\hat{H}\Psi(x)_{AB} &= (\frac{1}{2m}(-i\hbar\nabla + e\mathbf{A}(\mathbf{x}))^2 + V(\mathbf{x}))(e^{\int_{x_s}^{x} -i\frac{e}{\hbar}\mathbf{A}(\mathbf{x}')d\mathbf{x}'}\Psi_n(x)) \\
&= e^{\int_{x_s}^{x} -i\frac{e}{\hbar}\mathbf{A}(\mathbf{x}')d\mathbf{x}'}(\frac{1}{2m}(-i\hbar\nabla \int_{x_s}^{x} -i\frac{e}{\hbar}\mathbf{A}(\mathbf{x}')d\mathbf{x}' + e\mathbf{A}(\mathbf{x}) - i\hbar\nabla)^2 + V(\mathbf{x}))\Psi_n(x) \\
&= e^{\int_{x_s}^{x} -i\frac{e}{\hbar}\mathbf{A}(\mathbf{x}')d\mathbf{x}'}(\frac{1}{2m}(-e\mathbf{A}(\mathbf{x}) + e\mathbf{A}(\mathbf{x_s}) + e\mathbf{A}(\mathbf{x}) - i\hbar\nabla)^2 + V(\mathbf{x}))\Psi_n(x) \\
&= e^{\int_{x_s}^{x} -i\frac{e}{\hbar}\mathbf{A}(\mathbf{x}')d\mathbf{x}'}(\frac{(-i\hbar\nabla)^2}{2m} + V(\mathbf{x}))\Psi_n(x) \qquad (7.3)
\end{aligned}$$

Here, we have used that if $\mathbf{B}(\mathbf{x})$ is identically zero $\mathbf{A}$ can be written as a gradient of a scalar field, and so the integral is independent of the path taken from $\mathbf{x_s}$ to $\mathbf{x}$. Also we defined $\mathbf{A}(\mathbf{x_s}) = 0$, which can be done by choosing the appropriate gauge, corresponding to adding a constant to $\mathbf{A}(\mathbf{x})$ - even if we do not do this, $\mathbf{A}(\mathbf{x_s})$ is just a energy shift.

In the case of the CNT however, the problem is slightly more complicated, in that we do not start out from plane waves, but rather Bloch functions. We therefore need an argument to see what happens to these functions in the presence of a magnetic field, and such an argument have been outlined in chapter 6 of [21]:

Following the example of Luttinger in [24] (where he expands an intriguing theorem originally due to Wannier [22] and formalized by Slater [23]) we change our basic Bloch functions from those defined in (2.9) to include the magnetic field in a way very similar to the case of free electrons:

$$\Psi_{n\mathbf{k}}(\mathbf{r}) = \frac{1}{\sqrt{N}}\sum_{\mathbf{R}} e^{i\mathbf{k}\cdot\mathbf{R}}\phi(\mathbf{r}-\mathbf{R}) \rightarrow \Psi_{AB,n\mathbf{k}}(\mathbf{r}) = \frac{1}{\sqrt{N}}\sum_{\mathbf{R}} e^{i(\mathbf{k}\cdot\mathbf{R}+\frac{e}{\hbar}G_{\mathbf{R}})}\phi(\mathbf{r}-\mathbf{R}) \qquad (7.4)$$

where the $\phi(\mathbf{r}-\mathbf{R})$ are *molecular* wavefunctions, which we for the moment shall take to be the Wannier functions from (2.7) and the AB subscript stands for Aharonov-Bohm, ie. the wavefunction is modified to take the Aharonov-Bohm effect into account, and $G(\mathbf{R})$ is a phase factor defined as

$$G_{\mathbf{R}}(\mathbf{r}) = \int_{\mathbf{R}}^{\mathbf{r}} \mathbf{A}(\mathbf{r}')d\mathbf{r}' = \int_0^1 (\mathbf{r}-\mathbf{R})\cdot\mathbf{A}(\mathbf{R}+\lambda(\mathbf{r}-\mathbf{R}))d\lambda \qquad (7.5)$$

where the integral is taken along the straight line from $\mathbf{R}$ to $\mathbf{r}$ and $\mathbf{R}$ is a lattice point.

The reason for this replacement of the Bloch functions is the same as the above case for the free electrons, namely that we may "counter" the $\mathbf{A}$ part of the hamiltonian, which is readily seen:

$$\hat{H}\Psi_{AB,n\mathbf{k}}(\mathbf{r}) = \frac{1}{\sqrt{N}}\sum_{\mathbf{R}} e^{i\mathbf{k}\cdot\mathbf{R}}(\frac{1}{2m}(\mathbf{p}-e\mathbf{A}(\mathbf{r}))^2+V)e^{i\frac{e}{\hbar}G_{\mathbf{R}}(\mathbf{r})}\phi(\mathbf{r}-\mathbf{R}) =$$
$$\frac{1}{\sqrt{N}}\sum_{\mathbf{R}} e^{i(\mathbf{k}\cdot\mathbf{R}+\frac{e}{\hbar}G_{\mathbf{R}}(\mathbf{r}))}(\frac{1}{2m}(\mathbf{p}-e\mathbf{A}(\mathbf{r})+e\nabla G_{\mathbf{R}}(\mathbf{r}))^2+V)\phi(\mathbf{r}-\mathbf{R}) \tag{7.6}$$

where we have explicitly written the periodic potential V. We see then, that we need the gradient of $G_{\mathbf{R}}(\mathbf{r})$ with respect to $\mathbf{r}$, which we shall obtain using the definition in (7.5):

$$\nabla G_{\mathbf{R}}(\mathbf{r}) = \int_0^1 d\lambda\nabla((\mathbf{r}-\mathbf{R})\cdot\mathbf{A}(\mathbf{R}+\lambda(\mathbf{r}-\mathbf{R}))) =$$
$$\int_0^1 d\lambda((\mathbf{r}-\mathbf{R})\times(\nabla\times\mathbf{A})+\mathbf{A}\times(\nabla\times(\mathbf{r}-\mathbf{R}))+$$
$$(\mathbf{A}\cdot\nabla)(\mathbf{r}-\mathbf{R})+((\mathbf{r}-\mathbf{R})\cdot\nabla)\mathbf{A}) \tag{7.7}$$

where we have dropped the parameter on $\mathbf{A}$ in the last expression - it is implicitly understood that $\mathbf{A}\equiv\mathbf{A}(\mathbf{R}+\lambda(\mathbf{r}-\mathbf{R}))$, and used the wellknown rule of vector products:

$$\nabla(\mathbf{A}\cdot\mathbf{B}) = \mathbf{A}\times(\nabla\times\mathbf{B})+\mathbf{B}\times(\nabla\times\mathbf{A})+(\mathbf{A}\cdot\nabla)\mathbf{B}+(\mathbf{B}\cdot\nabla)\mathbf{A} \tag{7.8}$$

The terms of (7.7) can be treated one by one: First, notice that by the chain rule

$$\nabla\times\mathbf{A}(\mathbf{R}+\lambda(\mathbf{r}-\mathbf{R})) = \lambda\mathbf{B}(\mathbf{R}+\lambda(\mathbf{r}-\mathbf{R})) \tag{7.9}$$

Second, since $\mathbf{R}$ is independent of $\mathbf{r}$ we have $\nabla\times(\mathbf{r}-\mathbf{R})=0$. Third, since $\nabla(\mathbf{r}-\mathbf{R})=\mathbf{1}$ we find that $(\mathbf{A}\cdot\nabla)(\mathbf{r}-\mathbf{R})=\mathbf{A}$. Using these observations, we see that we may write (7.7)

$$\nabla G_{\mathbf{R}}(\mathbf{r}) = \int_0^1 d\lambda(\lambda(\mathbf{r}-\mathbf{R})\times\mathbf{B}+\mathbf{A}+((\mathbf{r}-\mathbf{R})\cdot\nabla)\mathbf{A}) \tag{7.10}$$

Finally we integrate $\mathbf{A}(\mathbf{R}+\lambda(\mathbf{r}-\mathbf{R}))$ by parts, taking the other function to be just 1:

$$\int_0^1 d\lambda\mathbf{A}(\mathbf{R}+\lambda(\mathbf{r}-\mathbf{R})) = [\lambda\mathbf{A}(\mathbf{R}+\lambda(\mathbf{r}-\mathbf{R}))]_0^1 - \int_0^1 d\lambda\lambda\frac{d}{d\lambda}\mathbf{A}(\mathbf{R}+\lambda(\mathbf{r}-\mathbf{R})) =$$
$$\mathbf{A}(\mathbf{r}) - \int_0^1 d\lambda((\mathbf{r}-\mathbf{R})\cdot\nabla)\mathbf{A}(\mathbf{R}+\lambda(\mathbf{r}-\mathbf{R})) \tag{7.11}$$

where the integrants in the last equality is most easily seen to be the same by defining $\xi = (\mathbf{R}+\lambda(\mathbf{r}-\mathbf{R}))$, and observing that, since $\mathbf{r}=(x,y,z)$, $\frac{d\xi_i}{d\lambda} = (\mathbf{r}-\mathbf{R})_i$ where i is a coordinate, and $\frac{\partial\xi_i}{\partial x_j} = \delta_{j,i}\lambda$, and

$$\frac{d\mathbf{A}}{d\lambda} = \frac{\partial\mathbf{A}}{\partial\xi_x}\frac{\partial\xi_x}{\partial\lambda}+\frac{\partial\mathbf{A}}{\partial\xi_y}\frac{\partial\xi_y}{\partial\lambda}+\frac{\partial\mathbf{A}}{\partial\xi_z}\frac{\partial\xi_z}{\partial\lambda} \tag{7.12}$$

finally leading to

$$((\mathbf{r}-\mathbf{R})\cdot\nabla)\mathbf{A} = \frac{d\xi_x}{d\lambda}\frac{d\mathbf{A}}{dx} + \frac{d\xi_y}{d\lambda}\frac{d\mathbf{A}}{dy} + \frac{d\xi_z}{d\lambda}\frac{d\mathbf{A}}{dz} =$$
$$\frac{d\xi_x}{d\lambda}\frac{d\mathbf{A}}{d\xi_x}\frac{d\xi_x}{dx} + \frac{d\xi_y}{d\lambda}\frac{d\mathbf{A}}{d\xi_y}\frac{d\xi_y}{dy} + \frac{d\xi_z}{d\lambda}\frac{d\mathbf{A}}{d\xi_z}\frac{d\xi_z}{dz} = \lambda(\frac{\partial\mathbf{A}}{\partial\xi_x}\frac{\partial\xi_x}{\partial\lambda} + \frac{\partial\mathbf{A}}{\partial\xi_y}\frac{\partial\xi_y}{\partial\lambda} + \frac{\partial\mathbf{A}}{\partial\xi_z}\frac{\partial\xi_z}{\partial\lambda}) = \lambda\frac{d\mathbf{A}}{d\lambda} \tag{7.13}$$

where we have again dropped the argument to $\mathbf{A}$ for greater readability.

Now we insert (7.11) into (7.10) to obtain

$$\nabla G_{\mathbf{R}}(\mathbf{r}) = \mathbf{A}(\mathbf{r}) + \int_0^1 d\lambda\lambda(\mathbf{r}-\mathbf{R})\times\mathbf{B}(\mathbf{R}+\lambda(\mathbf{r}-\mathbf{R})) \tag{7.14}$$

This is then inserted into (7.6) to obtain

$$\frac{1}{\sqrt{N}}\sum_{\mathbf{R}} e^{i(\mathbf{k}\cdot\mathbf{R}+\frac{e}{\hbar}G_{\mathbf{R}}(\mathbf{r}))}(\frac{1}{2m}(\mathbf{p}+e\int_0^1 d\lambda\lambda(\mathbf{r}-\mathbf{R})\times\mathbf{B}(\mathbf{R}+\lambda(\mathbf{r}-\mathbf{R})))^2 + V)\phi(\mathbf{r}-\mathbf{R}) \tag{7.15}$$

Recall that the idea of this exercise, analogous to the free electron calculation in the beginning of this subsection, is to arrive at a situation similar to that of the graphene sheet without a magnetic field. We therefore would like to have an approximation in which the integral in (7.15) evaluates to zero. But recall that the molecular orbitals, $\phi(\mathbf{r}-\mathbf{R})$ is only non-zero for $|\mathbf{r}-\mathbf{R}| \approx 0$. This means that we only need to consider the integrant for $\mathbf{r}\approx\mathbf{R}$, and if we furthermore assume that $\mathbf{B}$ is relatively constant on the scale of the unitcell [1], $\mathbf{B}$ part becomes a constant with respect to the integration, since λ going from 0 to 1 corresponds to the argument of $\mathbf{B}$ going from $\mathbf{R}$ to $\mathbf{r}$, and these were close due to the locality of the orbitals, and we therefore find

$$\int_0^1 d\lambda\lambda(\mathbf{r}-\mathbf{R})\times\mathbf{B}(\mathbf{R}+\lambda(\mathbf{r}-\mathbf{R})) \approx -\mathbf{B}(\mathbf{r})\times\int_0^1 d\lambda\lambda(\mathbf{r}-\mathbf{R}) \approx 0 \tag{7.16}$$

where the last approximation relies again on the molecular orbits locality, ie. $\mathbf{r}-\mathbf{R}\approx\mathbf{0}$. Thus, we finally end up with

$$\hat{H}\Psi_{AB,n\mathbf{k}}(\mathbf{r}) = \frac{1}{\sqrt{N}}\sum_{\mathbf{R}} e^{i(\mathbf{k}\cdot\mathbf{R}+\frac{e}{\hbar}G_{\mathbf{R}}(\mathbf{r}))}(\frac{1}{2m}\mathbf{p}^2 + V)\phi(\mathbf{r}-\mathbf{R}) \tag{7.17}$$

This, we notice, is almost exactly like the equation for the hamiltonian in the case without magnetic field in that we now have the hamiltonian from the graphene system, $\frac{1}{2m}\mathbf{p}^2+V$ working on the molecular orbitals - which may of cause be modified in the same manner as we have done in the previous sections, ie. perturbed by curvature and spin-orbit coupling - summed over all unitcells with an exponential factor. The only dependence on the $\mathbf{A}$ field that remains is the $G_{\mathbf{R}}(\mathbf{r})$ term in the phase factor.

In this derivation so far we have used the Wannier molecular functions for the sake of brevity and readability, but if we wish to determine the effect on the effective hamiltonians that we have

[1] an assumption that is indeed met in our case, since we consider a constant magnetic field

used so far, we need to split these up into the A and B sublattice blochfunctions, and we must consequently have two G phases, one for the A sublattice, which is as above, and another for the B sublattice in which $\mathbf{R}$ is exchanged with $\mathbf{R}-\mathbf{l_1}$, so we finally have

$$\hat{H}\Psi_{AB,n\mathbf{k}}(\mathbf{r}) = \frac{1}{\sqrt{N}}(\sum_{\mathbf{R}} e^{i(\mathbf{k}\cdot\mathbf{R}+\frac{e}{\hbar}G_{\mathbf{R}}(\mathbf{r}))}a(\frac{1}{2m}\mathbf{p}^2+V)\pi_A(\mathbf{r}-\mathbf{R})$$
$$+ e^{i(\mathbf{k}\cdot(\mathbf{R}+\mathbf{l_1})+\frac{e}{\hbar}G_{\mathbf{R}+\mathbf{l_1}}(\mathbf{r}))}b(\frac{1}{2m}\mathbf{p}^2+V)\pi_B(\mathbf{r}-\mathbf{R}-\mathbf{l_1})) \tag{7.18}$$

Now, in the spirit of the derivation for the graphene sheet (and therefore by extension the CNT with spin-orbit coupling), we wish to evaluate the hamiltonian element between two different blochwaves $\Psi_{AB,n\mathbf{k},A}$ and $\Psi_{AB,n\mathbf{k},B}$, where the last A or B denotes sublattice, in the nearest neighbour assumption:

$$\int d\mathbf{r}\Psi_{AB,n\mathbf{k},B}(\mathbf{r})^*\hat{H}\Psi_{AB,n\mathbf{k},A}(\mathbf{r})$$
$$= \int d\mathbf{r}\frac{1}{N}\sum_{\mathbf{R}}\sum_j e^{i\frac{e}{\hbar}(G_{\mathbf{R}}(\mathbf{r})-G_{\mathbf{R}+\mathbf{l_j}}(\mathbf{r}))}e^{i\mathbf{k}\cdot\mathbf{l_j}}(\pi_B(\mathbf{r}-\mathbf{R}-\mathbf{l_j})^*\hat{H}_0\pi_A(\mathbf{r}-\mathbf{R}))$$
$$= \sum_j e^{i\mathbf{k}\cdot\mathbf{l_j}}\int d\mathbf{r}e^{i\frac{e}{\hbar}(G_{\mathbf{0}}(\mathbf{r})-G_{\mathbf{0}+\mathbf{l_j}}(\mathbf{r}))}(\pi_B(\mathbf{r}-\mathbf{R}-\mathbf{l_j})^*\hat{H}_0\pi_A(\mathbf{r}-\mathbf{R})) \tag{7.19}$$

where we have made use of the analogy with the derivation leading to (2.13), and $\mathbf{0}$ in the last line refers to any given unitcell, since they are all equivalent.

We therefore find, that we need to evaluate the difference $G_{\mathbf{0}}(\mathbf{r}) - G_{\mathbf{0}+\mathbf{l_j}}(\mathbf{r})$. From the basic definition (7.5), we find

$$G_{\mathbf{0}}(\mathbf{r}) - G_{\mathbf{0}+\mathbf{l_j}}(\mathbf{r}) = \int_{\mathbf{0}}^{\mathbf{r}}\mathbf{A}(\mathbf{r}')d\mathbf{r}' - \int_{\mathbf{l_j}}^{\mathbf{r}}\mathbf{A}(\mathbf{r}')d\mathbf{r}' = \int_{\mathbf{0}}^{\mathbf{r}}\mathbf{A}(\mathbf{r}')d\mathbf{r}' + \int_{\mathbf{r}}^{\mathbf{l_j}}\mathbf{A}(\mathbf{r}')d\mathbf{r}'$$
$$+ \int_{\mathbf{l_j}}^{\mathbf{0}}\mathbf{A}(\mathbf{r}')d\mathbf{r}' - \int_{\mathbf{l_j}}^{\mathbf{0}}\mathbf{A}(\mathbf{r}')d\mathbf{r}' \equiv \Phi(\mathbf{r}) + \int_{\mathbf{0}}^{\mathbf{l_j}}\mathbf{A}(\mathbf{r}')d\mathbf{r}' \tag{7.20}$$

where we have identified the flux going through a triangle with corners in $\mathbf{0}$, $\mathbf{l_j}$ and $\mathbf{r}$ through

$$\int_{\mathbf{0}}^{\mathbf{r}}\mathbf{A}(\mathbf{r}')d\mathbf{r}' + \int_{\mathbf{r}}^{\mathbf{l_j}}\mathbf{A}(\mathbf{r}')d\mathbf{r}' + \int_{\mathbf{l_j}}^{\mathbf{0}}\mathbf{A}(\mathbf{r}')d\mathbf{r}' = \oint d\mathbf{r}'\cdot\mathbf{A}(\mathbf{r}') =$$
$$\int d\sigma\cdot(\nabla\times\mathbf{A}(\mathbf{r}')) = \int d\sigma\cdot\mathbf{B}(\mathbf{r}') = \Phi(\mathbf{r}) \tag{7.21}$$

where we have used stokes theorem, and where we see that Φs dependence on $\mathbf{r}$ is to be understood as the dependence on the position of the corner of the triangle through which we integrate the magnetic flux. Notice, that in (7.19), we integrate over all of space. But the flux terms from different points $\mathbf{r}$ in the integral approximately cancel out, since the path of the line integral for some point $\mathbf{r}$ is in the opposite direction as the line integral for a corresponding point $\mathbf{r}'$, and thus

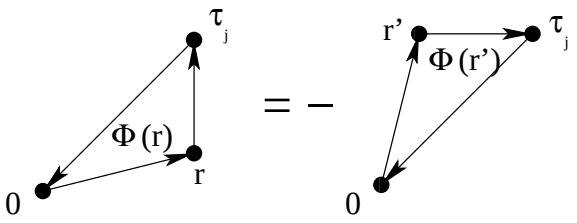

Figure 7.1: The flux going through the two triangles is assumed to be the same, but the direction of the line integral from (7.21) is anti-clockwise in the first, and clockwise in the second triangle, so they cancel out.

the flux from these to integrals cancel one another out as illustrated in figure 7.1, under the same assumption as above, namely that magnetic field does not change noticeably at an atomic length scale, so the magnitude of the fluxes are equal (there is also an atomic hamiltonian overlap in the position integral in (7.19), but at least for the dominant π, π orbital overlap in graphene in a position dependent Hückel approximation[2] this number is the same for the two points in figure 7.1, and so the argument still holds).

Thus, we may neglect the $\Phi(\mathbf{r})$ term in (7.20), and thus $G_{\mathbf{0}}(\mathbf{r}) - G_{\mathbf{0}+\mathbf{l_j}}(\mathbf{r})$ is independent on $\mathbf{r}$ and we may thus denote it by ϕ_j, where j denotes the bond $\mathbf{l_j}$. Inserting this into (7.19) we find

$$\sum_j e^{i\frac{2\pi}{\Phi_0}\phi_j} e^{i\mathbf{k}\cdot\mathbf{l_j}} \int d\mathbf{r}(\pi_B(\mathbf{r}-\mathbf{R}-\mathbf{l_j})^* \hat{H}_0 \pi_A(\mathbf{r}-\mathbf{R})) = \sum_j e^{i\frac{2\pi}{\Phi_0}\phi_j} e^{i\mathbf{k}\cdot\mathbf{l_j}} \gamma_0 \tag{7.23}$$

where we have inserted the magnetic flux quantum $\Phi_0 = \frac{h}{e}$[3]. This substitution, ie. the renormalization of the zero magnetic field overlap element with a phase factor is known as the Peierls substitution, and the phase ϕ_j is known as the Peierls phase first presented in [26].

The above derivations are all general in the sense that they apply irrespective of the direction of the magnetic field. We, however, have confined ourselves to a magnetic field in the axis direction, and in this case, a useful simplification is possible: Notice from the requirement that $b\mathbf{B} = B_z\hat{z}$ we may choose

$$\mathbf{A} = \frac{1}{2}\mathbf{B}\times\mathbf{r} = \frac{1}{2}Br\hat{\phi} \tag{7.24}$$

in cylindrical coordinates, so that the vector field points only in the $\hat{\phi}$ direction, leading to a

[2]that is to say, the approximation that not only the hamiltonian element between two orbitals is proportional to the overlap between the orbitals, but also that the integrants of these to overlaps is proportional, ie. point by point proportionality, or

$$\pi_B(\mathbf{r}-\mathbf{R}-\mathbf{l_j})^* \hat{H}_0 \pi_A(\mathbf{r}-\mathbf{R}) \propto \pi_B(\mathbf{r}-\mathbf{R}-\mathbf{l_j})^* \pi_A(\mathbf{r}-\mathbf{R}) \tag{7.22}$$

[3]note that this is twice the definition one typically finds for the flux quantum, since such a quantum was first anticipated by London[25] in a superconductor where the charge carriers are cooper pairs with a charge of $2e$

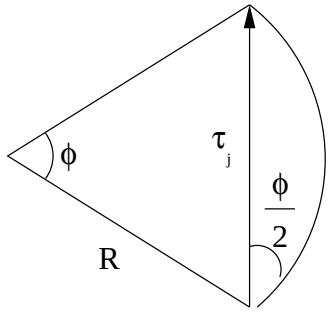

Figure 7.2: : Illustration of the sector of the CNT discussed in (7.26). The vector $\mathbf{l_j}$ connects two carbon atoms, and the flux we need to calculate is the flux going through the triangle: We approximate this by taking the flux through the entire sector, ie including the segment shown.

simplification of the integral in (7.20):

$$\phi_j = \int_{\mathbf{0}}^{\mathbf{l_j}} d\mathbf{r}' \cdot \mathbf{A}(\mathbf{r}') \tag{7.25}$$

We see that the integral is nothing else than the flux going through the triangle with corners in $\mathbf{0}$, j and the center of the tube, because we have that if $\mathbf{TC}$ denotes the corner on the tube axis,

$$\begin{aligned}\int_{\mathbf{0}}^{\mathbf{l_j}} d\mathbf{r}' \cdot \mathbf{A}(\mathbf{r}') &= \int_{\mathbf{0}}^{\mathbf{l_j}} d\mathbf{r}' \cdot \mathbf{A}(\mathbf{r}') + \int_{\mathbf{l_j}}^{\mathbf{TC}} d\mathbf{r}' \cdot \mathbf{A}(\mathbf{r}') + \int_{\mathbf{TC}}^{\mathbf{0}} d\mathbf{r}' \cdot \mathbf{A}(\mathbf{r}') \\ &= \oint d\mathbf{r}' \cdot \mathbf{A}(\mathbf{r}') = \int d\sigma \cdot \mathbf{B}(\mathbf{r}') = \frac{\phi}{2\pi}\pi R^2 B = \frac{\phi R^2 B}{2}\end{aligned} \tag{7.26}$$

where ϕ in the last to expressions denote the angle spanned by $\mathbf{l_j}$, as seen in figure 7.2 (so $|\mathbf{l_{j,\phi}}| \approx R\phi$), and where the first equality follows from the fact that $\mathbf{A}$ only has a component in the $\hat{\phi}$ direction, and the two additional line integrals are in the radial direction, so the scalar product is in fact identically zero, and the third equality follows from Stokes theorem and $\mathbf{B} = \nabla \times \mathbf{A}$. In deriving (7.26) we have made an approximation, in that we, without justification, add the flux going through the segment of the CNT outside the line from $\mathbf{0}$ to j. This error drops of with increasing radius of the CNT, since the area of the segment is $O(R^{-1})$, because the maximal distance from the straight line to the arc of the circle is $\frac{|\mathbf{l_j}|}{2}\sin(\frac{\phi}{2}) \approx \frac{|\mathbf{l_j}|^2}{R}$, and the length of the chord is of cause always $|l_{j,\phi}|$, and the area of the triangle that *is* included is $O(R)$, since it is approximately $R * sin(\phi) * R \approx R^2\frac{|l_{j,\phi}|}{R} = |l_{j,\phi}|R$, so the relative error is $O(R^{-2})$.

Notice that the phase from (7.26) can either be seen as a correction to the hamiltonian matrix element, or, equivalently, the orbital at $\mathbf{l_j}$. The latter interpretation means that orbitals next to j (other than $\mathbf{0}$) has an additional phase factor compared to the orbital at $\mathbf{0}$. We may continue that argument all the way around the CNT, until we come back to the orbital at $\mathbf{0}$, which alters the Bloch condition for the CNT, since if we wish to express the Bloch condition for the original, non-Aharonov-Bohm corrected blochwaves, we must now include the Peierls phase in the condition:

$$\Psi_{\mathbf{k}n}(\mathbf{r} + \mathbf{C}_h) = e^{i\mathbf{k}\cdot\mathbf{C}_h} e^{\frac{2\pi}{\Phi_0}\sum_i \int_{\mathbf{r_i}}^{\mathbf{r_{i+1}}} A(R,0,0) l_{i,i+1,\phi}} \Psi_{\mathbf{k}n}(\mathbf{r}) \tag{7.27}$$

where the sum over i is understood to run over a chain of nearest neighbour orbitals going around the circumference of the CNT, and $l_{i,i+1,\phi}$ is the length of the bond between the ith and the i+1st orbital in the circumference direction. In fact, this phase is easily calculated by realizing, that the integral of the sum corresponds, due to the argument below (7.26) to the total magnetic flux going through the CNT, so the blochcondition becomes

$$\Psi_{\mathbf{k}n}(\mathbf{r}+\mathbf{C}_h) = e^{i\mathbf{k}\cdot\mathbf{C}_h} e^{\frac{2\pi\Phi}{\Phi_0}} \Psi_{\mathbf{k}n}(\mathbf{r}) = e^{i2\pi(l_C+\frac{\Phi}{\Phi_0})} \Psi_{\mathbf{k}n}(\mathbf{r}) \tag{7.28}$$

where we have used (3.11) and (3.9). Now, in section 3 the periodic boundary conditions, ie. that $\Psi_{\mathbf{k}n}(\mathbf{r}+\mathbf{C}_h) = \Psi_{\mathbf{k}n}(\mathbf{r})$ meant that l_C should be an integer, but we now have the simple but powerful result that the Aharonov-Bohm effect changes this condition to

$$(l_C + \frac{\Phi}{\Phi_0}) \in \mathbb{Z} \tag{7.29}$$

This corresponds to shifting the allowed lines in figure 3.2 on page 18 in a direction perpendicular to the lines, ie. in the $\mathbf{k}_C$ direction. Remembering the low energy expression for the CNT (3.18),

$$E^{\pm}(\mathbf{k}) = \mp\frac{\gamma_0 a_0\sqrt{3}}{2}\sqrt{|k_C + ik_T|^2} = \mp\frac{\gamma_0 a_0\sqrt{3}}{6R}\sqrt{9R^2k_T^2 + (\nu + \frac{\Phi}{\Phi_0})} \tag{7.30}$$

where we remember that $\nu = \pm 1$ or 0 distinguishes the three chirality families, we see that the lowest lying energy states is changed differently by the re normalized quantization condition on l_C in (7.29) depending on ν: For a given $\nu = \pm 1$ (ie. semiconducting nanotube), the allowed k_C value moves away from one valley and towards the other, so one of the energies, that are equal without the magnetic field, increases, and the other decreases with an energy that, for $k_T = 0$ in (7.30) is proportional to the magnetic flux going through the CNT.

This lends itself to an intuitive, phenomenological description: Since the low energy states are always on opposite sides of the K versus the K' point, and the dispersion relation is approximately linear around the K(') points, we see that the group velocity in the circumference direction ($\frac{dE}{dk_C}$) of the states close to the K point is the same size, but opposite sign, as the lowenergy states close to the K' point, ie. the wavefunctions go around the circumference with the same speed, but in opposite directions. This could then be interpreted as a magnetic dipole moment, since the wavefunctions are of cause *electron*-wavefunctions and we thus have a charge in orbital motion around the CNT, and we recall the classical result (from eg [31]) that such a dipole moment has least energy when it is parallel to the magnetic field and highest energy when they are antiparallel, and that the energy of such a *classical* dipole moment is proportional to $\mathbf{B}\cdot\mathbf{L}$, $\mathbf{B}$ being the magnetic field, and $\mathbf{L}$ the angular momentum of the orbital motion. We see that this has the same functional form as the above result for the energy from the magnetic field due to the Aharonov-Bohm effect, but it is important to stress that the arguments are completely different, and that the classical result differs in some crucial points from the Aharonov-Bohm effect: For one, the functional dependence, ie. the linear dependence on velocity, was the same only because of the curious, Dirac-like linear dispersion relation around the K and K' points of the CNT, since this was used to get (7.30). Another very peculiar difference is, that while the classical argument relies on the Lorenz force on the electrons in a wire, ie. the magnetic field, $\mathbf{B}$, has to be non-zero at the

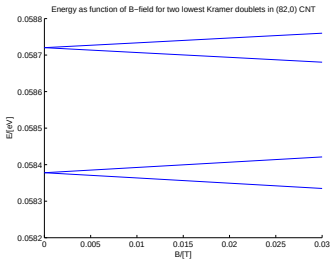

Figure 7.3: Energy as function of magnetic field for the four conduction bands in a (82,0) CNT. The valence band has the same form, ie. the energy has a linear dependence on the magnetic field, which is the result for all nanotubes tested. Note the splitting of the Kramer doublets: There is no degeneracy left when we apply a magnetic field.

position of the electrons, the Aharonov-Bohm effect refers only to the vector potential $\mathbf{A}$, or, as we saw, the flux going through the CNT: The magnetic field need not extend to the wall of the CNT, the electrons will "feel" it simply by going around it. This illustrates the general principle that while the $\mathbf{B}$ field is the "physical" entity in classical electrodynamics, and the $\mathbf{A}$ field is just a convenient, mathematical construction, in quantum mechanics, the $\mathbf{A}$ field is the fundamental physical field.

Another thing to note about the effect of the magnetic field is the breaking of the time-inversion symmetry: as we have seen, since the magnetic field defines a direction, one can no longer employ inversion symmetry to obtain degeneracy between the states close to the K versus the K' point, as we have seen. Thus we should expect the Kramer doublets to be split, and, when taking spin-orbit coupling and/or the Zeeman effect into account, the 4-fold degenerate LUMO and HOMO states, to split up into 4 different energies. This is indeed what happens in the numerical simulations, which we shall turn to now.

7.2.1 Numerical results

The results of the numerical simulations concerns two hypothesises which would be consequences of the above: First, that the energy has a linear dependence on the magnetic field: This is predicted from the conclusion reached in the end of section 7.2 above and from the fact that the Zeeman term from section 7.1 is also linear in the magnetic field. This was tested for various families of CNTs, namely the zigzag, armchair, $(n, \frac{n}{2})$ and $(n, \frac{n}{3})$ nanotubes for n up to 50 (and up to 90 for the zigzag nanotubes) [4], and in figure 7.3 we see a representative result for this calculation: A linear correspondence was confirmed in all cases tested.

The second hypothesis concerns the proportionality constant of this linear function. First, it should be admitted that this has still not been fully understood, and we therefore present only a heuristic argument based on the correspondence with a classical dipole moment presented above, ie. we shall treat the problem as if though it concerned charged particles moving on the circumference

[4] the reason for choosing these particular families will become clear in the next chapter

of the CNT in a magnetic field. We then know from basic magnetism, that the energy of the particle due to the magnetic field is

$$E_{mag} = -\mu \cdot \mathbf{B} \tag{7.31}$$

(see e.g. [31]) where μ is the magnetic dipole moment, which, for an electron going around a the circumference of a CNT of radius R is

$$\mu = \frac{-eRv_{Cg}}{2}\hat{y} \tag{7.32}$$

, where

$$v_{Cg} \equiv \frac{\partial E}{\hbar \partial k_C} \tag{7.33}$$

is the group velocity around the circumference.

Now, since we have discrete allowed values values for k_C due to the rotational boundary conditions, we may feel slightly uneasy about the derivative in (7.33). However, remembering that we consider the CNT to be a rolled up sheet of graphene, the group velocity around the circumference is the same as the group velocity in the appropriate direction in the graphene, ie. the direction of the $\mathbf{C}$ vector in the graphene sheet. Remembering (2.16) then, we see that, if we neglect the overlap matrix (which is justified, since the overlap, $s_0|\Gamma(\mathbf{k})|$ is small for $\mathbf{k}$ values around the K(') point that we are interested in, since here $|\Gamma(\mathbf{k})|$ is small) we have

$$E(\mathbf{k}) = -\gamma_0|\Gamma(\mathbf{k})| \tag{7.34}$$

and using (2.18) we find

$$E(\mathbf{k}) = -\gamma_0\frac{\sqrt{3}a}{2}|k_C + ik_T| \tag{7.35}$$

close to the Fermi points. In this thesis we wish to study the lowest lying energy states, and so we set $k_T = 0$ since we assume an infinitely long CNT. Thus we end up with

$$v_{Cg} = \frac{\partial E}{\hbar \partial k_C} = \pm\frac{-\gamma_0 a\sqrt{3}}{2\hbar} \approx \pm\frac{3.033eV 2.46\text{Å}\sqrt{3}}{2 \cdot 6.582 \cdot 10^{-16}eVs} \approx \pm 9.82 \cdot 10^5 \frac{m}{s} \tag{7.36}$$

which, due to the linear dispersion relation in graphene, is the value typically given for the Fermi velocity of graphene[19]. Inserting this into (7.32) and (7.31) we find that the proportionality factor between the magnetic field and the energy is

$$g_l = \frac{ev_{Cg}R}{2} = 4.91 \cdot 10^{-5} R[\text{Å}]\frac{eV}{T\text{Å}} \tag{7.37}$$

where the l subscript denotes that this is the proportionality constant for the orbital (or more correctly, Aharonov-Bohm) part of the magnetic coupling: There is also the coupling to the spin, seen in 7.1, where we know that g_s, ie the proportionality between the magnetic field and the energy, from (7.2) is

$$g_s = \mu_B s = \pm 5.79 \cdot 10^{-5}\frac{eV}{T} \tag{7.38}$$

where $s = \pm 1$ indicates the spin in the axial direction.

The numerical experiments for this hypothesis is shown for the zigzag CNTs in figure 7.4. As may be seen, given the assumptions made to reach the theoretical results (lines in figure 7.4) the correspondence with numerical data is quite good, leading us to the conclusion, that the phenomenological system of an electron on a cylinder is surprisingly good, even though it has little grounding in the quantum physical treatment of the system. The agreement between theory and numerical experiment holds also for the $(n, n/2)$, $(n, n/3)$ and armchair nanotubes, although we should note that, since there is no curvature gap in armchair nanotubes, and since they are all metallic, the states are four fold degenerate for no magnetic field. There is still, however, four different g-factors, corresponding to 2 orbital direction times 2 spin values, and so the pattern seen in figure 7.4 is still seen. The valence band exhibits a pattern similar to the one seen in 7.4, except that the structure of each triplet of radii is slightly different: in the conduction band, the absolute value of the g factors are seen to be slightly higher for the $\nu = -1$ family compared to the corresponding $\nu = 0$ (semi-metallic) family. This is not so in the valence band (shown in figure 7.5): Here the $\nu = -1$ family has a smaller g factor than the following $\nu = 0$ family. This is one example of the lack of particle-hole symmetry that appears in the system when both spin-orbit coupling, curvature and magnetic field are taken into consideration. Since this effect is very small, however, we don't attempt to explain it theoretically in this thesis.

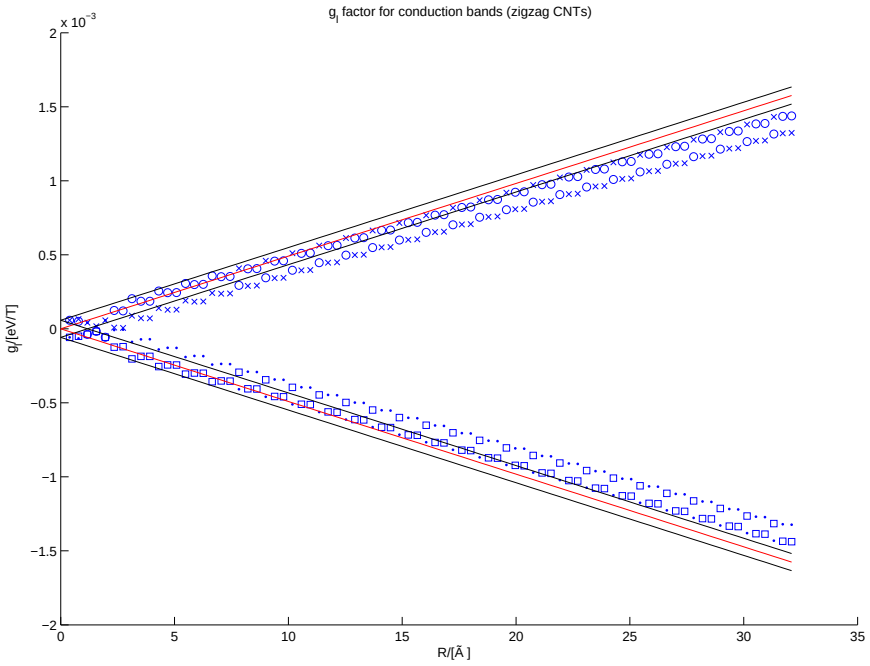

Figure 7.4: The proportionality constant between energy and magnetic field for zigzag CNTs (conduction band), ie. the slopes of the lines in figure 7.3. The circles and squares (crosses and dots) represent the g factor of the states from the lower (upper) Kramer doublet. The red lines is the theoretical value for g_l, ie. the proportionality constant between energy and the magnetic field due only to the Aharonov-Bohm effect, and the black lines correspond to the proportionality due to both Aharonov-Bohm and Zeeman effect.

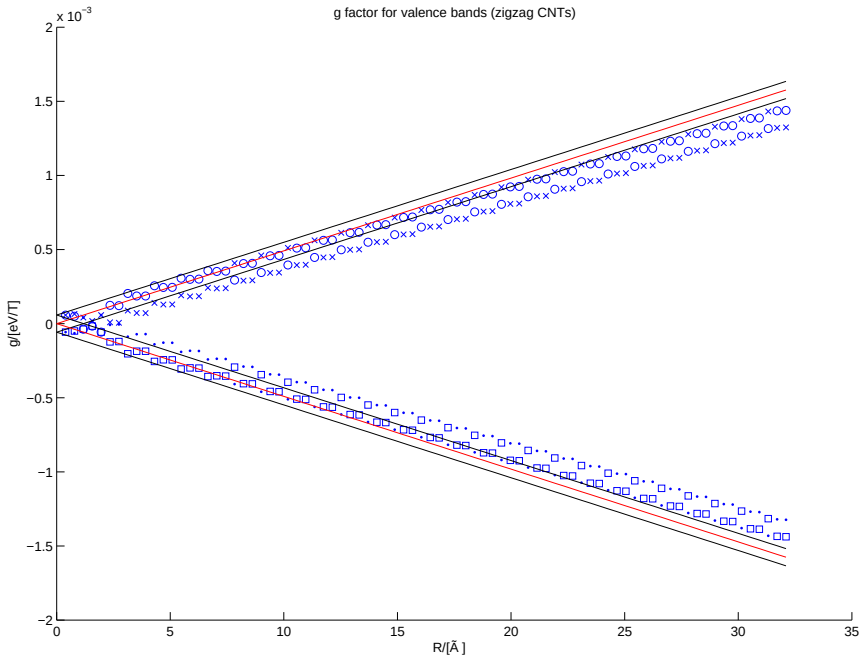

Figure 7.5: The proportionality constant between energy and magnetic field for zigzag CNTs (valence band). As for the conduction band, the circles and squares (crosses and dots) represent the g factor of the states from the lower (upper) Kramer doublet, and the red(black) lines are the theoretical g values without(with) Zeeman effect taken into account. Note that for the $\nu = -1$ family there is a difference compared to the conduction band in figure 7.4

Chapter 8

Nummerical Hückel calculations

This final chapter concerns the numerical method used to obtain the results presented in previous chapters. While we shall present as many mathematical arguments for the plausibility of this method, it is worth noting from the beginning that it is essentially an empirical method: The basic reason for believing the results of the algorithm is not theoretical but that it produces results that agree with experiments and/or more advanced algorithms, such as DFT.

We start out by simply presenting the method, then making as much progress as is possible from a purely theoretical viewpoint and further referring to the empirical data that reassures us that the method is plausible. We shall then make a few considerations on the subject of spin-orbit coupling and magnetic field in an EHT framework. Ending this chapter is a section elaborating on the method used by both [28] and [19] that allows a significantly more thorough search of the chirality space.

The extended Hückel theory framework for CNTs is described in [11], which describes the EHT method in general, and provides the parameters used by our numerical code.

8.1 The extended Hückel method

One benefit of the method is in the simplicity of its prescription: It assumes the geometry of the carbon nanotube, ie. the positions of the nuclei, and uses linear combinations of Slater type orbitals (STOs) at the nuclei as basis functions, which may be viewed as parametrized versions of the wellknown hydrogenic wavefunctions:

$$\Phi_{nlm}(\mathbf{r}) = Ne^{-\xi r}r^{n-1}Y_l^m(\theta,\phi) \tag{8.1}$$

which were suggested by Slater in [34], and where Y_l^m is the usual spherical harmonics. This gives us a set of parameters to determine for the problem, namely ξ_i for each STO and a coefficient c_i for each of them to determine the linear combination used. Note, that the units typically given in references are the Bohr units, ie. r has the numerical value 1 for the Bohr radius, and consequently ξ is given in reciprocal Bohr radii in table 8.1 below.

Further, the EHT method assumes that the diagonal elements of the hamiltonian, ie. the self-energy of a given orbital, is to be benchmarked against the difference between the electron affinity

and the ionization energy for that orbital. It is important to note that in the EHT method, the selfenergy is treated as a parameter, but we are able to make a heuristic argument for the size of these elements: Adding an electron in a given orbital yields an energy which is per definition the electron affinity (assuming that the atom being added to was neutral before adding the extra electron), but this electron has to come from some other atom, and removing it from that atom will cost the ionization energy. This argument is admittedly very crude and approximate, but it yields an understanding of the fact that the Hückel method has one parameter for each kind of orbital in the system: In our case the 2s and 2p orbitals in carbon.

Of these two we should expect a higher energy of the 2p orbitals, based on repulsion between the electron being added and the core 1s electrons: the 2p orbitals have a smaller average distance from the nuclei (and therefore a higher Coulomb repulsion energy) with these electrons: Thus less energy will be freed by putting an electron into the 2p orbital than the 2s orbital.

EHT explicitly assumes that the core electrons are deep in the Fermi sea, and thus can be neglected, but it is possible (and [11] gives parameters) to could include $n = 3$ or higher orbitals in the model. In this thesis we choose to work with the $n = 2$ orbitals only, and so there are two different parameters for the diagonal elements, namely ϵ_p and ϵ_s for the 2p and 2s orbitals respectively.

Once the orbitals and selfenergies are set, the EHT method defines a way to determine the off-diagonal matrix elements of the hamiltonian from the elements of the overlap matrix and the diagonal matrix elements. The overlap matrix is determined by (numerical) integration given the functional form of the STOs (8.1)

Notice that the selfenergy values do *not* take into account the crystal field: The geometrical dependencies are assumed to be contained in the overlap matrix exclusively: one finds the off-diagonal elements by multiplying the corresponding overlap matrix element by the average of the two diagonal matrix elements and a model parameter K_{EHT} which is set to 2.8, a value found from [33]. This is a major assumption: One may show relatively rigorously that an orbital pair dependent constant could be reasonably assumed, but the only reason for assuming the systemwide constant K_{EHT} lies in the empirical agreement with more advanced methods or experiments.

So, finally we see that, given a set of orbitals $\phi_\nu(\mathbf{r})$ (in our case linear combinations of STOs and where ν denotes the orbital) and the energies of electrons in these orbitals (E_ν), we can set up the necessary elements for the secular equation presented in the previous chapters, ie. (2.11), using three rules:

$$S_{\nu\mu} = \int d(\mathbf{r})\phi^*_\nu(\mathbf{r})\phi_\mu(\mathbf{r}) \tag{8.2}$$

$$H_{\nu\nu} = E_\nu \tag{8.3}$$

$$H_{\nu\mu} = K_{EHT}S_{\nu\mu}\frac{H_{\nu\nu} + H_{\mu\mu}}{2} \tag{8.4}$$

This problem is then in principle easy to solve, since it is a simple secular equation, although in practice, since the dimensionality of the problem can easily be of the order of 10000, advanced methods are used for diagonalizing the matrix, in our case the Lanczos algorithm.

8.1.1 Semi-heuristic argument for EHT

There are two classes of situations, where one may theoretically explain (8.4), ie. a central assumption of EHT, namely in two distinct situations where $H_{\nu\mu} = 0$. One is the case when the two orbitals are very far from one another. In this case we would heuristically not expect any hopping between the orbitals, and, since the STOs decay exponentially with distance from the nucleus, the overlap integral will go towards zero, and by (8.4) we get $H_{\nu\mu} \to 0$.

The other case is that the overlap integral is zero due to the parity properties of the two orbitals, ie. we have that

$$S_{\nu\mu} = \int d(\mathbf{r})\phi^*_\nu(\mathbf{r})\phi_\mu(\mathbf{r}) = 0 \tag{8.5}$$

because the integrant is odd in one or more of the coordinates x,y or z.

In this case, (8.4) yields a zero hopping element between these orbitals: This is actually a reasonable assumption in our case, at least for nearest neighbours - assume that the hamiltonian is simply described by

$$\hat{H} = -\hbar^2\hat{\nabla}^2 + \hat{V}(\mathbf{x}) \tag{8.6}$$

where the potential is simply the sum of the centrosymetric atomic potentials generated by the nuclei. Observe first, that the kinetic energy operator $-\hbar^2\hat{\nabla}^2$ is even in all coordinates. This is due to the fact that $\frac{d}{dx_i}$ is odd in x_i and thus $(\frac{d}{dx_i})^2$ is even in x_i and therefore $\hat{\nabla}^2 \equiv \frac{d}{dx}^2 + \frac{d}{dy}^2 + \frac{d}{dz}^2$ is even in all coordinates since a sum of even functions is itself even. Thus we have that the kinetic part of the hamiltonian element is

$$\int d\mathbf{r}\phi^*_\nu(\mathbf{r})(-\hbar^2\hat{\nabla}^2)\phi_\mu(\mathbf{r}) = -\hbar^2 \int d\mathbf{r}\phi^*_\nu(\mathbf{r})\psi_\mu(\mathbf{r}) \tag{8.7}$$

where $\psi_\mu(\mathbf{r})$ is some function with the same parity as $\phi_\mu(\mathbf{r})$. But if we then use the assumption that the overlap integral between the orbits is zero due to parity, we see that the kinetic energy is also zero: The same parity argument can be applied to (8.7) as could, by assumption, be applied to (8.5).

This leaves the potential part of the hamiltonian. Now, assuming that the two orbitals in question are nearest neighbours, it is reasonable to assume that the relevant part of the potential is the sum of the two centrosymetric potentials from each nuclei. Here we see that the sum of these potentials is rotationally invariant around a line connecting the two nuclei. This means that, if we define the directions y' and z' perpendicular to one another and to the line between the nuclei, the potential operator preserves parity in these two directions, since $V(\mathbf{r})$ is dependent only on the distance from this axis, and the position along it, not on the angular coordinate in a cylindrical coordinate system with the line between the atoms defining the axial coordinate. Remembering table 3.1, we know that all the cases where the overlap matrix element is zero (due to parity) involves at least one orbital which is odd along either y' or z', since the parity properties of the STOs are the same as for standard, hydrogenic atomic orbitals. Together, these observations mean, that if we examine the potential part of the hamiltonian,

$$\int d\mathbf{r}\phi^*_\nu(\mathbf{r})V(\mathbf{r})\phi_\mu(\mathbf{r}) = -\hbar^2 \int d\mathbf{r}\phi^*_\nu(\mathbf{r})\psi_\mu(\mathbf{r}) \tag{8.8}$$

Orbital	E	ξ_1	c_1	ξ_2	c_2
2s	-20.316	2.037	0.741	0	0
2p	-13.670	1.777	0.640	3.249	0.412

Table 8.1: The parameters used for the linear combinations of STOs used in the EHT calculations. The last parameter is the hückel constant, K_{EHT} which is 2.8. All the parameters are taken from [11].

we find, that $\psi_\mu(\mathbf{r})$ has the same parity properties in y' and z' as the original orbital function $\phi_\mu(\mathbf{r})$, and thus, coupled with table 3.1, we see that the assumption (8.5) leads to the potential integral in (8.8) being zero.

Finally, remembering that the atomic orbitals are localized around their nuclei, we may make the further assumption, that even if the two orbitals are not on neighbouring atoms, the only relevant terms of the potential in the integral determining the hamiltonian matrix element are the potentials of the "parent" nuclei, since the potential of all other nuclei is small at the positions where the two orbitals are non vanishing.

The above considerations does not, of cause, prove the plausibility of the extended hückel method: In particular there is no reason to believe that a single constant for the entire system, K_{EHT} is determinable. Here, we turn to the fact that, in [11] the authors show that it is possible to find parameters for K_{EHT} and the STO orbitals (ie. sets of $c_{i,\nu}$,$\xi_{i,\nu}$ and E_ν), so that the resulting dispersion relations of the hückel method for CNTs agree with those found in using DFT. Since the parameters are simply taken as input in our model, we shall not elaborate further on this. The parameters are found in table 8.1, which is a copy of table 1 in [11].

8.2 EHT for magnetic field and spin-orbit coupling

The method covered so far, and indeed in the literature [11] immediately apply to our problem of a CNT, however, it is not clear how to augment it to function with spin-orbit coupling and a magnetic field as well, without which the model is of no use to us. This section gives the arguments for the applicability of the above to the full problem of this thesis.

The magnetic field is easily introduced by observing that nothing was assumed about the atomic orbitals for the derivation of the Peierls phase (7.23) in the previous chapter, except that the orbitals should be localized at the atomic sites, which is certainly fulfilled for the STOs (8.1), since the value of ξ yielding the standard hydrogenic orbitals would be 0.5[1], and the orbitals used have a minimum ξ value of $1,777a_0^{-1}$. Thus we may avail ourselves of the Peierls substitution in augmenting (8.4) to

$$H_{\nu\mu} = K_{EHT} S_{\nu\mu} e^{i2\pi \frac{\int d\sigma \cdot \mathbf{B}(\mathbf{r})}{\Phi_0}} \frac{H_{\nu\nu} + H_{\mu\mu}}{2} \tag{8.9}$$

where we remember that the integral may be approximated well by the magnetic flux going through the section of the CNT from the ν atom to the μ atom, ie. if the magnetic flux going through the

[1] note, that a_0 here is the Bohr radius 0.53Å, not the lattice constant of graphene

CNT is Φ, we have that $\int d\sigma \cdot \mathbf{B}(\mathbf{r}) = \frac{\phi_{\nu\mu}}{2\pi}\Phi$, so we find the result

$$H_{\nu\mu} = K_{EHT} S_{\nu\mu} e^{i\phi_{\nu\mu}\frac{\Phi}{\Phi_0}} \frac{H_{\nu\nu} + H_{\mu\mu}}{2} \tag{8.10}$$

where $\phi_{\nu\mu}$ (the difference in angular coordinate between ν and μ) is known in EHT, since it presumes the geometry of the atoms in the CNT.

Spin-orbit coupling can in fact be included by (obviously) adding a spin degree of freedom to the STOs (8.1) and using the same formulas as was developed using hydrogenic orbitals in chapters 4 and 6. This is possible due to the fact that the spin-orbit hamiltonian

$$\hat{H}_{SO} \propto \hat{\mathbf{L}} \cdot \hat{\mathbf{S}} = \hat{L}_z \hat{S}_z + \frac{1}{2}(\hat{L}_+ \hat{S}_- + \hat{L}_- \hat{S}_+) \tag{8.11}$$

only contains operators that depend on the angular part of the spatial wavefunction, plus the spin degree of freedom, or, equivalently depends only on the quantum numbers m_l and m_s, and neither of these are dependent on the radial part of the basis functions. But since we see in (8.1) that the angular part of the STOs is the same as it is for the hydrogenic wavefunctions, ie. spherical harmonics, there is no difference in the application of the spin-orbit coupling hamiltonian.

8.3 A more efficient method

The method used for the calculations in this thesis depends on the translational unitcell, and the overlap integrals between all pairs of orbitals in this unitcell must be calculated and a matrix of dimension "number of overlaps" must be diagonalized. Now, given that each atom have 4 orbitals relevant for overlap calculation (since spin overlaps is trivially $\delta_{s,s'}$, $s(')$ being the spin of the orbitals), and the number of atoms pr. helical unit cell is 2, and remembering (3.8), we see that the number of orbitals that is to be used is

$$N_{orbs} \equiv 2 \cdot 8 \frac{2(n^2 + m^2 + nm)}{\gcd(2n + m, 2m + n)} \tag{8.12}$$

while the dimensionality the hamiltonian is 2 times bigger (due to spin), for a given chirality (n, m). A relevant figure to compare this number to is the circumference of the nanotube, since we need to see the radial dependence of the effective hamiltonians found from theory, and compare with numerical results. Now using $\mathbf{C} = n\mathbf{a}_1 + m\mathbf{a}_2$, we see, using (2.1), that

$$|\mathbf{C}|^2 = (n\mathbf{a}_1 + m\mathbf{a}_2) \cdot (n\mathbf{a}_1 + m\mathbf{a}_2) = a_0^2(n^2 + m^2 + 2nm(\mathbf{a}_1 \cdot \mathbf{a}_2)) = a_0^2(n^2 + m^2 + nm) \tag{8.13}$$

so that we get

$$\frac{N_{orbs}}{|\mathbf{C}|} = \frac{16\sqrt{n^2 + m^2 + nm}}{a_0 \gcd(2n + m, 2m + n)} \tag{8.14}$$

In order for the hückel method to use as few computational resources as possible, we wish to minimize this fraction. Simultaneously, we also might want to study families of chiralities that have equidirectional chiral vectors, or equivalently have some fixed factor $f \equiv \frac{n}{m}$. It is from these

two demands that we get the idea first presented in chapter 7: let f be some small integer. Then we have

$$\frac{N_{orbs}}{|\mathbf{C}|} = \frac{16m\sqrt{f^2+f+1}}{a_0 \gcd((f+2)m,(2f+1)m)} = \frac{16}{a_0}\frac{\sqrt{f^2+f+1}}{\gcd(f+2,2f+1)} \tag{8.15}$$

where we see that, assuming the worst-case scenario that $\gcd(f+2,2f+1)=1$, the fraction is linear in f, thus the demand that f should be small. In practice, it turns out that the largest f for which a reasonably large set of chiralities can be calculated was 3 - this limits the method used severely in terms of scouring the chirality space, as mentioned in the final effect presented in chapter 7. Note that achiral CNTs are always "easy", since here $\gcd(2n+m,2m+n) \propto n$, and $|\mathbf{C}| \propto n$, leading to a small fraction in (8.15).

There is a better way of doing this, using the arguments first presented in [19], namely using the crystal structure of the CNT in the numerical calculation, so that we reduce the size of the hamiltonian that is to be diagonalized from the translational unitcells size to the 16x16 hamiltonian natural to the helical unitcell. This is a situation, where the symmetry adapted blochfunctions (6.48) becomes important, since they allow us to maintain delta functions in the angular momentum, since these functions have been adapted to *total* angular momentum, which is not altered by spin-orbit coupling (as there is no coupling to any environment that could absorb the angular momentum). Thus, if we calculate the overlap between the Bloch functions explicitly we find

$$\begin{aligned}\langle j'\sigma'\tilde{s}\mathbf{k}_{J'}||j\sigma\tilde{s}\mathbf{k}_J\rangle &= \frac{1}{N_s}\sum_{l,l'} e^{i((k_t z_l - k'_t z_{l'})+(J\theta_l - J'\theta_{l'}))}\langle j'\sigma'\theta_{l'}z_{l'}s_{l'}||j\sigma\theta_l z_l s_l\rangle \\ &= \sum_l e^{i(k_t z_l+\mu\theta_l)}e^{i\frac{1-s}{2}\theta_l}\langle j'\sigma'\theta_0 z_0 s||j\sigma\theta_l z_l s\rangle\delta_{\mathbf{k}_{J'},\mathbf{k_J}} \equiv S_{j'\sigma'\tilde{s},j\sigma\tilde{s}}\delta_{\mathbf{k}_J,\mathbf{k}_{J'}}\end{aligned} \tag{8.16}$$

where we have implicitly used that there is no overlap between spin up and spin down, and where we used in the third equality that the inner of the two sums over the crystal always gives the same result. There is a completely analogous derivation for the hamiltonian overlap, ie. giving us $H_{j'\sigma'\tilde{s},j\sigma\tilde{s}}$. Notice how we get a angular dependence from the rotation of spin coordinatesystems which comes from the fact, that in order to evaluate the overlap between atomic orbitals, we need them represented in the same coordinatesystems, ie. the global spin system, and, recalling (6.46), this gives us a spin-dependent phase, even though the atomic overlap itself is spin-independent. The above calculation takes care of both the graphene and the curvature part of the hamiltonian: We make no assumptions of nearest neighbour coupling only, rather we simply calculate overlaps based on either the Hückel approximation presented above (ie. calculate the atomic overlaps in directly as integrals in (8.16) and use (8.4) to find the hamiltonian overlaps), or use a, possibly superior, way of approximating the integrals using ab initio calculations directly[27], rather than the somewhat crude approximations made in the Hückel method, ie. finding the overlaps from fitting the dispersion relation to ab initio calculations.

We also need the spin-orbit coupling matrix in this numerical effective hamiltonian, but this turns out to be very simple, due to the fact that in (6.48) we define the symmetry adapted wavefunctions as a sum over wavefunctions where the spin is defined in the local coordinate system, and since the spin-orbit coupling is still assumed to be intra-atomic only, the spin-orbit overlap is

either 0, or can be calculated using e.g. (4.14), and so we find

$$\begin{aligned}
\langle x\sigma\tilde{s}'\mathbf{k}_{J'}|\hat{H}_{so}|y\sigma\tilde{s}\mathbf{k}_J\rangle &= \frac{1}{N_s}\sum_{l,l'} e^{i((k_t z_l - k'_t z_{l'})+(J\theta_l - J'\theta_{l'}))}\langle x\sigma\theta_{l'}z_{l'}s_{l'}|\hat{H}_{so}|y\sigma\theta_l z_l s_l\rangle \\
&= -i\frac{V_{so}}{2}\delta_{\tilde{s}',-\tilde{s}_{l'}}\delta_{\mathbf{k}_J,\mathbf{k}_{J'}} \equiv \hat{H}_{SO,x\sigma\tilde{s}',y\sigma\tilde{s}}\delta_{\tilde{s}',-\tilde{s}_{l'}}\delta_{\mathbf{k}_J,\mathbf{k}_{J'}} \qquad (8.17) \\
\langle z\sigma\tilde{s}'\mathbf{k}_{J'}|\hat{H}_{so}|y\sigma\tilde{s}\mathbf{k}_J\rangle &= \frac{1}{N_s}\sum_{l,l'} e^{i((k_t z_l - k'_t z_{l'})+(J\theta_l - J'\theta_{l'}))}\langle z\sigma\theta_{l'}z_{l'}s_{l'}|\hat{H}_{so}|y\sigma\theta_l z_l s_l\rangle \\
&= \tilde{s}\frac{V_{so}}{2}\delta_{\tilde{s}',-\tilde{s}_{l'}}\delta_{\mathbf{k}_J,\mathbf{k}_{J'}} \equiv \hat{H}_{SO,z\sigma\tilde{s}',y\sigma\tilde{s}}\delta_{\tilde{s}',-\tilde{s}_{l'}}\delta_{\mathbf{k}_J,\mathbf{k}_{J'}} \qquad (8.18) \\
\langle z\sigma\tilde{s}'\mathbf{k}_{J'}|\hat{H}_{so}|x\sigma\tilde{s}\mathbf{k}_J\rangle &= \frac{1}{N_s}\sum_{l,l'} e^{i((k_t z_l - k'_t z_{l'})+(J\theta_l - J'\theta_{l'}))}\langle z\sigma\theta_{l'}z_{l'}s_{l'}|\hat{H}_{so}|x\sigma\theta_l z_l s_l\rangle \\
&= -i\tilde{s}\frac{V_{so}}{2}\delta_{\tilde{s}',\tilde{s}_{l'}}\delta_{\mathbf{k}_J,\mathbf{k}_{J'}} \equiv \hat{H}_{SO,z\sigma\tilde{s}',x\sigma\tilde{s}}\delta_{\tilde{s}',\tilde{s}_{l'}}\delta_{\mathbf{k}_J,\mathbf{k}_{J'}} \qquad (8.19)
\end{aligned}$$

plus the hermitian conjugates of the above.

Now, one can simply set up the 16x16 effective hamiltonian, which can easily be solved *no matter the size of the translational unitcell*, ie. irrespective of chirality. This enables both [19] and [28] to make numerical experiments for any realistic chirality - the reason this was not used in this thesis, is that we used a commercial implementation of the Hückel method, which was developed to examine general systems, rather than crystals, and thus is not capable of employing the above simplification.

Finally, it should be stressed, however, that the results obtained from our numerical experiments are qualitatively consistent with the results in [28] and [19] - quantitatively, however there are some differences, most likely due to the difference described in the methods of obtaining the atomic overlaps.

Chapter 9

Conclusion

In summary, we found the explanation for the main problems of the thesis posed in chapter 5, thus explaining the surprising fact, that the spin-orbit induced energy gaps vary wildly as a function of chirality: Even though the geometry of two carbon nanotubes is almost the same, this energy gap can be several orders of magnitude different for them. Simultaneously we found the explanation for the lack of particle-hole symmetry when spin-orbit coupling in the spin-orbit gap.

We also found a good correspondence between the theoretical expectations of the effect of a magnetic field, and the numerical data.

Thus having established a more refined understanding of spin-orbit coupling in carbon nanotubes, we can continue the effort to establish the spin of electrons in quantum dots in carbon nanotubes as a physical basis for qubits, and thus eventually as parts for a physical implementation of the quantum computing which have attracted such attention in the last 25 years.

Appendix A

$\sigma - \sigma$ coupling elements

We wish to derive the parameters $\mathbf{p}_{\sigma_{\mathrm{l}',\mathbf{B}}} \cdot \mathbf{p}_{\sigma_{\mathrm{l},\mathbf{A}}}$ and $\mathbf{p}_{\sigma_{\mathrm{l}',\mathbf{B}}} \cdot \hat{\mathbf{R}}_{\mathbf{A}}$, defined in section 3.3.

First we need to find the $\mathbf{p}_{\sigma_{\mathbf{1},\mathbf{B}}}$ vector, ie. the unitvector pointing in the direction of the σ orbital of the target atom pointing towards the origo (see section 3.3 for definitions of the atom positions). This is done through noticing, that the demand that it must point towards the origo atom implies that

$$\frac{p_{\sigma_{1,B},C}}{p_{\sigma_{1,B},T}} = \frac{\hat{R_{i,C}}}{\hat{R_{i,T}}} = \frac{cos(\alpha_i)}{tan(\beta_i)} \tag{A.1}$$

where the C/T subscripts denote the respective coordinates. Also, in order for $\mathbf{p}_{\sigma_{\mathbf{1},\mathbf{B}}}$ to point in the direction of a *sigma* orbital, it needs to be perpendicular to the π orbital at the target atom, ie. we also have that

$$\mathbf{p}_{\sigma_{\mathbf{1},\mathbf{B}}} \cdot \pi_{\mathbf{B}} = 0 \tag{A.2}$$

And finally, in order for the vector to be a *unit*vector, we also demand that

$$|\mathbf{p}_{\sigma_{\mathbf{1},\mathbf{B}}}|^2 = {\mathbf{p}_{\sigma_{\mathbf{1},\mathbf{B}},\mathbf{T}}}^2 + {\mathbf{p}_{\sigma_{\mathbf{1},\mathbf{B}},\mathbf{C}}}^2 + {\mathbf{p}_{\sigma_{\mathbf{1},\mathbf{B}},\mathbf{R}}}^2 = 1 \tag{A.3}$$

Starting out from (A.2), we have, given that, since $\pi_{\mathbf{B}} = (sin(2\alpha_i), 0, cos(2\alpha_i))$,

$$\mathbf{p}_{\sigma_{\mathbf{1},\mathbf{B}}} \cdot \pi_{\mathbf{B}} = \mathbf{p}_{\sigma_{\mathbf{1},\mathbf{B}},\mathbf{C}} sin(2\alpha_i) + \mathbf{p}_{\sigma_{\mathbf{1},\mathbf{B}},\mathbf{R}} cos(2\alpha_i) \implies \mathbf{p}_{\sigma_{\mathbf{1},\mathbf{B}},\mathbf{C}} = -\frac{\mathbf{p}_{\sigma_{\mathbf{1},\mathbf{B}},\mathbf{R}}}{tan(2\alpha_i)} \tag{A.4}$$

and this, along with (A.1),

$$\mathbf{p}_{\sigma_{\mathbf{1},\mathbf{B}},\mathbf{T}} = -\frac{\mathbf{p}_{\sigma_{\mathbf{1},\mathbf{B}},\mathbf{R}} tan(\beta_i)}{cos(\alpha_i) tan(2\alpha_i)} \tag{A.5}$$

We thus have both $\mathbf{p}_{\sigma_{\mathbf{1},\mathbf{B}},\mathbf{C}}$ and $\mathbf{p}_{\sigma_{\mathbf{1},\mathbf{B}},\mathbf{T}}$ in terms of $\mathbf{p}_{\sigma_{\mathbf{1},\mathbf{B}},\mathbf{R}}$, and we can therefore insert (A.4) and (A.5) into (A.3), and, after some algebraic manipulations, we reach

$$\mathbf{p}_{\sigma_{\mathbf{1},\mathbf{B}},\mathbf{R}} = +\sqrt{\frac{tan^2(2\alpha_i)}{1 + (\frac{tan(\beta_i)}{cos(\alpha_i)})^2 + tan^2(2\alpha_i)}} \tag{A.6}$$

where we explicitly take the positive solution (taking the negative value of the square root in (A.6) would of cause also have worked, as (A.3) is only a constraint on ${\mathbf{p}_{\sigma_{\mathbf{1},\mathbf{B}},\mathbf{R}}}^2$). This is to insure that

we get the solution that points *towards*, rather that away from, the origo atom: We should always have that $\mathbf{p}_{\sigma_{\mathbf{1,B,R}}} \geq 0$, since the R direction is defined as the *Cartesian* direction along the radial direction at the position of the origo atom. Now we can combine (A.6) with (A.4) and (A.5) to find

$$\mathbf{p}_{\sigma_{\mathbf{1,B,C}}} = -\frac{1}{tan(2\alpha_i)}\sqrt{\frac{tan^2(2\alpha_i)}{1+(\frac{tan(\beta_i)}{cos(\alpha_i)})^2+tan^2(2\alpha_i)}} \tag{A.7}$$

and

$$\mathbf{p}_{\sigma_{\mathbf{1,B,T}}} = -\frac{tan(\beta_i)}{cos(\alpha_i)tan(2\alpha_i)}\sqrt{\frac{tan^2(2\alpha_i)}{1+(\frac{tan(\beta_i)}{cos(\alpha_i)})^2+tan^2(2\alpha_i)}} \tag{A.8}$$

We then have to find the two other unitvectors corresponding to $\sigma_{2,B}$ and $\sigma_{3,B}$. In total analogy with the case for the origo atom, we may find these vectors be rotating the $\mathbf{p}_{\sigma_{\mathbf{1,B,R}}}$ vector ± 120 degrees around the $\pi_{\mathbf{B}}$ vector. This is done by performing a coordinatesystem shift on the rotation matrix already used in (3.36), ie.

$$\mathbf{O}_\sigma = \begin{pmatrix} cos(\frac{2\pi}{3}) & -sin(\frac{2\pi}{3}) & 0 \\ sin(\frac{2\pi}{3}) & cos(\frac{2\pi}{3}) & 0 \\ 0 & 0 & 1 \end{pmatrix} = \begin{pmatrix} -\frac{1}{2} & -\frac{\sqrt{3}}{2} & 0 \\ \frac{\sqrt{3}}{2} & -\frac{1}{2} & 0 \\ 0 & 0 & 1 \end{pmatrix} \tag{A.9}$$

, and since we have $\pi_{\mathbf{B}} = (sin(2\alpha_i), 0, cos(2\alpha_i))$, the rotation matrix that takes the radial direction into $\pi_{\mathbf{B}}$ and preserves the tube axis is $\mathbf{O}_\pi = \begin{pmatrix} cos(2\alpha_i) & 0 & -sin(2\alpha_i) \\ 0 & 1 & 0 \\ sin(2\alpha_i) & 0 & cos(2\alpha_i) \end{pmatrix}$, and we find that the desired rotation matrix is

$$\mathbf{O}_{\sigma,\mathbf{B}} = {\mathbf{O}_\pi}^{-1}\mathbf{O}_\sigma\mathbf{O}_\pi = \begin{pmatrix} \frac{1}{4}(1-3cos(4\alpha_i)) & -\frac{1}{2}\sqrt{3}cos(2\alpha_i) & \frac{3}{4}sin(4\alpha_i) \\ \frac{1}{2}\sqrt{3}cos(2\alpha_i) & -\frac{1}{2} & -\sqrt{3}cos(\alpha_i)sin(\alpha_i) \\ \frac{3}{4}sin(4\alpha_i) & \sqrt{3}cos(\alpha_i)sin(\alpha_i) & \frac{1}{4}(1+3cos(4\alpha_i)) \end{pmatrix} \tag{A.10}$$

At this point the algebraic expressions regrettably become somewhat more complex but clearly we now have

$$\mathbf{p}_{\sigma_{\mathbf{2,B,R}}} = \mathbf{O}_{\sigma,\mathbf{B}}\mathbf{p}_{\sigma_{\mathbf{1,B,R}}} \qquad \mathbf{p}_{\sigma_{\mathbf{3,B,R}}} = {\mathbf{O}_{\sigma,\mathbf{B}}}^2\mathbf{p}_{\sigma_{\mathbf{1,B,R}}} \tag{A.11}$$

and with these it is in principle trivial to calculate the necessary inner products, but we choose not to present them here because of their complexity.

Appendix B

Explicit H_{SO} matrix

B.1 Explicit H_{so} matrix

$$\begin{pmatrix}
0 & -\frac{i}{\sqrt{3}} & \frac{i}{\sqrt{3}} & 0 & 0 & 0 & 0 & -\sqrt{\frac{2}{3}}e^{i\beta} \\
\frac{i}{\sqrt{3}} & 0 & -\frac{i}{\sqrt{3}} & 0 & 0 & 0 & 0 & \frac{\left(-3i+\sqrt{3}\right)e^{i\beta}}{3\sqrt{2}} \\
-\frac{i}{\sqrt{3}} & \frac{i}{\sqrt{3}} & 0 & 0 & 0 & 0 & 0 & \frac{\left(3i+\sqrt{3}\right)e^{i\beta}}{3\sqrt{2}} \\
0 & 0 & 0 & 0 & \sqrt{\frac{2}{3}}e^{i\beta} & -\frac{\sqrt{2}\left(-3i+\sqrt{3}\right)e^{i\beta}}{6} & -\frac{\sqrt{2}\left(3i+\sqrt{3}\right)e^{i\beta}}{6} & 0 \\
0 & 0 & 0 & \sqrt{\frac{2}{3}}(e^{-i\beta} & 0 & \frac{i}{\sqrt{3}} & -\frac{i}{\sqrt{3}} & 0 \\
0 & 0 & 0 & -\frac{\left(3i+\sqrt{3}\right)e^{-i\beta}}{3\sqrt{2}} & -\frac{i}{\sqrt{3}} & 0 & \frac{i}{\sqrt{3}} & 0 \\
0 & 0 & 0 & -\frac{\left(-3i+\sqrt{3}\right)e^{-i\beta}}{3\sqrt{2}} & \frac{i}{\sqrt{3}} & -\frac{i}{\sqrt{3}} & 0 & 0 \\
-\sqrt{\frac{2}{3}}e^{-i\beta} & \frac{\sqrt{2}\left(3i+\sqrt{3}\right)e^{-i\beta}}{6} & \frac{\sqrt{2}\left(-3i+\sqrt{3}\right)e^{-i\beta}}{6} & 0 & 0 & 0 & 0 & 0
\end{pmatrix} \tag{B.1}$$

Appendix C

Oddness of derivative operator

The derivative function is odd, ie. if $E(x)$ is an even function in x, $\frac{dE}{dx}$ is odd in x, and if $O(x)$ is odd in x, $\frac{dO}{dx}$ is even in x

Proof: let E be an even function in x. We then have

$$\frac{dE(-x)}{dx} = \lim_{\Delta\to 0} \frac{E(-x+\Delta) - E(-x)}{-x+\Delta-(-x)} = \lim_{\Delta\to 0} \frac{E(x-\Delta) - E(x)}{x+\Delta-x}$$
$$= \lim_{\Delta\to 0} \frac{E(x') - E(x'+\Delta)}{x'+\Delta-x'} = -\frac{dE(x')}{dx'} \approx -\frac{dE(x)}{dx} \tag{C.1}$$

where in the second equality we use that $E(x)$ is even in x, and $x' = x - \Delta$, ie. for the relevant limit of $\Delta \to 0$, $x' = x$ so the last $\approx$ is actually an equality. The other case, ie. the derivative of an odd function, proceeds in exactly the same way, except we get an extra minus in the second equality, which carries through to the final expression proving that the derivatives of odd functions are even.□

Appendix D

Electromagnetic field in quantummechanics. Canonical and Kinematic impulse

In order to understand the second effect, the Aharonov-Bohm effect, we must first state the basics of electromagnetics in quantum physics: we seek therefore the proper hamiltonian to use for a charged particle in an electromagnetic field. The way we shall proceed is to state the proper hamiltonian to use in the classical system, and then employ the correspondence principle to get the quantum mechanical operator. We wish to find a hamiltonian that yields the Lorenz force when we find $m\ddot{\mathbf{x}}$, where, as usual, the dots denote time derivatives, ie. $\dot{\mathbf{x}} \equiv \frac{d\mathbf{x}}{dt}$. From analytical mechanics (eg. [20]) we know, that from the hamiltonian we may find the kinematic and canonical impulse as

$$m\dot{x_i} = m\frac{\partial H}{\partial p_i} \tag{D.1}$$

$$\dot{p_i} = -\frac{\partial H}{\partial x_i} \tag{D.2}$$

Here we must emphasize that p_i (the canonical impulse) is *not* necessarily the same as $m\dot{x_i}$ (the kinematic impulse). For brevity we now propose the hamiltonian which is indeed the correct answer, and then proceed to prove, that the expression obtained for $m\ddot{x_i}$ is indeed the ith component of the Lorenz force, $q(\mathbf{v} \times \mathbf{B} + \mathbf{E})$. Let

$$H = \frac{1}{2m}(\mathbf{p} - q\mathbf{A}(\mathbf{x}, \mathbf{t}))^2 + q\phi(\mathbf{x}) \tag{D.3}$$

where $A(\mathbf{x}, t)$ is the vector potential defined from $\mathbf{B} = \nabla \times \mathbf{A}$ and $\phi(x)$ is the electric potential, ie.

$$\mathbf{E}(\mathbf{x}) = -\frac{\partial \mathbf{A}(\mathbf{x}, t)}{\partial t} - \nabla\phi(\mathbf{x}) \tag{D.4}$$

and q and m is the charge and mass of the particle, respectively. It is important to realize that in the hamiltonian formulation of analytical mechanics, H is considered to be a function of $\mathbf{x}$, $\mathbf{p}$ and

t only, as this will come into play when distinguishing between total and partial derivatives. From (D.1) we find

$$m\ddot{x_i} = m\frac{d}{dt}(\frac{\partial H}{\partial p_i}) = \frac{d}{dt}(p_i - qA_i(\mathbf{x},t)) = \dot{p_i} - q\sum_j \frac{\partial A_i(\mathbf{x},t)}{\partial x_j}\dot{x_j} - q\frac{\partial A_i(\mathbf{x},t)}{\partial t} \tag{D.5}$$

Now, inserting (D.3) into (D.2) we find

$$\dot{p_i} = -\frac{1}{m}\sum_j (p_j - qA_j(\mathbf{x},t)(-q\frac{\partial A_j(\mathbf{x},t)}{\partial x_i})) - q\frac{\partial \phi(\mathbf{x})}{\partial x_i} = \sum_j (\dot{x_j}q\frac{\partial A_j}{\partial x_i}) - q\frac{\partial \phi(\mathbf{x})}{\partial x_i} \tag{D.6}$$

We can insert this into (D.5) we find

$$\begin{aligned} m\ddot{x_i} &= q\sum_j (\dot{x_j}(\frac{\partial A_j(\mathbf{x},t)}{\partial x_i} - \frac{\partial A_i(\mathbf{x},t)}{\partial x_j})) + q(-\frac{\partial A_i(\mathbf{x},t)}{\partial t} - \frac{\partial \phi(\mathbf{x})}{\partial x_i}) \\ &= q(\sum_j (\dot{x_j}\epsilon_{ijk}B_k) + E_i(\mathbf{x})) = q((\dot{\mathbf{x}}\times\mathbf{B})_i + E_i(\mathbf{x})) \end{aligned} \tag{D.7}$$

which, as we required is exactly the equation of motion of a charged particle in a electromagnetic field, and where we have used that

$$\epsilon_{ijk}B_k = \epsilon_{ijk}(\nabla\times\mathbf{A})_k = \epsilon^2_{ijk}(\frac{\partial \mathbf{A}(\mathbf{x},t)_j}{\partial x_i} + \frac{\partial \mathbf{A}(\mathbf{x},t)_i}{\partial x_j}) \tag{D.8}$$

and the expression of the electric field $\mathbf{E}$ from (D.4). We should thus (by the correspondence principle) use the quantum mechanical hamiltonian operator

$$\hat{H} = \frac{1}{2m}(\hat{\mathbf{p}} - q\mathbf{A})^2 + q\phi(\mathbf{x}) = \frac{1}{2m}(-i\hbar\nabla - q\mathbf{A})^2 + q\phi(\mathbf{x}) \tag{D.9}$$

where, for brevity I have dropped the parameters of $\mathbf{A}$. Now, if we write out the square we find that

$$\begin{aligned} \hat{H}\Psi &= \frac{1}{2m}(-\hbar^2\nabla^2\Psi + q^2\mathbf{A}^2\Psi + iq\hbar(\nabla\cdot\mathbf{A}\Psi + \mathbf{A}\cdot\nabla\Psi)) \\ &= \frac{1}{2m}(-\hbar^2\nabla^2\Psi + q^2\mathbf{A}^2\Psi + iq\hbar(\Psi\nabla\cdot\mathbf{A} + 2\mathbf{A}\cdot\nabla\Psi)) \\ &= \frac{1}{2m}(-\hbar^2\nabla^2 + q^2\mathbf{A}^2 + iq\hbar(2\mathbf{A}\cdot\nabla))\Psi \end{aligned} \tag{D.10}$$

where in the last equality I have used the Coulomb gauge, ie. $\nabla\cdot\mathbf{A} = 0$.

The formula (D.9) forms the outset for the explanation of the Aharonov-Bohm effect.

Bibliography

[1] J. I. Cirac and P. Zoller, Phys. Rev. Lett. **74**, 4091 (1995)

[2] Feynman, R. P., Int. J. Theor. Phys. **21**, 467 (1982)

[3] Kitaev, A. Y., Russ. Math. Surveys **52**, 11917 (1997)

[4] DiVincenzo, D.P., Phys. Rev. A **51**, 1015 (1995)

[5] Deutsch, D., Proc. Roy. Soc. Lond. A **400**, 97 (1985)

[6] Grover, L. K.,quant-ph/9605043 (1996)

[7] Shor, P. , SIAM J. Comput. 26 (5): 1484-1509 (1999)

[8] Kuemmeth, F. *et al*, Nature **452**, 448-452 (2008)

[9] Ashcroft/Mermin *Solid state physics* Int'l edition, 1976

[10] R. Saito *et al*, Phys. Rev. B **46**, 1804 (1992).

[11] D. Kienle *et al.*, J. Appl. Phys. **100**, 043714 (2006)

[12] C.T. White, D.H. Robertson and J.W. Mintwire, Phys. Rev. B **47**, 5485 (1993)

[13] D.V. Bulaev *et al.*, Phys. Rev. B **77**, 235301 (2008)

[14] T. Ando, J. Phys. Soc. Jpn. **69**, 1757 (2000)

[15] A. Kleiner and S. Eggert, Phys. Rev. B **64**, 113402 (2001)

[16] D. Huertas-Hernando, F. Guinea, A. Brataas, Phys. Rev. B **74**, 155426 (2006)

[17] F. Schwabl *Quantenmechanik für Fortgeschrittene*, 2nd edition, (2000)

[18] H. Ajiki and T. Ando, J. Phys. Soc. Japan **62**, 1255 (1993)

[19] W. Izumida, K. Sato, R. Saito: J. Phys. Soc. Jpn. **78** (2009) No. 7 074707

[20] Goldstein *et al.*: Classical mechanics, 3rd eddition, Addison/Wesley (2002)

[21] R. Saito,G. Dresselhaus,M. S. Dresselhaus, *Physical properties of carbon nanotubes* (1998)

[22] G.H. Wannier, Phys. Rev. **52**, 191 (1937)

[23] J.C. Slater, Phys. Rev. **76**, 1592 (1949)

[24] J.M. Luttinger, Phys. Rev. **84**, 814 (1951)

[25] F. London, Phys. Rev. **74**, 562 (1948)

[26] R. Peierls, Z. Phys. **80**, 763 (1933)

[27] D. Porezag *et al.* Phys. Rev. B **51**, 12947 (1995)

[28] Jeong, J.S and Lee, H.W. Phys. Rev. B **80**, 075409 (2009)

[29] J. Serrano *et al.*, Solid State Commun. **113**, 411 (2000)

[30] Wallace, P.R., Phys. Rev. **71**, 622 (1947)

[31] Blundell, S., *Magnetism in condensed matter* (2006)

[32] Sakurai, J.J., *Modern quantum mechanics* Rev. eddition (1994)

[33] http://www.icmm.csic.es/jcerda/index.html

[34] J.C. Slater, Phys. Rev., **36** 57 (1930)

[35] L. Chico *et al.* Phys. Rev. B **79**, 235423 (2009)